DEVELOPMENT AND CHARACTERIZATION OF T-SLICE: A CANCER MODELING PLATFORM TO MODEL IMPORTANT FEATURES OF THE TUMOUR MICROENVIRONMENT IN VITRO

by

Nicholas Dawe

Submitted in partial fulfilment of the requirements
for the degree of Master of Applied Science

at

Dalhousie University
Halifax, Nova Scotia
June 2022

Dalhousie University is located in Mi'kma'ki,
the ancestral and unceded territory of the Mi'kmaq.
We are all Treaty people.

Dedication Page

To my parents Peter and Barbara for their support and encouragement throughout my academic journey. I will continue to value your advice as I navigate through the next chapter of my life. Thank you for being excellent role models and teaching me the importance of patience and work ethic. I would not be where I am today without your unwavering support.

Table of Contents

List of Figures

Abstract

The tumour microenvironment is composed of several types of non-cancerous cells (e.g., cancer-associated fibroblasts, endothelial cells, immune cells), extracellular matrix proteins, and cell signaling molecules. The various components of the tumour microenvironment work together to generate biochemical and biophysical pressures that promote tumour growth, invasion, metastasis, and multidrug resistance. Hypoxia gradients in the tumour microenvironment are significant because they are responsible for driving many of the tumour cell responses that allow the cancer to progress. The current landscape of *in vitro* cancer modeling relies largely on methods that fail to incorporate important features of the tumour microenvironment. As a result, investigations into tumour biology and anti-cancer drug efficacy can be misrepresentative of what occurs in the natural tumour *in vivo*. Cancer modeling platforms that do mimic important features of the tumour microenvironment are often limited due to their incompatibility with live-imaging techniques, lack of tunability, and lack of usability due to cost or the need for user expertise. The aim of this research project was to create a cancer disease modeling device that can recapitulate important features of the tumour microenvironment while remaining imageable to acquire spatiotemporal information. We have combined 2D tissue culture with 3D spheroid culture to create the "Tumour Spheroids Layered in an Imageable Cancer Environment" (T-SLICE), which harnesses the advantages of currently established cancer research methods while circumventing their limitations. This study demonstrated that T-SLICE generates hypoxia gradients that impact tumour cell response in two different breast cancer cell lines, including viability, proliferation rate, and changes in gene expression. T-SLICE provides a live snapshot of cancer cell behaviour in response to different biochemical pressures and has the potential to advance anti-cancer drug testing and diagnosis in the future.

List of Abbreviations & Symbols Used

2D	Two-dimensional
3D	Three-dimensional
AA	Antibiotic-antimycotic
ATP	Adenosine triphosphate
bFGF	Basic fibroblast growth factor
BSA	Bovine serum albumin
CAD	Computer aided design
CAF	Cancer-associated fibroblast
cDNA	Complementary DNA
CSC	Cancer stem cell
Cy3	Cyanine 3
Cy5	Cyanine 5
DMEM	Dulbecco's modified eagle medium
DNA	Deoxyribonucleic acid
EC	Endothelial cell
ECM	Extracellular matrix
eGFP	Enhanced green fluorescent protein
ER	Estrogen receptor
FBS	Fetal bovine serum
FISH	Fluorescence *in situ* hybridization
FUT11	Fucosyltransferase 11
GAPDH	Glyceraldehyde 3-phosphate

GFP	Green fluorescent protein
HDP	Hanging drop plate
HER2	Human epidermal growth factor receptor 2
HIF	Hypoxia-inducible factor
HRE	Hypoxia responsive element
ITH	Intratumour heterogeneity
LDHA	Lactate dehydrogenase A
M.M.P.	Mitochondrial membrane potential
MDR	Multidrug resistance
MGAT2	Alpha-1,6-Mannosyl-Glycoprotein 2-Beta-N-Acetylglucosaminyltransferase
miRNA	micro ribonucleic acid
PBS	Phosphate buffered saline
PDGFB	Platelet-derived growth factor subunit b
PDMS	Polydimethylsiloxane
PDX	Patient-derived xenograft
PEG	Poly(ethylene) glycol
PFA	Paraformaldehyde
PLAU	Plasminogen activator, urokinase
PR	Progesterone receptor
qRT-PCR	Quantitative reverse transcription polymerase chain reaction
RFP	Red fluorescent protein
RNA	Ribonucleic acid

ROS	Reactive oxygen species
scRNA-seq	Single cell RNA-sequencing
T-SLICE	Tumour Spheroids Layered in an Imageable Cancer Environment
TAM	Tumour-associated macrophage
TGFB3	Transforming growth factor beta 3
TIC	Tumour initiating cell
TIMP1	Tissue inhibitor metallopeptidase 1
TME	Tumour microenvironment
TOAC	Tumour-on-a-chip
UGT1A1	UDP Glucosyltransferase Family 1 Member A1
UV	Ultraviolet

Acknowledgements

I would like to sincerely thank my supervisor Dr. Brendan Leung for giving me the opportunity to pursue my MASc degree in his lab and allowing me to contribute to such an interesting research project. You have been an outstanding mentor and role model and immediately supported me and my goals from the day I joined your research team. You have given me the opportunity to develop in both a personal and academic setting and I will cherish my time in the Leung Lab forever. I would also like to thank the entire Leung Lab Team, current and past, for their support and friendship over the last two years. This also extends to the entire SBME student body and 4th floor Dentistry group. There are way too many of us to name, but you have all made my graduate school experience so enjoyable and filled with memories and friendships that will last a lifetime. Thank you to my advisory committee members, Dr. Paola Marcato, Dr. Leigha Rock, and Dr. John Frampton for all your advice and support. You created a supportive environment that left me feeling more motivated and excited to conduct my research after every committee meeting. Thank you to Dr. Jeanette Boudreau and her lab team, especially Morgan Pugh-Toole, for helping move this project forward and being such a pleasure to collaborate with. Thank you to my father Peter, mother Barbara, and brother Brad for all your support and encouragement throughout my graduate studies. I also want to thank my friends who stuck by my side when school became busy and always pushed me to keep working hard to achieve my academic goals. Finally, thank you to my loving partner Erin for always supporting me in my academic endeavours. You have always been such an excellent academic role model and motivate me to step outside of my comfort zone to continue growing as a person.

Chapter 1: Introduction

1.1 Breast cancer statistics, classification, and treatment

It is estimated that there will be 233,900 new cancer diagnoses and 85,100 cancer deaths in Canada in 2022 (Brenner et al., 2022). Breast cancer is expected to be the most diagnosed cancer in females with an anticipated 28,600 new diagnoses and will account for 6.5% of deaths caused by cancer, which is the fourth highest among cancer types (Brenner et al., 2022). These figures have increased since 2020 when there were an estimated 225,800 new cancer diagnoses and 83,000 cancer deaths in Canada, with breast cancer accounting for 6.1% of all cancer deaths (Brenner et al., 2020). A 2022 study published by Garaszczuk et al. that examined the economic impact of cancer in Canada from a societal perspective found that cancer-related costs in Canada surpassed CAD 26 billion in 2021, with a staggering 30% of costs being assumed by patients and their families in terms of direct and indirect costs and productivity loss. The overall rate of new cancer diagnoses has been declining in Canada since the 1990s, but the incidence of breast cancer has remained stable over the last three decades (Brenner et al., 2022). It must also be noted that despite overall incidence decreasing, the total number of new cancer cases and deaths continues to increase due to Canada's growing and aging population and predisposing factors such as genetics (Brenner et al., 2022; Torre et al., 2016). Cancer remains at the forefront of public health concern and research efforts into early detection programs, therapeutics, and fundamental research must be continued.

Breast cancer is a complex, dynamic disease that can be categorized based on a variety of factors. *In situ* breast carcinomas are localized and have not spread to other parts of the body and can be further divided into ductal carcinoma *in situ* (DCIS) or

lobular carcinoma *in situ* (LCIS) (Ullah, 2019). Invasive breast carcinomas represent greater risk to an individual's health and are further divided into histological subtypes, with invasive ductal carcinoma being the most common of the subtypes (Ullah, 2019). Breast cancer is also staged from 0 – 4 based on the extent of cancer in the body, which is based on the size of the tumour, where it is in the breast, and whether it has spread to the lymph nodes or metastasized to other parts of the body (Canadian Cancer Society). Higher stage number is associated with greater cancer spread and poorer prognosis (Canadian Cancer Society). In addition to classifying breast cancer based on location, size, and spread, it can be further classified at the molecular level based on the expression of estrogen receptor (ER), progesterone receptor (PR), and human epidermal growth factor receptor 2 (Her2).

Immunophenotyping breast cancer based on ER, PR, and HER2 holds significant prognostic value for invasive ductal carcinomas (Ullah, 2019). Immunohistochemical analysis of breast tumour biopsies is performed to measure the expression of ER, PR, and HER2 to further classify these tumours: ER+/PR+/HER2- tumours are Luminal A; ER+/PR+/HER2+ tumours are Luminal B; ER-/PR-Her2+ tumours are HER2-enriched; ER-/PR-/HER2- tumours are triple negative breast cancer (TNBC) and classified as Basal Like (Ullah, 2019). Patients with TNBC often have a poor prognosis due to the rapid rate of growth and spread of these tumours and lack of therapeutic options compared to hormone receptor-positive breast cancers (Ullah, 2019). Several targeted therapies to treat breast tumours expressing ER, PR, or overexpressing HER2 have been developed.

First line treatment for non-metastatic breast cancer is surgical intervention via lumpectomy if negative margins can be achieved or mastectomy (Trayes & Cokenakes,

2021). Patients receiving surgical intervention are often preoperatively treated systemically to reduce the size of the tumour to make it more operable (Trayes & Cokenakes, 2021). Surgical intervention is followed by postoperative radiation treatment to eliminate any remaining cancerous tissue and lower the risk of recurrence (Trayes & Cokenakes, 2021). Endocrine therapy, targeted therapy, and chemotherapy can also be administered postoperatively depending on the needs of the patient and their cancer diagnosis. Endocrine therapy used to treat hormone receptor-positive breast cancers include aromatase inhibitors, which prevents the conversion of androstenedione to estrone and testosterone to estradiol, and selective estrogen receptor modulators, which competitively bind estrogen receptors on tumour cells (Trayes & Cokenakes, 2021). Immunotherapy is used to treat HER-2-positive breast cancers with a monoclonal antibody that binds the extracellular domain of ERBB2 and prevents the activation of downstream signaling pathways (e.g., Trastuzumab) (Trayes & Cokenakes, 2021). Finally, breast cancer can also be treated with chemotherapies with a wide range of mechanisms of action that target DNA replication and cell division (Trayes & Cokenakes, 2021). Chemotherapy is the only systemic treatment option available for patients with TNBC and is often associated with severe adverse effects (e.g., cardiotoxicity). These treatments are also administered to patients with metastatic breast cancer but are often focused on extending life and improving quality of life versus curing the disease. Patients with metastatic breast cancer currently have a 29% 5-year survival rate (Cancer.net, 2022). Treatment of breast cancer has improved drastically over the last fifty years, but there are still many challenges to overcome.

One of the most remarkable improvements in the treatment of breast cancer has been the use of localized, breast conserving therapies versus full mastectomies and therapeutics that are becoming more targeted with less systemic adverse effects (Sledge, 2014). There are still areas of breast cancer treatment that can be improved despite these advances, particularly in TNBC where targeted therapies have not yet been developed. One of the difficulties associated with developing targeted therapies for TNBC is that it is a highly heterogeneous disease that presents differently among patients, making selection of an appropriate chemotherapy at the correct dosage difficult (Sledge, 2014). Resistance to systemic therapy is also a major hurdle faced in breast cancer treatment. Resistance can be caused by changes in the tumour microenvironment and the development of tumour heterogeneity throughout tumour progression, along with the selection of sub-clonal multidrug resistant (MDR) tumour cell populations that expand and diversify to further complicate treatment (Chatterjee & Bivona, 2019). Oncology drug development has the lowest probability of success across therapeutic groups with an abysmal 3.4%, an approximate 50% decrease since a 2014 report (Wong et al., 2019). This problem is exacerbated by the fact that most oncology drug candidates fail in Phase 3 clinical trials that have had millions of dollars poured into their development. Several factors contribute to the failure of oncology drug candidates in clinical trials, including off-target effects and misidentification of biomarkers, but it can also be attributed to pre-clinical *in vitro* testing in unrepresentative models of cancer disease that do not incorporate important aspects of tumour biology (Wong et al., 2019). There is an urgent need to better mimic the tumour microenvironment *in vitro* to recapitulate tumour heterogeneity

to provide improved evidence for advancement of oncology drug candidates into clinical trials.

1.2 Tumour microenvironment

Tumour initiation occurs when genomic alterations occur within a cell to facilitate the evasion of pro-apoptotic and growth-inhibitory signals while providing signals to survive and proliferate (Bajaj et al., 2020). Cells that accumulate mutations in oncogenes or tumour suppressor genes are termed cancer stem cells (CSCs) or tumour initiating cells (TICs), which is attributed to their ability to self-renew and tumorigenicity (Bajaj et al., 2020; Qureshi-Baig et al., 2017). Tumour initiating cells must also accumulate mutations that promote angiogenesis, invasion, and metastasis to support tumour development and progression. It has previously been thought that cancer development and progression was solely due to intracellular abnormalities in cancerous cells, however more recent cancer research has demonstrated that the extracellular environment of a tumour plays crucial roles in initiation, progression, and metastasis (Hansen et al., 2016). Cells that have accumulated the proper set of driver mutations must also be subject to an altered extracellular matrix (ECM) with disrupted biophysical and biochemical properties to successfully initiate tumour development (Evans et al., 2019). Tumours influence their surrounding environment as they develop and generate selective pressures for the tumour microenvironment (TME) to be supportive of the needs of the tumour to grow and metastasize (Junttila & de Sauvage, 2013). A tumour will recruit fibroblasts, immune cells, vascularize, and remodel the ECM to shape its stroma to create a supportive TME (Figure 1.2.1), ultimately helping in the acquisition of the hallmarks of cancer (Hanahan & Weinberg, 2000; Hanahan & Weinberg, 2011; Hanahan, 2022). The role of the TME

varies significantly depending on the location and needs of the tumour that it supports. The phenotypic differences of a tumour and its environment combined with intracellular genotypic variations of cancer cells drives tumour heterogeneity, which plays a major role in MDR and relapse.

Most of the stromal cells in the TME are cancer-associated fibroblasts (CAFs) that are mainly derived from resident fibroblasts that have been reprogrammed in response to cell signaling molecules abundant within the TME (Wu & Dai, 2017). CAFs are identified in the tumour stroma based on their morphology and lack of epithelial, endothelial, and immune cell markers along with the lack of mutations found within the cancer cells (Sahai et al., 2020). It is difficult to pinpoint an exact mechanism explaining how CAFs are generated and seems to vary based on tumour location. Interactions between breast cancer cells and stromal fibroblasts activates Notch signalling to promote a CAF phenotype (Sahai et al., 2020). One of the main functions of fibroblasts under normal physiology is the production and secretion of ECM molecules and proteolytic enzymes (e.g., matrix metalloproteinases) to promote ECM remodeling and mechanical tissue integrity (Wu & Dai, 2017). Extracellular matrix remodeling is required for proper wound healing and development but can be exploited by tumours to facilitate invasion into surrounding tissue and metastasize to other sites in the body. Disrupted ECM remodeling in the breast TME leads to the generation of a fibrotic, stiff stroma that can be up to 20 times stiffer than a healthy mammary gland (Elwakeel & Weigert, 2021). The increased rigidity disturbs tissue homeostasis and facilitates invasion of breast cancer cells into surrounding breast tissue. The stiffened ECM also plays a major role in the prevention of cancer cell elimination by the immune system and systemic therapy.

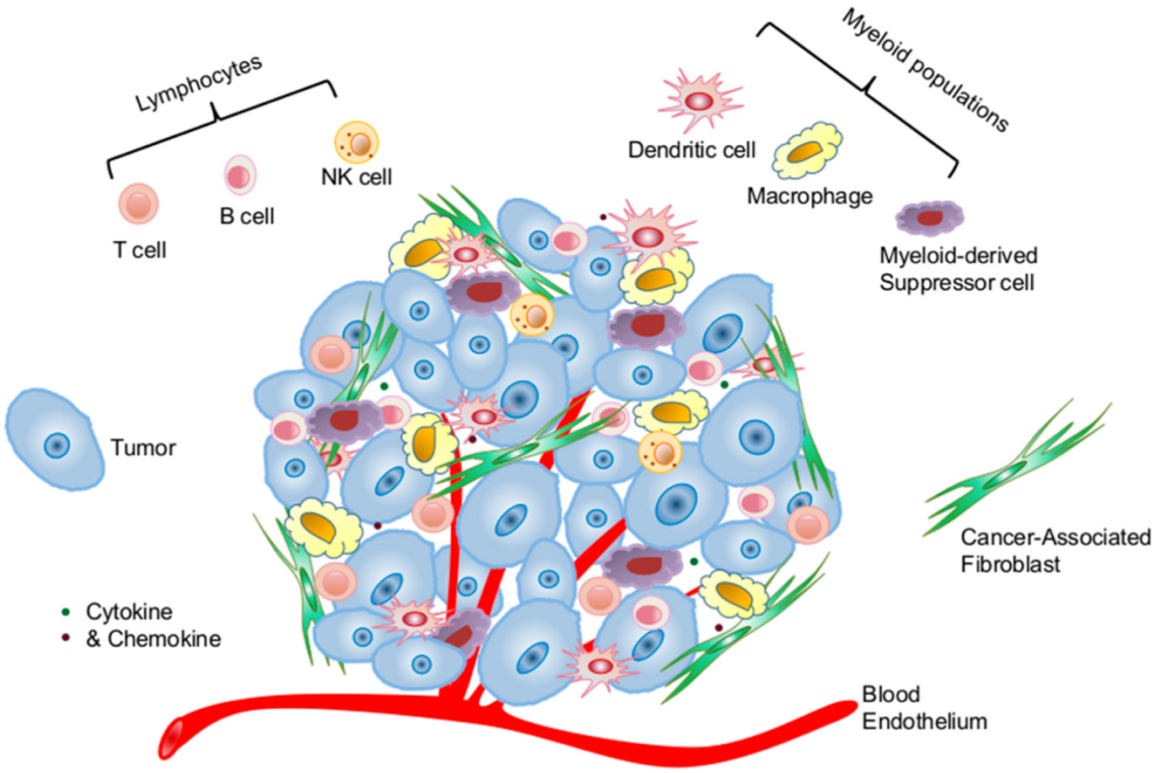

Figure 1.2.1. Main constituents of the tumour microenvironment. The tumour microenvironment can be divided into two compartments: (i) the stromal cellular compartment consisting of cancer-associated fibroblasts, endothelial cells composing the vasculature, and a variety of immune cell populations and (ii) the extracellular compartment consisting of extracellular matrix molecules, cytokines, and growth factors. Dynamic interactions between the tumour microenvironment and tumour cells impacts tumour biology and drives heterogeneity. Reprinted with permission from MDPI, Basel, Switzerland: International Journal of Molecular Sciences (Cui & Guo, 2016), Copyright © 2016: http://creativecommons.org/licenses/by/4.0/.

Immune cells are unable to infiltrate the tumour mass to kill cancerous cells (Elwakeel & Weigert, 2021). Direct immunomodulation arising from cell-cell communication between CAFs and tumour-associated macrophages (TAMs) has also been found in breast cancer. Chitinase-3-like-1 secreted by CAFs interacts with TAMs to promote an immunosuppressive M2 phenotype (Cohen et al., 2017). The stiffened ECM in breast cancer also prevents the dispersal of chemotherapeutics into the tissue. Cytokines secreted by CAFs interact with breast cancer cells and have been shown to confer resistance to doxorubicin and enhance their CSC-like properties (Elwakeel & Weigert, 2021). Taken together, the disrupted ECM reorganization facilitated by CAFs and the secretion of various cell signaling molecules that interact with cancer and stromal cells in the TME enhances tumorigenicity, drug resistance, and immune evasion.

The immune cell compartment of the tumour microenvironment is complex and dynamic. Immunosurveillance in the breast eliminates transformed cells that acquire driver mutations that would ultimately lead to the development of a breast tumour. When cells that have acquired these mutations evade immune detection, they will communicate with immune cells residing in the breast to prevent their elimination in the future (Salemme et al., 2021). The TICs that escape immune destruction will proliferate and grow into a solid tumour. The breast cancer cells will continue to acquire mutations and generate an increasingly immunosuppressive TME every time they are able to avoid immune detection (Salemme et al., 2021).

The breast TME has both immunosuppressive cells (e.g., M2-like TAMS, innate lymphoid cells type 2 and 3, regulatory T cells) and immunostimulatory cells (natural killer cells, tumour infiltrating lymphocytes, innate lymphoid cells type 1) that

communicate with the cancer cells and influence tumour progression (Salemme et al., 2021). Tumour-associated macrophages typically assume an M2-like phenotype. Correlations between high TAM density and poor prognosis are well-documented in breast cancer (Choi et al., 2017). The poor prognosis associated with high TAM density is attributed to several factors. The CAFs and TAMs in the breast TME work in unison to disrupt healthy ECM remodeling to facilitate breast cancer cell invasion (Choi et al., 2017). Immunostimulatory cells (e.g., $CD8^+$ T cells) can also be suppressed by TAMs via secretion of anti-inflammatory cytokines (e.g., IL-10), leading to the escape of breast cancer cells from immune detection (Cha & Koo, 2020). Regulatory T-cells exert much of their immunosuppression via the production of immunosuppressive cytokines, which helps cancer cells avoid immune clearance (Salemme et al., 2021). Hypoxia in the TME, which will later be discussed in detail, increases the expression of CXCR4 on regulatory T cells and CXCL12 in breast cancer cells, which recruits regulatory T cells to the tumour to create an immunosuppressive phenotype (Yan et al., 2011). High regulatory T cell infiltration into the breast TME correlates with poor prognosis, as seen with other immunosuppressive immune cells (Yan et al., 2011). M2-like TAMs, regulatory T cells, and other immunosuppressive cells in the TME aid in tumour progression through mechanisms independent of immune function. For example, immunosuppressive cells secrete vascular endothelial growth factor (VEGF) and other pro-angiogenic cytokines to stimulate vascularization of a growing tumour (Salemme et al., 2021).

Solid tumours must vascularize to adequately supply oxygen and nutrients to cancerous cells to facilitate continued proliferation and tumour growth. A consequence of dysregulated ECM remodeling and pro-angiogenic signaling is aberrant vascularization

within the TME. Breast tumours are limited in growth to just 2 mm if they do not activate angiogenesis because inadequate oxygen and nutrient supply leads to a balanced rate of cancer cell death and proliferation (Madu et al., 2020). Healthy tissue with well perfused vasculature at a typical venous pressure enables oxygen to diffuse up to 150 μm through the tissue (Grimes et al., 2016). The poorly developed vasculature of solid tumours decreases this diffusion distance down to approximately 100 μm (Grimes et al., 2016). The decreased oxygen diffusion distance is exacerbated by the high metabolic demand of cancerous cells that consume oxygen more rapidly. The poorly developed vascular networks within the TME result in hypoxic regions of solid tumours, typically observed in the middle of a large mass, that induce hypoxic responses mediated by hypoxia inducible factors and other pro-angiogenic factors in cancerous and supporting stromal cells (Petrova et al., 2018).

Low O_2 tension (i.e., hypoxia) in the breast TME will stabilize hypoxia inducible factors (HIFs) to activate a wide range of transcriptional responses to stimulate angiogenesis (Madu et al., 2020). Endothelial cells (ECs) in the TME are the cells that compose the capillary networks that make up the vasculature within the tumour, but they are incapable of multiplying. To extend the vascular network throughout the breast tumour, precursor cells are recruited to the site of blood vessel extension, differentiate into ECs, and form tubular networks to vascularize the poorly oxygenated areas of the tumour (Madu et al., 2020). Both breast cancer cells and supporting stromal fibroblasts are responsible for the upregulation and secretion of pro-angiogenic factors in the hypoxic TME (Madu et al., 2020).

As previously mentioned, cellular hypoxic responses are mainly attributed to HIF transcription factors that regulate the expression of a large set of genes involved in cell metabolism, proliferation, and ECM remodeling (Madu et al., 2020). Hypoxia-inducible factors contain an oxygen-sensitive alpha subunit that is transiently activated when cells are exposed to a low oxygen environment, and a beta subunit (HIF1-B) that is constitutively expressed. HIF-a and HIF1-B subunits dimerize when cells are under hypoxic stress (e.g., in the hypoxic TME) to induce HIF-driven transcriptional changes in cancer and stromal cells (Petrova et al., 2018). One of the major HIF-driven transcriptional responses in cancerous cells is the upregulation of TGFB, bFGF, and PDGFB secretion to reprogram fibroblasts into CAFs (Petrova et al., 2018). The hypoxic conditions then stimulate a HIF-mediated response in CAFs to secrete CXCL12 to enhance tumour growth (Petrova et al., 2018). As previously mentioned, CAFs secrete ECM components and proteolytic enzymes that lead to abnormal ECM formation that is pro-tumorigenic. Collagen is one of the main dysregulated ECM proteins secreted by CAFs in breast cancer that results in the development of the stiff, fibrotic ECM in the TME. Studies have shown that these fibrotic regions within the TME coincide with the location of hypoxic zones in the TME (Colpaert et al., 2003). Mechanical signaling between the stiffened ECM and breast cancer cells stimulates breast epithelial cell proliferation, which is stimulated further by the downregulation of miRNA-203 and upregulation of Akt activation resulting from the mechanical stiffness of the breast ECM (Jiang et al., 2022). Mechanical stimuli and the biophysical environment of the TME will be discussed further in a future subsection, but this highlights the complex interplay

between hypoxic responses in cancerous cells and CAFs that function together to promote cancer progression and metastasis.

Cells displaying a hypoxic response shift their metabolism from aerobic respiration to glycolysis to generate adenosine triphosphate (ATP) from glucose molecules. The stabilization of HIF-1 is thought to be a major mediator of this metabolic alteration observed in solid tumours. Specifically, HIF-1 mediates the transcriptional activation of genes encoding glucose transporters and glycolytic enzymes (Zeng et al., 2015). Studies have found hypoxia-mediated upregulation of glucose transport GLUT1 in breast cancer and suggest a link between GLUT1 expression and aggressiveness (Chen et al., 2010). Hypoxia in the breast TME also increases lactate dehydrogenase A (LDHA) expression in breast cancer cells that catalyzes the conversion of pyruvate to lactate, which subsequently increases breast cancer cell proliferation rate, invasion, and the conversion of stromal fibroblasts to CAFs (Martinez-Ordonez et al., 2021). HIF-1 also prevents oxidative phosphorylation in the mitochondria to further drive glycolysis over aerobic respiration (Zeng et al., 2015). The shift from aerobic respiration to glycolysis allows cancer cells to survive under conditions of prolonged hypoxia in large, poorly vascularized tumours.

The cellular hypoxic response is implicated in DNA damage and repair and tumour cell apoptosis. Acute hypoxic stress leads to the accumulation of reactive oxygen species (ROS) that cause DNA damage. Chronic hypoxia impairs DNA repair mechanisms in cancer cells (Zeng et al., 2015). Acute and chronic hypoxic responses in cancer cells leads to the accumulation of DNA mutations and the inability to repair them, giving rise to malignancies (Zeng et al., 2015). Base excision repair, mismatch repair, and DNA

double-strand break repair are downregulated at the transcriptional and translational level by hypoxia in breast cancer (Venkatesh et al., 2020). The mutational burden in hypoxic breast cancer cells allows them to evade immunosurveillance (Venkatesh et al., 2020). In addition to the pro-tumorigenic effects of hypoxia, it is implicated in therapeutic resistance through a variety of mechanisms.

The shifted metabolism of cancer cells in the hypoxic TME creates an acidic extracellular environment (Gao et al., 2020). The decreased pH in the hypoxic TME leads to MDR in solid tumours (Jing et al., 2019). This occurs through reduced apoptosis, genetic alterations in tumour suppressor genes, and elevated expression of drug efflux transporters (Jing et al., 2019). The disrupted proton gradient across cancer cell membranes leads to decreased intracellular accumulation of systemic drugs (e.g., chemotherapeutics), thereby directly impacting their efficacy. Paclitaxel, a commonly used chemotherapy in the treatment of breast cancer, is often rendered ineffective in the hypoxic breast TME due to apoptosis inhibition mediated through the inactivation of several caspases (van Loo et al., 2002). Hypoxia also impacts the efficacy of radiotherapy as it relies on the generation of ROS to kill cancer cells. Interestingly, a 2022 study published by West found that using a hypoxia biomarker was ineffective in predicting efficacy of adjuvant radiotherapy in patients following surgery. The hypoxic response of cancer cells also contributes to intratumour heterogeneity (ITH) by activating genes containing hypoxia responsive elements (HRE), which significantly contributes to metastasis and MDR (Qian & Rankin, 2019).

Biophysical cues resulting from the dynamic interactions between cancer cells and the TME play an important role in shaping cancer progression and metastasis (Emon et

al., 2018). Increasing bodies of evidence support that in addition to genetic alterations, cell-cell and cell-ECM interactions are responsible for neoplasia (Katira et al., 2013). The ECM stiffness, porosity, and composition are all important factors to consider in biophysical interactions. Mechanotransduction can occur in many ways, leading to a multitude of cell responses to shape tumour biology (Emon et al., 2018). The ECM of breast cancer is stiffer than that of healthy breast tissue and is mainly due to the increased deposition of collagens and crosslinking glycoproteins (Emon et al., 2018; Jiang et al., 2022). Increased ECM stiffness also correlates with later stage (III/IV) breast cancer, highlighting the importance of the biophysical nature of the TME in cancer progression (Acerbi et al., 2015). The stiffened ECM of cancerous tissue also impacts the ECs in the TME by driving their mechanically induced upregulation of N-cadherin expression to interact with cancer cells undergoing epithelial-to-mesenchymal transition (EMT) and permitting their entry into circulation (Reid et al., 2017). The biochemical and biophysical cues in the TME must be considered together in determining tumour growth, MDR, and metastasis.

1.3 Tumour heterogeneity

Tumour heterogeneity can be defined as intertumour heterogeneity or intratumour heterogeneity; intertumour heterogeneity refers to the differences in cancer cells and their surrounding TME between tumours, whether it is between different cancer patients or the primary and metastatic sites, whereas intratumour heterogeneity is defined as the genotypic and phenotypic variation observed within a single tumour (Figure 1.3.1) (Seoane & De Mattos-Arruda, 2014). It is important to consider both types of tumour heterogeneity in the context of cancer progression and treatment, but the focus of this

section will be intratumour heterogeneity, which I will abbreviate 'ITH'. The combination of ITH and the TME alter tumour metabolism, leading to hypoxia, acidemia, and fluctuations in nutrient availability and consumption rate compared to matched healthy tissues due to altered biochemical pathways. Experiments using single-cell sequencing have found that metastatic sites have a higher frequency of variation (single nucleotide polymorphisms, insertions, deletions) compared to the primary tumour, indicating that ITH in the primary tumour plays a crucial role in metastasis (Lawson et al., 2018). Intratumour heterogeneity complicates chemotherapeutic treatment as therapy-resistant sub-clonal cancer cell populations are selected for during treatment, which then expand and give rise to a drug resistant tumour (Dagogo-Jack & Shaw, 2018). The TICs in a tumour tend to be responsible for this relapse after treatment as they are frequently resistant to first-line therapies. The discovery of the roles played by the TME and ITH in tumour progression and susceptibility to treatment highlights the importance of investigating the implications that they have on tumour development, progression, and drug response.

Intratumour heterogeneity can be genetic, transcriptomic, epigenetic, or phenotypic (Dagogo-Jack & Shaw, 2018). All these factors contribute to ITH and are required for its dynamicity. Neoplasia arises from genetic alterations (i.e., driver mutations) that arise in a single cell, combined with biochemical and biophysical cues from their surrounding environmental niche, and undergo clonal expansion (Yuan, 2016; Katira et al., 2013). Additional mutations accumulate as the cancerous cells replicate their genome and divide, leading to the development and expansion of sub-clonal populations. Cooperation among sub-clonal populations leads to a genetically diverse tumour with

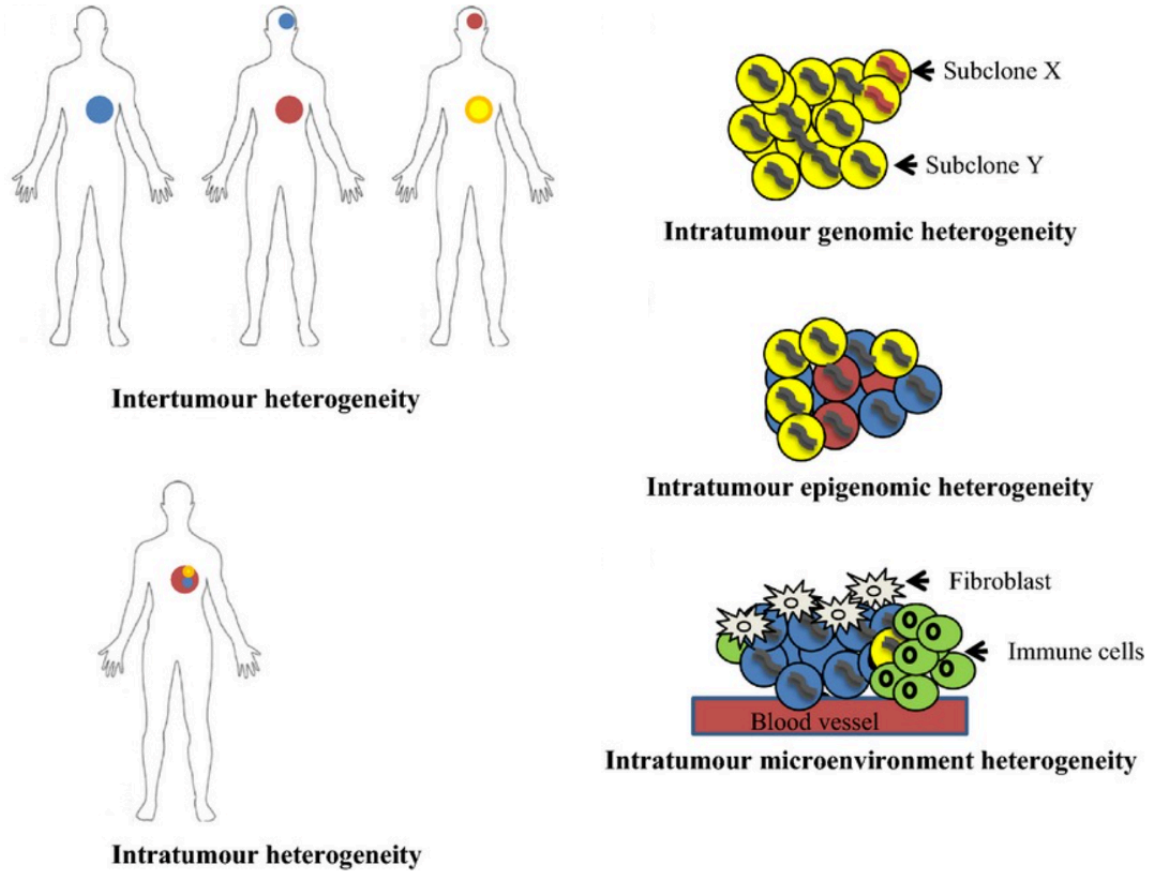

Figure 1.3.1. Intertumour versus intratumour heterogeneity. Intertumour heterogeneity describes differences in tumours between patients with different types of cancer, the same type of cancer, and between the primary and metastatic site within a single patient. Intratumour heterogeneity describes the genotypic and phenotypic variation observed within a single tumour. Tumour heterogeneity can refer to differences among the tumour cell population or within the tumour microenvironment. Reprinted with permission from Wiley Online Library: Journal of Internal Medicine (Seoane & De Mattos-Arruda, 2014), Copyright © 2014: http://creativecommons.org/licenses/by/4.0/.

high levels of ITH (Yuan, 2016). The mutational profile of the different cellular populations gives rise to different therapeutic responses among cancer cells within a single tumour. Phenotypic ITH extends beyond the rigid genetic heterogeneity and facilitates highly diverse cell populations within a single tumour. These can be influenced both spatially and temporally by the TME.

The TME is heterogeneous itself and thus drives cellular ITH via selective pressures (Lawson et al., 2018). Research has started to elucidate mechanisms in which gene expression changes can vary depending on the biochemical and biophysical gradients imposed by the TME (Black et al., 2015). As stated previously, HIFs interact with the hypoxia responsive elements in the promoter of HIF-regulated genes to control the expression of genes involved in metabolism, angiogenesis, proliferation, and MDR. As hypoxia fluctuates within the TME, so will the gene expression in cancer cells to generate a phenotypically diverse tumour with additional layers of complexity contributing to ITH. The TME is not only diverse within a single tumour mass but is also very different depending on the type of cancer and site of the tumour. This directly contributes to the level of ITH observed in different cancer types. Breast cancer is known to be a highly heterogeneous disease whose progression and drug resistance is often attributed to ITH (Januskeviciene & Petrikaite, 2019).

Breast cancer cells display high plasticity and can adapt to their environmental niche to drive ITH. (Yeo & Guan, 2018). This phenomenon extends beyond CSCs and into differentiated breast cancer cells, further complicating the matter of ITH. A 2016 study by Sflomos and colleagues injected ER^+/PR^+ MCF7 breast cancer cells intraductally or into the mammary fat pad of mice, which subsequently exhibited gene expression

patterns characteristic of luminal-A or basal-like breast cancers depending on the site of injection, demonstrating the possible influence that the TME has on breast cancer subtype plasticity. Given the difficulty in choosing systemic therapy for a given subtype of cancer described earlier, this becomes an even more difficult clinical problem when multiple breast cancer subtypes are present within a single tumour.

The last few decades have seen significant advancements in the treatment of breast cancer as researchers continue to gain a better understanding of targetable molecular markers in breast tumours. Unfortunately, breast cancer remains the second-highest cause of cancer-related death in women worldwide (Januskeviciene & Petrikaite, 2019). This is largely due to the complications in treating aggressive metastatic breast cancer that results from high levels of ITH. The heterogeneity within a tumour leads to improper diagnosis as not all cell populations are captured, leading to the resistance of certain sub-populations of tumorigenic cells and relapsed disease (Januskeviciene & Petrikaite, 2019). Biochemical gradients and interactions with the stromal cell compartment of the TME drive heterogeneity in breast tumours and cause differences in cell morphology, gene expression, metastatic potential, and MDR (Januskeviciene & Petrikaite, 2019). The ability to study and understand the impact of the TME on ITH in breast cancer, and other cancers, will be ground-breaking in improving cancer diagnosis, treatment, and ultimately prognosis.

1.4 Current landscape of disease modeling

Many disease modeling methods and platforms are used to study characteristics of cancer disease. Standard two-dimensional (2D) cell culture is a commonly used *in vitro* method used in cancer research to investigate cancer biology and drug response

(Imamura et al., 2015). Although a single cell is still three dimensional (3D), growing cells in a single monolayer on tissue culture polystyrene is considered 2D cell culture (Kapalczynska et al., 2018). 2D cell culture techniques are frequently used due to their low cost, high throughput, and reproducibility (Kapalczynska et al., 2018). There are numerous disadvantages associated with modeling cancer using 2D cell culture. Cancer cells grown as a monolayer on a plastic dish do not receive the same biophysical cues that cancerous cells in a tumour receive (Kapalczynska et al., 2018). This lack of cell-cell and cell-ECM interactions relative to a tumour do not capture the changes in gene expression, proliferation, and other behaviours observed *in vivo*. The absence of biochemical gradients in 2D cell cultures exacerbates this problem (Kapalczynska et al., 2018). The inability to mimic important features of the TME in 2D cell culture leads to the failure to recapitulate ITH. As a result, drug screening performed in 2D cell culture platforms does not represent drug response in a natural tumour. This leads to oncology drug candidate failure in late phase clinical trials after millions of dollars have been invested into their development (Wong et al., 2019).

In vitro modeling of cancer disease has shifted to 3D tissue culture methods that are better able to mimic the biophysical and biochemical properties of a solid tumour. Some of the most popular 3D *in vitro* culture methods being used in cancer research are spheroid culture, organoid culture, and growing cells in a biocompatible scaffold that mimics the tumour ECM for cancer cells to grow in a more native-like microenvironment (Imparato et al., 2015). Spheroids are cells grown in suspension that form 3D spherical aggregates and are much better than 2D cell culture at capturing the biophysical and biochemical complexity of the TME (Imparato et al., 2015). One of their limitations in

modeling cancer disease is that they are not grown in a representative ECM, which is implicated in tumour invasiveness and drug permeability (Imparato et al., 2015). Another problem with spheroid culture is that they must be grown several hundred micrometers in diameter to generate physiologically relevant biochemical gradients, which limits their imageability and researchers cannot investigate spatiotemporal dynamics within the spheroid once it becomes a certain size. Organoids are another 3D *in vitro* model used to study cancer. They are self-organized structures derived from stem cells that are strong *in vitro* models of tissue architecture and complexity relative to spheroid and 2D cell culture (Mohan et al., 2021). One of the other advantages of organoids over spheroids is that they are grown in a matrix that is more representative of an *in vivo* ECM compared to spheroids that are grown in suspension. Breast organoids have been used to study gene expression, tissue remodeling, and drug response (Mohan et al., 2021). One limitation of organoid culture is the inability to grow them beyond the micrometer scale, making it difficult to generate biochemical gradients that are representative of the TME (Huang et al., 2021). Organoids also present technical difficulties and irreproducibility as possible disadvantages associated with this culture technique.

An alternative to *in vitro* models of cancer disease is an *in vivo* patient-derived xenograft (PDX) in an immunocompromised rodent. PDXs can more faithfully maintain ITH than conventional *in vitro* culture methods and offer an improved model to study tumour biology and therapeutic response (Siolas & Hannon, 2014). Growing cells in an *in vivo* environment is much more representative of the TME than growing cells in an *in vitro* culture platform due to its innate ability to generate biochemical gradients and biophysical stimuli. The use of PDX in cancer research is still limited due to several

factors, including cost, success rate of engraftment, the tendency of drug response to differ between rodent and human, and the difficulties associated with observing and assaying the tumour while it grows in the rodent (Siolas & Hannon, 2014).

Researchers have recently shifted their focus to designing tumour-on-a-chip (TOAC) and microfluidic devices to model specific types of cancer *in vitro* and bridge the gap between current *in vitro* disease modeling techniques and PDX. Microfluidic devices and TOAC are often designed to model the TME as faithfully as possible to recapitulate physiologically relevant biochemical and biophysical features (Wan et al., 2020). McGuigan and colleagues (2016) developed the TRACER culture platform that generates hypoxia and other biochemical gradients observed in the TME of an *in vivo* tumour but is limited by its lack of imageability and inability to assess spatiotemporal dynamics during culture. Gioiella and colleagues (2016) created a TOAC device that incorporated both breast epithelial and stromal cells to assess the *in vitro* replication of the stromal activation during tumour epithelial invasion. This device was useful for the function that it was developed to model, but it is not tunable to model other cancers and requires user expertise. Ayuso et al. (2016) constructed a microfluidic device that was imageable to provide a 'window' into the TME to investigate spatiotemporal dynamics of cancer cells. This device generated biochemical gradients comparable to those observed in the TME but failed to incorporate any 3D cell-cell interactions and is not tunable to model a multitude of cancers (Ayuso et al., 2016). Microfluidic devices and TOAC hold promise in mimicking the TME *in vitro* but are currently limited by a variety of factors.

There is a gap in the field of cancer research that requires a high-content, high-throughput, cost-effective, and user-friendly *in vitro* culture platform that can faithfully

recapitulate the TME and maintain ITH while remaining imageable, tunable, and scalable.

1.5 Thesis aim, objectives, and hypothesis

This research project aimed to develop and optimize a novel *in vitro* culture platform that combines conventional 2D cell culture with 3D spheroid culture to mimic important features of the TME and resulting cell responses. The device was named "**T**umour **S**pheroids **L**ayered in an **I**mageable **C**ancer **E**nvironment" (T-SLICE) and takes advantage of the previously established method of culturing cells between two impermeable surfaces to generate biochemical gradients due to cellular consumption rate outpacing the rate of diffusion (Figure 1.5.1). Murine NIH/3T3 embryonic fibroblasts were seeded as a monolayer in T-SLICE and were primarily responsible for generating the cell-driven biochemical gradients in the device. Small diameter (<150 μm) MCF7 and HCC1806 breast cancer cells spheroids were cultured on top of the fibroblast monolayer to subject them to the cell-consumption defined gradients in T-SLICE.

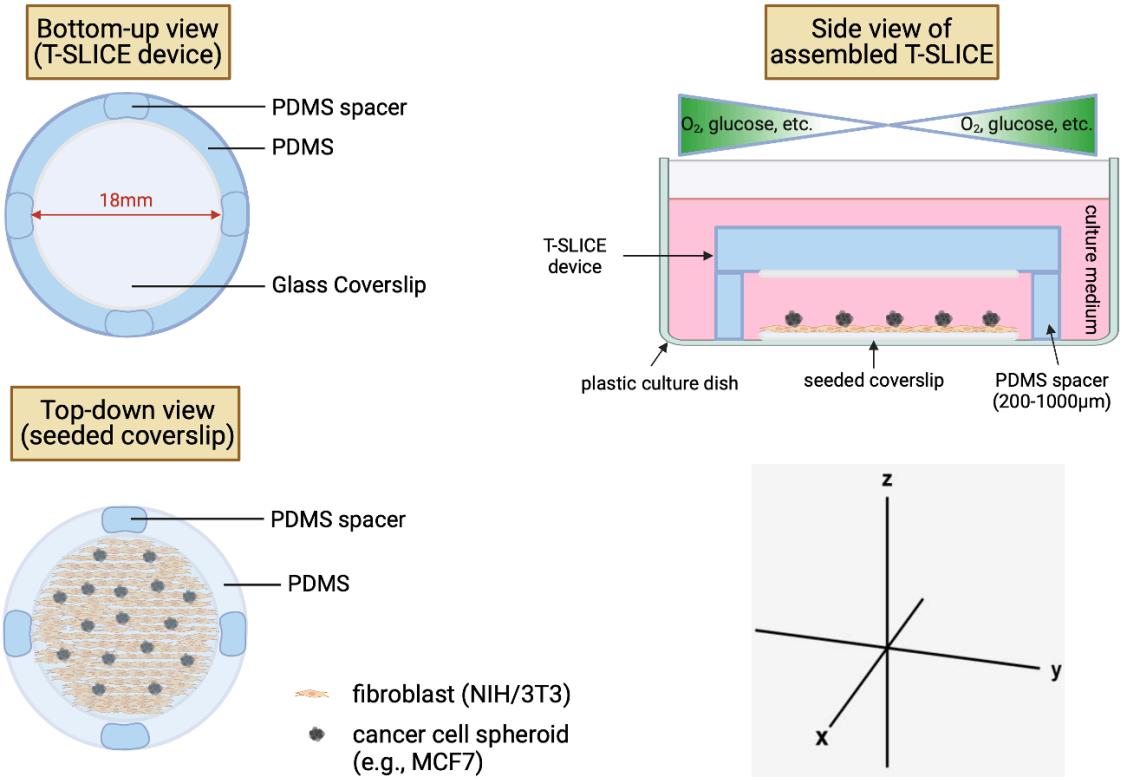

Figure 1.5.1. Schematic of T-SLICE design. T-SLICE is based on culturing cells between two parallel, closely spaced glass plates to generate cell consumption-defined biochemical gradients that are analogous to those observed in the *in vivo* tumour microenvironment (e.g., hypoxia, nutrient depletion). Biochemical gradients are generated in the X-Y plane of T-SLICE as oxygen and nutrients diffuse into the device from surrounding cell culture medium but are metabolized by cells before they reach the centremost regions of the device. Cells are grown between two round glass coverslips with an 18 mm diameter that are spaced 300 to 700 µm apart. The spacing is achieved using PDMS as the housing substrate, which is an optically transparent elastomer that maintains imageability of the device. To establish T-SLICE culture, a 2D monolayer of fibroblasts is seeded between the two glass coverslips. These are the cells that are responsible for generating the cell-consumption defined biochemical gradients within the device. I then seed breast cancer cell spheroids on top of the fibroblast layer to subject them to the gradients generated by the fibroblasts. Created with BioRender.com.

The overarching aim of this research project was divided into three main objectives:

1. Build the T-SLICE device and demonstrate its ability to maintain the desired cell culture. This involved determining the size of the device, space between the two oxygen-impermeable surfaces where cells are cultured, and the materials used. Objective 1 also included optimization of cell seeding densities to (i) generate desired biochemical gradients in T-SLICE and (ii) create breast cancer cell spheroids with a diameter less than 150 μm.
2. Robustly characterize the hypoxia gradients generated in T-SLICE to demonstrate that they are generated and sustained throughout the duration of T-SLICE culture.
3. Determine if the hypoxia gradients generated in T-SLICE can recapitulate cell responses in breast cancer cells that are observed *in vivo*. These included cell viability, cell proliferation, mitochondrial membrane potential, and changes in gene expression.

I hypothesized that T-SLICE would be able to generate and sustain cell consumption-defined hypoxia gradients analogous to those observed in the native TME and recapitulate important cell responses in the breast cancer cell spheroids. T-SLICE represents an imageable, tunable, cost-effective, and user-friendly device to more accurately model cancer disease *in vitro* compared to similar culture platforms while circumventing some of the main limitations in the field of TOAC development. In the future, T-SLICE has the potential to offer researchers a better method to investigate tumour biology and drug response in various cancers, ultimately leading to enhanced chemosensitivity predictive power and better cancer patient prognosis.

Chapter 2: Materials and Methods

2.1 T-SLICE conceptualization and design

The T-SLICE device is based on culturing cells between two parallel, closely spaced glass plates to generate cell consumption-defined biochemical gradients that are analogous to those observed in the *in vivo* tumour microenvironment (e.g., hypoxia, nutrient depletion). Biochemical gradients are generated in the X-Y plane of T-SLICE as oxygen and nutrients diffuse into the device from surrounding cell culture medium but are metabolized by cells before they reach the centremost regions of the device (Figure 1.5.1). The device geometry, cell growth surface area, and distance between the two parallel spaced glass plates are interrelated and must be considered together during conceptualization and design.

The following criteria were incorporated into the conceptualization and design of the T-SLICE device: T-SLICE must be imageable, easily tunable, user-friendly, cost-effective, high content, and high throughput. Polydimethylsiloxane (PDMS) and glass coverslips were used in combination to construct T-SLICE to meet these design criteria. The PDMS was used as the housing substrate to create separation between two parallel, closely spaced (<1 mm) glass coverslips. Devices with circle and square geometries were constructed. Circle glass coverslips with 18 mm, 22 mm, and 25 mm diameters and square glass coverslips with 18 mm x 18 mm and 22 mm x 22 mm side lengths were tested. T-SLICE devices of all sizes were fabricated with spacer heights ranging from 300 μm – 700 μm.

2.2 T-SLICE fabrication

T-SLICE devices were constructed by PDMS soft lithography followed by covalent attachment of a glass coverslip using plasma oxidation. 3D-printed molds of the T-SLICE devices were made to facilitate PDMS soft lithography for device fabrication. The mold designs were created using Autodesk® Fusion 360™ Computer-Aided Design (CAD) software and saved as '.stl' files. The '.stl' files were then converted to '.ctb' files using Chitubox® 3D printing preprocessing software. Molds were then printed using the ELEGOO Mars 2 Pro MSLA 3D Printer using ELEGOO Standard LCD UV-Curing Photopolymer Rapid Resin in 0.05mm layers with a UV light exposure time of 6 seconds per layer. Resin molds were washed with isopropanol for 20 minutes and UV-cured for 30 minutes using the ELEGOO Mercury Plus Washing and Curing Machine. The molds then underwent solvent extraction in 95% ethanol for 72 hours, with ethanol renewal every 24 hours, to remove any residual compounds that would interfere with PDMS curing during T-SLICE device fabrication.

Polydimethylsiloxane elastomer and curing agent (SYLGARD™ 184 Silicon Elastomer Kit, DOW) were mixed in a 10:1 ratio and poured into the 3D-printed molds. The PDMS was degassed in a vacuum chamber for 15 minutes or until no air bubbles remained. The degassed PDMS was cured at 60°C for 24 hours and then removed from the mold using forceps. A No. 1 glass coverslip was permanently attached to the PDMS via plasma oxidation for 1 minute to complete T-SLICE device fabrication. T-SLICE devices were rinsed in 70% ethanol and UV sterilized for 30 minutes prior to use.

2.3 General cell culture

NIH/3T3, MCF7, and HCC1806 cell lines were originally obtained from the American Type Culture Collection and maintained in a humidified incubator at 37°C, 5% CO_2. NIH/3T3 cells were maintained between 30% - 95% confluence in Dulbecco's Modified Eagle Medium (DMEM; ThermoFisher Scientific, Gibco, Cat. No. 11965092) supplemented with 10% calf bovine serum, iron fortified (ATCC, Cat. No. 30-2030) and 1% antibiotic-antimycotic (AA; ThermoFisher Scientific, Gibco, Cat. No. 15240062). MCF7 cells were maintained between 30% - 95% confluence in DMEM supplemented with 10% fetal bovine serum (FBS; ThermoFisher Scientific, Gibco, Cat. No. 12483020) and 1% AA. HCC1806 cells were maintained between 30% - 95% confluence in RPMI 1640 medium (ThermoFisher Scientific, Gibco, Cat. No. 11875119) supplemented with 10% FBS and 1% AA. All cell lines were subcultured at a ratio of 1:2 – 1:4 when 95% confluence was reached.

2.4 Spheroid culture using 384-well hanging drop plates

MCF7 and HCC1806 breast cancer cell spheroids were fabricated in 384-well hanging drop plates (HDP) for culture in T-SLICE. Prior to seeding, 384-well HDP were soaked overnight in 0.1% w/v Pluronic® F-108 (Sigma-Aldrich, Cat. No. 542342) solution in distilled water, rinsed with distilled water, and UV-sterilized for 30 minutes. Sterile strips of gauze were packed along the sides of the UV-sterilized HDP using a 1% AA solution in water. HDPs were then placed inside a 24-well plate containing 500 µL 1% AA solution in water per well to create a humid chamber and prevent droplet evaporation during spheroid culture. At this stage, the HDPs are prepared for cell seeding.

MCF7 and HCC1806 cell lines were seeded at densities of 50 cells and 100 cells per 25 µL droplet, respectively, to yield spheroids with a diameter less than 150 µm. Spheroid seeding medium was the complete cell culture medium for the respective cell line supplemented with 2.4 mg/mL Methocel® A4M (Sigma-Aldrich, Cat. No. 94378). Spheroids were seeded in a zippered pattern in HDP to prevent adjacent droplets from physically contacting each other, therefore yielding 192 spheroids per 384-well HDP. MCF7 and HCC1806 cell spheroids formed within 24 hours and 48 hours of seeding, respectively. Spheroids were cultured in a humidified incubator at 37°C, 5% CO_2.

2.5 T-SLICE culture

T-SLICE culture is performed in a 6-well plate (VWR®, Cat. No. 10062-892) with cells seeded on 18 mm diameter circular glass coverslips (VWR®, Cat. No. 16004-300). Glass coverslips were placed in the wells of a 6-well plate and treated with a 10 µg/mL fibronectin (Sigma-Aldrich, Cat. No. F1141) solution in phosphate buffered saline (PBS) (ThermoFisher Scientific, Gibco, Cat. No. 10010023) for 45 minutes. The fibronectin solution was then aspirated from the coverslips, and they were air-dried for 30 minutes or until all residual fibronectin solution had evaporated. NIH/3T3 fibroblasts were seeded on the fibronectin-coated coverslips overnight (24 hr) at a density of 200,000 cells per coverslip (400,000 cells/mL). Once a confluent fibroblast monolayer was generated on the coverslips, MCF7 and HCC1806 spheroids were harvested from HDP, centrifuged at 200 x g, and resuspended in 500 µL complete cell culture medium and seeded overnight (16-24 hr) on top of the NIH/3T3 fibroblast monolayer. One full HDP of spheroids (192 spheroids) was seeded per coverslip. Once the spheroids had adhered to the fibroblast monolayer, medium was aspirated from the coverslips, the T-SLICE device

was placed directly on top of the cell-seeded coverslips, and 2 mL of complete cell culture medium for the cell lines used to make the breast cancer cell spheroids was added to the well. Medium was changed in 500 µL increments every 24 hours to prevent metabolic waste buildup.

2.6 Image-IT Green Hypoxia Reagent for hypoxia detection

Image-IT Green Hypoxia Reagent (ThermoFisher Scientific, Invitrogen, Cat. No. I14834) is a live-cell permeable fluorogenic compound that becomes fluorescent in cells when oxygen tension drops below 5%. MCF7 cells were seeded in a 96-well plate at a density of 10,000 cells/well and grown for 24 hours. Image-IT Green Hypoxia reagent was then added to the cell culture medium at a final concentration of 1 – 10 µM and incubated at 37°C, 5% CO_2 for 30 minutes. The medium was exchanged with fresh growth medium following the 30-minute incubation and cells were then grown for 4 hours at 21% O_2 (normal growth conditions) or 1% O_2 ("hypoxia") using the EVOS™ Onstage Incubator (ThermoFisher Scientific, Cat. No. AMC1000). Cells were imaged on the Thermo Scientific™ Invitrogen™ EVOS™ FL Auto 2 Cell Imaging System (ThermoFisher Scientific, Invitrogen, Cat. No. AMAFD2000) with the EVOS™ Light Cube, GFP 2.0 (ThermoFisher Scientific, Invitrogen, Cat. No. AMEP4951) that has excitation and emission maxima near 482 nm and 524 nm, respectively.

2.7 Enzo Life Sciences ROS-ID Hypoxia/Oxidative Stress Detection Kit for hypoxia detection

ROS-ID Hypoxia/Oxidative Stress Detection Kit (Enzo Life Sciences, Cat. No. ENZ-51042) is designed to identify hypoxic cells using a fluorogenic probe. NIH/3T3 cells were seeded in a 96-well plate at a density of 10,000 cells/well and grown for 24

hours at 37°C, 5% CO_2 in complete growth medium. Cells were then incubated at 1% O_2 in the EVOS™ Onstage Incubator or at 21% O_2 as a control for 24 hours. ROS-ID Hypoxia Detection Reagent was added to the cells at a final concentration of 0.5 µM in complete cell culture medium for 30 minutes at 37°C, 5% CO_2. ROS-ID Hypoxia Detection Reagent was aspirated, and cells were rinsed three times with PBS. Cells were immersed in 100 µl PBS and imaged on the EVOS™ FL Auto 2 Cell Imaging System using the EVOS™ Light Cube, Texas Red 2.0 (ThermoFisher Scientific, Invitrogen, Cat. No. AMEP4955) that has excitation and emission maxima near 585 nm and 628 nm, respectively.

2.8 EF5 assay to characterize hypoxic response of MCF7 and HCC1806 cells in T-SLICE

EF5 (2-(2-Nitro-1*H*-imidazol-1-yl)-*N*-(2,2,3,3,3-pentafluoropropyl) acetamide) is a compound that was developed at the University of Pennsylvania by Dr. Cameron Koch and Dr. Sydney Evans that selectively binds hypoxic cells and forms adducts at the cell membrane, which can then be detected using an anti-EF5 fluorophore-conjugated antibody. EF5 Hypoxia Detection Kit, Cyanine 3 (Sigma-Aldrich, Cat. No. EF5-30C3) was used to detect cellular hypoxic responses in T-SLICE. T-SLICE culture was established as described above (section 2.5) and cultured in the presence of 100 µM EF5 for 6, 12, 24, or 48 hours. Medium containing 100 µM EF5 was replenished daily for timepoints exceeding 24 hours. T-SLICE devices were removed at desired timepoints, and cells were fixed in 4% paraformaldehyde (PFA) solution in PBS (ThermoFisher Scientific, Cat. No. J19943.K2) overnight at 4°C. Cells were rinsed twice with ice-cold PBS and permeabilized with 0.2% (v/v) Triton X-100 (Sigma-Aldrich, Cat. No. X100) for 5 minutes at room temperature. Cells were washed three times with PBS for 5 minutes

each to remove all permeabilization solution and blocked for 30 minutes at room temperature with 1% Bovine Serum Albumin (BSA) (Sigma-Aldrich, Cat. No. A9418) solution in PBS. Blocking solution was removed and cells were stained with anti-EF5, clone ELK3-51 Cyanine 3 conjugate mouse monoclonal antibody at a concentration of 5 µg/ml in 1% BSA solution in PBS for 16-24 hours at 4°C, protected from light. Cells were rinsed once and washed twice with PBS for 5 minutes prior to imaging. Imaging was performed using the EVOS™ FL Auto 2 Cell Imaging System using the EVOS™ Light Cube, RFP 2.0 (ThermoFisher Scientific, Invitrogen, Cat. No. AMEP4952) that has excitation and emission maxima near 542 nm and 593 nm, respectively. Fluorescence intensity was quantified in ImageJ.

2.9 Immunofluorescent staining of Hypoxia-Inducible Factor 1- and 2-alpha

MCF7 and HCC1806 cell spheroids were cultured in T-SLICE for up to 48 hours according to protocols outlined in section 2.5. Cells were fixed at desired timepoints with 4% PFA solution in PBS overnight at 4°C. Cells were rinsed twice with ice-cold PBS and permeabilized with 0.2% (v/v) Triton X-100 for 5 minutes at room temperature. Cells were washed three times with PBS for 5 minutes each to remove all permeabilization solution and blocked for 30 minutes at room temperature with 1% BSA solution in PBS. Blocking solution was aspirated, and cells were incubated with the following primary antibodies for 16-24 hours at 4°C: monoclonal mouse anti-human HIF-1a (Abcam, Cat. No. ab1) at a concentration of 10 µg/ml in 1% BSA solution in PBS; monoclonal rabbit anti-human HIF-2a (Abcam, Cat. No. ab243861) diluted 1/100 from manufacturer's stock in 1% BSA solution in PBS. Cells were rinsed twice and washed three times for 5 minutes each with PBS and stained for 2 hours at room temperature, protected from light,

with the following secondary antibodies: goat anti-mouse IgG H&L (Alexa Fluor® 488) (ab150113) at a dilution of 1/1000 from manufacturer's stock in 1% BSA solution in PBS; donkey anti-rabbit IgG H&L (Alexa Fluor® 647) (ab150075) at a dilution of 1/1000 from manufacturer's stock in 1% BSA solution in PBS. Cells were simultaneously stained for HIF-1a and HIF-2a. Imaging was performed using the EVOS™ FL Auto 2 Cell Imaging System using the EVOS™ Light Cube, GFP 2.0 (482 nm/524 nm) and EVOS™ Light Cube, Cy5 2.0 (ThermoFisher Scientific, Invitrogen, Cat. No. AMEP4956) that has excitation and emission maxima near 635 nm and 692 nm, respectively.

2.10 Transfection of MCF7 cells with 5HRE/GFP to generate a hypoxia-reporter cell line

MCF7 cells were transfected with plasmid 5HRE/GFP using the QIAGEN Superfect® Transfection Reagent (QIAGEN, Cat. No. 301305). 5HRE/GFP was a gift from Martin Brown & Thomas Foster (Addgene plasmid # 46926; http://n2t.net/addgene:46926; RRID:Addgene _46926). 200,000 MCF7 cells were seeded per well in a 6-well plate and incubated overnight at 37°C, 5% CO_2 prior to transfection. 5 µg 5HRE/GFP was diluted in 150 µl DMEM containing no serum or antibiotics. 30 µl Superfect Transfection Reagent was added to the 5HRE/GFP solution and vortexed for 10 seconds, followed by a 10-minute incubation at room temperature to allow transfection-complex formation to occur. 1 mL of complete cell culture medium (DMEM supplemented with 10% FBS, 1% AA) was added to the reaction tube and mixed by pipetting. Cells were washed once with 1 mL PBS and incubated with the transfection complexes at 37°C, 5% CO_2 for 3 hours. The medium containing the transfection complexes was then removed and cells were cultured under standard tissue culture

conditions with complete cell culture medium supplemented with 500 µg/ml G-418 (Sigma-Aldrich, Cat. No. G8168) to select transfected cells. Selective medium was used to maintain the cells but was not used when the transfected cells were used in experiments. Cells were imaged on the EVOS™ FL Auto 2 Cell Imaging System using the EVOS™ Light Cube, GFP 2.0 (Ex: 482 nm, Em: 524 nm).

2.11 Assessing cell viability in T-SLICE using calcein AM and ethidium homodimer-1

Cell viability in T-SLICE was assessed using calcein AM (ThermoFisher Scientific, Invitrogen, Cat. No. C1430) and ethidium homodimer-1 (ThermoFisher Scientific, Invitrogen, Cat. No. E1169) in tandem to create a live/dead assay, where calcein AM labels live cells and ethidium homodimer-1 labels dead cells. MCF7 and HCC1806 cell spheroids were cultured in T-SLICE as described in section 2.5 for 72 hours, with medium renewal every 24 hours to prevent metabolic waste accumulation. T-SLICE devices were removed after 72 hours, and cells were washed once with 1 ml PBS. A 1 µM calcein AM, 1 µM ethidium homodimer-1 solution in PBS was used to stain the cells for 30 minutes at room temperature, protected from light. The staining solution was removed, and cells were washed twice with 1 ml PBS and immersed in 1mL PBS for imaging. Imaging was performed on the EVOS™ FL Auto 2 Cell Imaging System using the EVOS™ Light Cube, GFP 2.0 (Ex: 482 nm, Em: 524 nm) and EVOS™ Light Cube, RFP 2.0 (Ex: 542 nm, Em: 593 nm).

2.12 Assessing cell proliferation in T-SLICE using the EdU Cell Proliferation Kit

EdU (5-ethynyl-2'-deoxyuridine) is a thymidine analog that is incorporated into newly synthesized DNA and can be used as a direct marker of cell proliferation. MCF7 and HCC1806 cell spheroids were cultured in T-SLICE as described in section 2.5 for 72

hours, with medium renewal every 24 hours to prevent metabolic waste accumulation. Cell culture medium contained 10 μM EdU (ThermoFisher Scientific, Invitrogen, Cat. No. C10337) for the entire duration of the culture period. After 72 hours, T-SLICE devices were removed, and cells were fixed with 4% PFA solution in PBS for 15 minutes at room temperature. The cells were washed twice with 1 ml 3% BSA solution in PBS for 5 minutes each. The wash solution was removed, and cells were permeabilized with a 0.5% (v/v) Triton X-100 solution in PBS for 20 minutes at room temperature. The permeabilization solution was removed, and cells were washed twice with 1 ml 3% BSA solution in PBS for 5 minutes each. The cells were labeled with 500 μL Click-IT® Reaction Cocktail for 30 minutes at room temperature, protected from light. The cells were washed once with 1 ml 3% BSA solution in PBS for 5 minutes and immersed in 1 ml PBS for imaging. Imaging was performed on the EVOS™ FL Auto 2 Cell Imaging System using the EVOS™ Light Cube, GFP 2.0 (Ex: 482 nm, Em: 524 nm).

2.13 Assessing changes in mitochondrial membrane potential in T-SLICE with MitoView 633

MitoView™ 633 is a potential-dependent dye that accumulates in the mitochondria and can be used to assess changes in mitochondrial membrane potential in cells. MCF7 and HCC1806 cells were cultured in T-SLICE as described in section 2.5 for 72 hours, with medium renewal every 24 hours to prevent metabolic waste accumulation. Cell culture medium was supplemented with 100 nM MitoView 633 (Biotium, Cat. No. 70055) for the entire duration of T-SLICE culture. T-SLICE cultures were imaged every 24 hours on the EVOS™ FL Auto 2 Cell Imaging System using the EVOS™ Light Cube,

Cy5 2.0 (Ex: 635 nm, Em: 692 nm). Images were acquired while cells were actively being cultured in T-SLICE.

2.14 RNA isolation and quantification

RNA was isolated from NIH/3T3, MCF7, and HCC1806 cells cultured in 6-well plates and in T-SLICE devices with a 500 µm spacer height using the QIAGEN RNeasy Mini Kit (QIAGEN, Cat. No. 74106). Cells were seeded at a density of 200,000 cells/well in a 6-well plate and allowed to adhere to the plate overnight. Cells were cultured for an additional 24 hours and then harvested for RNA isolation. RNA was isolated by adding 350 µl Buffer RLT to each well and scraping the cells off the growth surface. The cells were lysed by pipetting 20 times and transferred to a microcentrifuge tube. 350 µL of 70% ethanol was added to the cell lysate and mixed by pipetting 10 times. The cell lysate was transferred to a RNeasy spin column placed in a 2 ml collection tube and centrifuged at 9000 x g for 15 seconds. The flow-through was discarded and 700 µl of Buffer RW1 was added to the spin column and centrifuged at 9000 x g for 15 seconds. The flow-through was discarded and 500 µl of Buffer RPE was added to the spin column and centrifuged at 9000 x g for 15 seconds. The flow-through was discarded and an additional 500 µl of Buffer RPE was added to the spin column and centrifuged at 9000 x g for 2 minutes. The spin column was transferred to a new 2 ml collection tube and centrifuged at 9000 x g for 1 minute to completely dry the membrane of the spin column. The spin column was then placed in a new 1.5 ml collection tube and 30 µl of nuclease-free water was added to the spin column and centrifuged at 9000 x g for 1 minute to elute the RNA.

T-SLICE culture was established, as detailed in section 2.5, for 6 and 24 hours prior to RNA isolation. To isolate RNA from all cells cultured in T-SLICE, the T-SLICE device was removed from the culture at the desired timepoint, cell culture medium was aspirated, and 1 ml of RNAprotect Cell Reagent (QIAGEN, Cat. No. 76526) was added to the cells. The cells in RNAprotect Cell Reagent were transferred to a 15 ml conical tube and centrifuged at 3000 x g for 6 minutes to pellet the cells. The supernatant was discarded, and the cells were lysed with 350 µl Buffer RLT, and RNA was isolated as described above. To isolate RNA from cells cultured in the middle of T-SLICE (0-5 mm from the centre of the coverslip), the 3D-printed construct shown in Figure 2.14.1 was placed on the coverslip and cells were scraped off the middle-zone of the coverslip using a sterile toothpick. The 3D-printed construct served as a stencil to ensure consistent collection of cells from the same region of T-SLICE across experiments. 1 ml of RNAprotect Cell Reagent was added to the coverslip and the scraped off cells were immediately transferred to a 15 ml conical tube. An additional 1 ml of RNAprotect Cell Reagent was then added to the coverslip to harvest the cells cultured around the periphery of T-SLICE (5-9 mm from the centre of the coverslip) for subsequent RNA isolation. Once the cells from the middle and peripheral zones of T-SLICE were harvested, cell lysis and RNA isolation was performed as described above for RNA isolation from the entire T-SLICE culture.

RNA concentration was measured using the NanoDrop™ 2000 Spectrophotometer (ThermoFisher Scientific, Cat. No. ND-2000) or the µDrop™ Plate (ThermoFisher Scientific, Cat. No. N12391) in the Varioskan™ Lux multimode plate reader (ThermoFisher Scientific, Cat. No. VL0000D0). RNA was stored at -80°C and re-

quantified every freeze-thaw cycle. RNA samples were freeze-thawed a maximum of twice prior to cDNA synthesis.

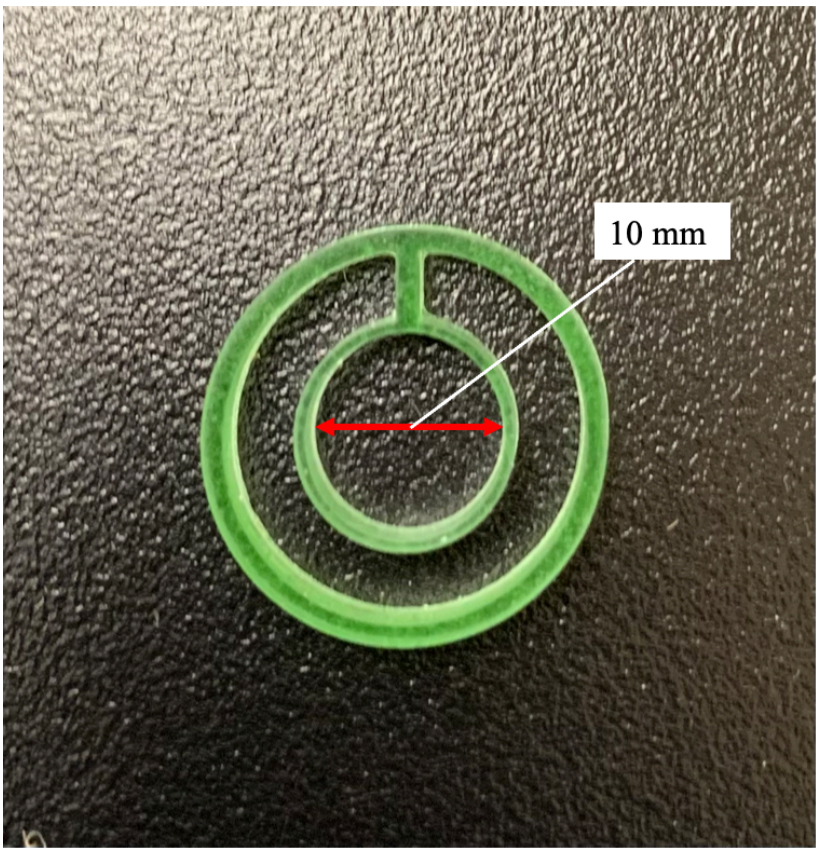

Figure 2.14.1. 3D-printed construct to isolate cells from the middle and edge of T-SLICE for qRT-PCR analysis. A 3D-printed stencil was created to isolate cells from the middle (0 – 4 mm from the centre) and edge (4 – 9 mm from the centre) of T-SLICE for downstream RNA isolation and qRT-PCR analysis.

2.15 cDNA synthesis

Complementary DNA (cDNA) was synthesized from RNA using the iScript Reverse Transcription Supermix for RT-qPCR (Bio-Rad Laboratories Inc., Cat. No. 1708841). Reverse transcription (RT) reactions were prepared in 8-strip 0.2 ml Polymerase Chain Reaction (PCR)
tubes (Axygen™, Cat. No. PCR0208CPC) on ice. Each RT reaction consisted of 4 µl of iScript RT Supermix, 250 ng RNA template (variable volumes), and nuclease-free water (variable volumes to make final reaction volume 20 µl). The reactions were gently mixed by pipetting 5 times and incubated in a thermal cycler (Applied Biosystems 2720) using the following protocol:

1) Priming: 5 minutes at 25°C
2) Reverse transcription: 20 minutes at 46°C
3) RT inactivation: 1 minute at 95°C
4) Hold at 4°C

cDNA was transferred to a 2 ml microcentrifuge tube and diluted 1/25 with nuclease-free water. Diluted cDNA was stored at -20°C.

2.16 qRT-PCR to assess HIF-regulated gene expression in cells cultured in T-SLICE

Quantitative Reverse Transcription Polymerase Chain Reaction (qRT-PCR) was performed to assess differences in HIF-regulated gene expression in MCF7 and HCC1806 cells cultured in T-SLICE compared to standard 2D tissue culture and between different zones of T-SLICE. qRT-PCR reactions were prepared on ice in 384-well PCR plates (Bio-Rad Laboratories Inc., Cat. No. HSP3805). Each qRT-PCR reaction consisted of 5 µl SsoAdvanced™ Universal SYBR® Green Supermix (Bio-Rad Laboratories Inc.,

Cat. No. 1725274), 1 µl of forward/reverse primers at a final concentration of 400 nM, and 4 µl of cDNA generated as described in section 2.15, yielding a final reaction volume of 10 µl per well. Primers were designed using the NCBI Primer-BLAST tool and *in silico* analysis was performed to predict species specificity. Primers were validated to be human-specific prior to use in qRT-PCR experiments. Primer sequences are listed in Appendix A. The PCR plates were sealed with a Microseal 'B' PCR Plate Sealing Film (Bio-Rad Laboratories Inc., Cat. No. MSB1001) and gently tapped on the laboratory benchtop to mix the reaction components. PCR plates were spun at 200 x g to remove any air bubbles and collect the reaction mixture at the bottom of the wells. qRT-PCR reactions were performed in the CFX384 Touch Real-Time PCR Detection System (Bio-Rad Laboratories Inc.) using the following reaction protocol:

1) Polymerase Activation and DNA Denaturation: 30 seconds at 95°C
2) Denaturation: 10 seconds at 95°C
3) Annealing/Extension and Plate Read: 30 seconds at 60°C
4) Perform 40 cycles of steps 2 and 3
5) Melt Curve Analysis: 65°C - 95°C in 0.5°C increments at 5 seconds per step

Relative expression of target genes was normalized to reference gene beta-actin at matched timepoints from standard 2D tissue culture. Relative expression of target genes was calculated using the Comparative Ct (ΔΔCt) method.

2.17 Statistical analysis

Statistical analysis of qRT-PCR data was performed in GraphPad Prism 9 (GraphPad Software). One-way analysis of variance (ANOVA) with Dunnett's multiple

comparisons test was performed to assess multi-group comparisons. *p*-values are represented as follows: *$p < 0.05$; **$p < 0.01$; ***$p < 0.001$; ****$p < 0.0001$.

Chapter 3: Results

Synopsis

The first objective of this research project was to design and fabricate the T-SLICE device, which involved the selection and optimization of materials, size, and geometries. My second objective was to test if T-SLICE was able to generate cell-consumption defined hypoxia gradients. Finally, my third objective investigated cancer cell behaviours such as proliferation rate, viability, and gene expression profiles to assess how they are impacted by the biochemical gradients generated in T-SLICE. Throughout this project, two human breast cancer cell lines were used: MCF7 and HCC1806. MCF7 breast cancer cells are positive for estrogen receptor (ER) and progesterone receptor (PR), but negative for the HER-2 receptor. HCC1806 breast cancer cells are ER, PR, and HER-2 negative (TNBC). These cell lines were chosen for analysis in T-SLICE due to their differing immunophenotypes and ability to form 3-dimensional spheroids. Two breast cancer cell lines were used to investigate differences in response to environmental pressures within the same type of cancer (i.e., breast cancer). Murine NIH/3T3 embryonic fibroblast cell line was used to drive the biochemical gradients in T-SLICE, which breast cancer cell spheroids were subject to.

3.1 T-SLICE with circular geometry, 18 mm diameter, and made via polydimethylsiloxane soft lithography yields consistent device dimensions

The first objective of this study was to design and construct the Tumour Spheroids Layered in an Imageable Cancer Environment (T-SLICE) device. T-SLICE is based on culturing cells between two parallel, closely spaced glass coverslips to generate cell-consumption defined biochemical gradients (e.g., hypoxia, nutrient depletion). Design criteria for T-SLICE were determined based on unmet needs in the field of *in vitro* cancer disease modeling and are listed in Appendix B (Table B), along with how these criteria were met. Square and circular geometries ranging in width or diameter from 18 mm – 25 mm were tested for device fabrication. Circular glass coverslips with an 18 mm diameter were determined to be the optimal shape and size for T-SLICE design (Figure 3.1.1). PDMS was chosen as the housing substrate used to separate the two circular 18 mm diameter glass coverslips 300 μm – 700 μm apart (Figure 3.1.1). T-SLICE was constructed using 3D-printed molds used for PDMS soft lithography, with subsequent covalent attachment of a circular 18 mm diameter glass coverslip to its underside. One-piece and two-piece 3D-printed molds were tested for T-SLICE fabrication. A two-piece 3D-printed mold was superior to a one-piece 3D-printed mold and facilitated easy and consistent removal of the PDMS (Figure 3.1.1).

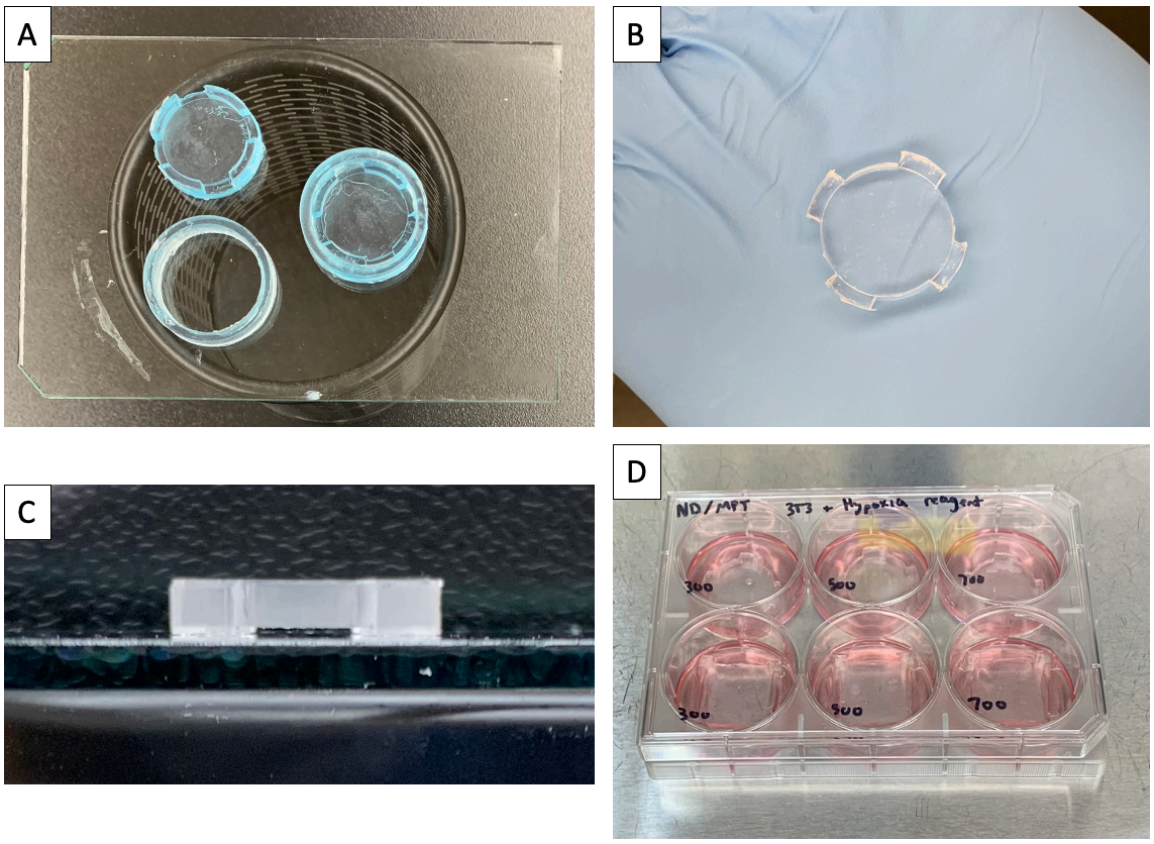

Figure 3.1.1. T-SLICE with an 18 mm diameter cell growth surface area and 300 µm – 700 µm spacer height achieved using PDMS yielded consistent device fabrication in terms of manufacturing quality. Two-piece 3D-printed molds for PDMS soft lithography were optimal for device removal following PDMS curing (A). Top view (B) and side view (C) of T-SLICE following removal from the 3D-printed mold. T-SLICE devices can be used in 6-well cell culture plates (D).

3.2 200,000 NIH/3T3 fibroblasts per coverslip is the optimal seeding density in T-SLICE

Fibroblasts are an abundant cell type found in the tumour microenvironment and serve important roles in tumour progression (Wu & Dai, 2017). Murine NIH/3T3 embryonic fibroblasts were selected as the cell type used to generate the cell-consumption defined biochemical gradients in T-SLICE. I tested NIH/3T3 seeding numbers ranging from 120,000 – 220,000 cells per coverslip at densities ranging from 240,000 cells/mL – 440,000 cells/mL (Figure 3.2.1 A). I initially selected 200,000 cells per coverslip as the optimal seeding density because it created an approximate 80% confluent monolayer on the 18 mm diameter circular glass coverslip after overnight seeding, lending room for proliferation over the course of an experiment (Figure 3.2.1 A). When breast cancer cell spheroids were seeded on top of the ~80% confluent fibroblast monolayer, they adhered to the fibronectin-coated coverslip in the gaps between fibroblasts and lost all their 3D-geometry (Figure 3.2.1 B). To combat this, I selected a seeding density 200,000 NIH/3T3 cells per coverslip since it creates a confluent monolayer on the coverslip after overnight seeding (Figure 3.2.1 A). Breast cancer cell spheroids maintained their 3D-geometry much better when seeded on top of a confluent fibroblast monolayer (Figure 3.2.1 C). 200,000 NIH/3T3 fibroblasts per 18 mm diameter circular glass coverslip was chosen as the optimal fibroblast seeding density in T-SLICE.

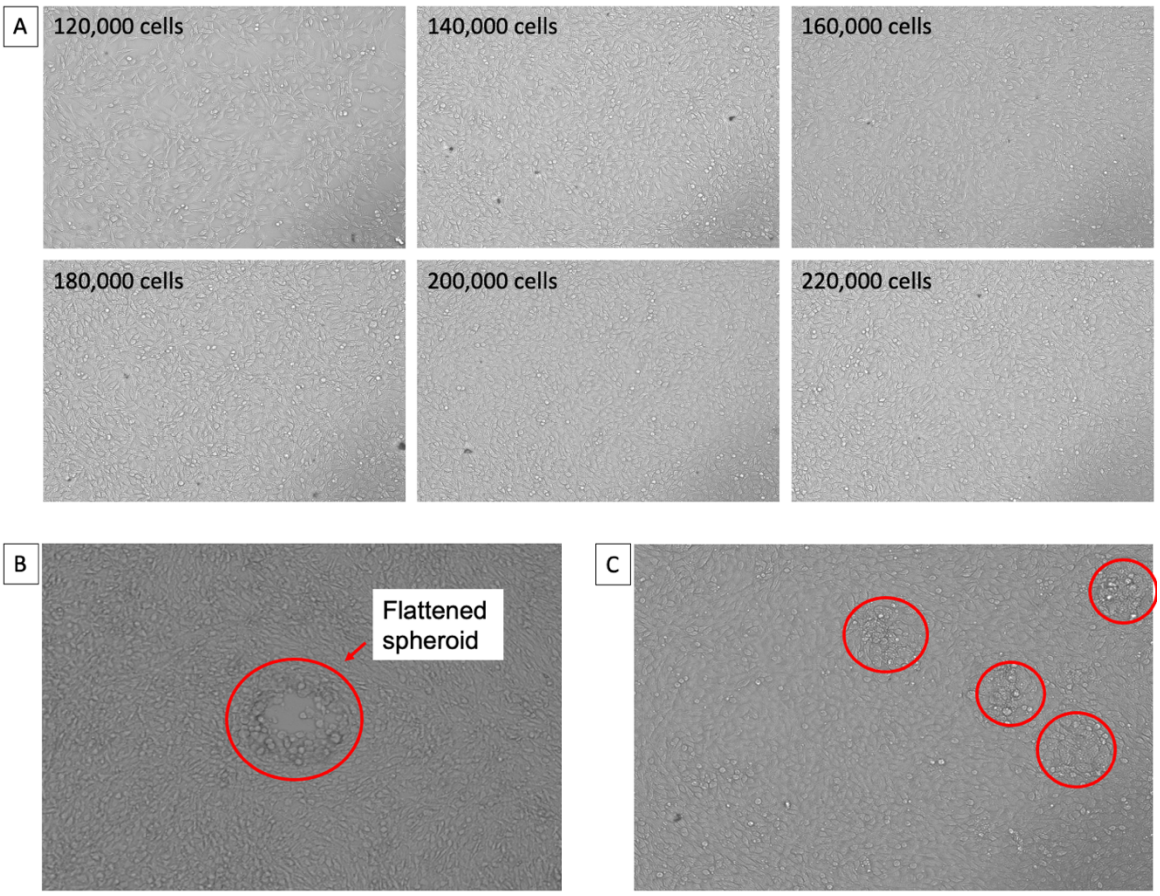

Figure 3.2.1. Optimizing NIH/3T3 fibroblast seeding density in T-SLICE. NIH/3T3 fibroblasts were seeded on an 18 mm diameter circular glass coverslip at densities of ranging from 120,000 – 220,000 cells per coverslip (A). Seeding MCF7 spheroids on top of fibroblasts seeded at a density of 120,000 cells per coverslip led to complete loss of 3D geometry of the spheroids (B). Seeding MCF7 spheroids on top of fibroblasts seeded at a density of 200,000 cells per coverslip helped maintain 3D geometry of the spheroids (C).

3.3 50 MCF7 cells and 100 HCC1806 cells per droplet in a 384-well hanging drop plate yield spheroids with diameter <150 µm in 24 – 48 hours

Breast cancers with different immunophenotypes have been shown to exhibit differences in tumour biology and metastatic potential. MCF7 (ER+/PR+/HER2-) and HCC1806 (TNBC) human breast cancer cell lines were used to assess how biochemical gradients generated in T-SLICE impact cancer cell behaviour. These cell lines were chosen due to their different immunophenotypes and established use in 3D cell culture applications. Oxygen has a diffusion limit of approximately 150 µm in tissues and there should therefore be no more than 300 µm between blood vessels in the tissue (i.e., the oxygen source) (Grimes et al., 2016). This distance is even smaller for metabolically active tissues, such as a tumour. Spheroid seeding densities were optimized to generate spheroids with a diameter less than 150 µm to prevent the generation of intra-spheroid hypoxia gradients. MCF7 breast cancer cells were seeded at densities of 50, 400, and 3200 cells per 25 µL droplet in 384-well hanging drop plates. Seeding 50 MCF7 cells per 25 µL droplet consistently generated spheroids with a diameter ranging from 100 µm – 130 µm in 24 hours (Figure 3.3.1 A). Given this information, HCC1806 breast cancer cells were seeded at densities of 50 and 100 cells per 25 µL droplet in 384-well hanging drop plates. Seeding 100 HCC1806 cells per 25 µL droplet consistently generated spheroids with a diameter ranging from 100 µm – 130 µm in 48 hours (Figure 3.3.1 B). 50 MCF7 cells and 100 HCC1806 cells per 25 µL droplet were chosen as the optimal seeding densities to consistently generate spheroids with a diameter less than 150 µm for subsequent use in T-SLICE. Spheroid seeding medium had to be supplemented with 2.4 mg/mL MethoCel A4M® for efficient spheroid formation. Finally, I determined that

seeding one 384-well hanging drop plate of spheroids (192 spheroids due to ‘zig-zag’ seeding pattern) per coverslip was sufficient to have numerous spheroids cultured in all areas of T-SLICE.

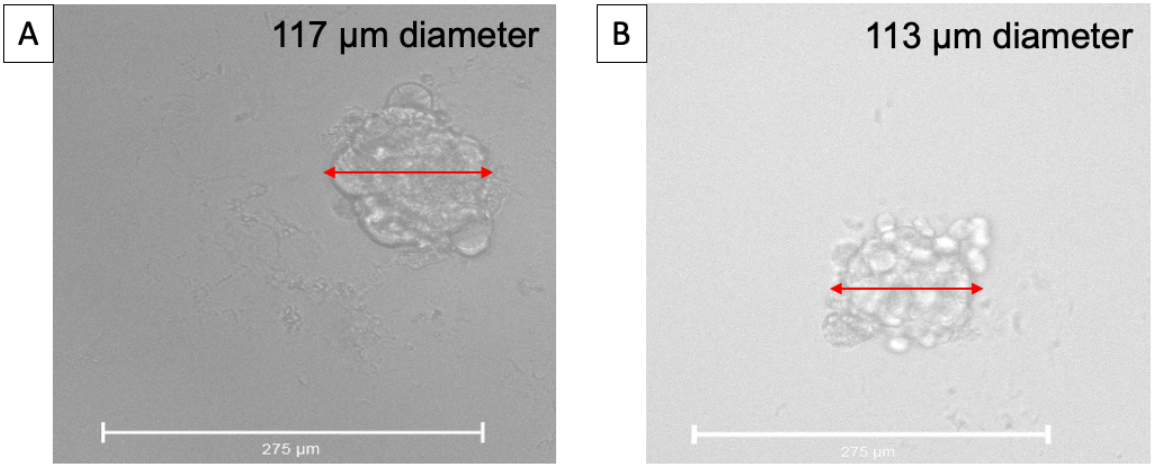

Figure 3.3.1. Optimizing MCF7 and HCC1806 cell seeding densities for small diameter (<150 µm) spheroid formation. MCF7 and HCC1806 cells were seeded in 384-well hanging drop plates at densities ranging from 50 cells to 3200 cells per 25 µL droplet containing 2.4 mg/mL MethoCel® A4M. Seeding 50 MCF7 cells per 25 µL droplet produced spheroids with diameters ranging from 100 µm – 130 µm in 24 hours (A). Seeding 100 HCC1806 cells per 25 µL droplet produced spheroids with diameters ranging from 100 µm – 130 µm in 48 hours (B).

3.4 Image-iT Green Hypoxia Reagent and ROS-ID Hypoxia Detection Reagent are not suitable for characterizing hypoxia gradients in T-SLICE

Hypoxia is a biochemical gradient that develops in the microenvironment of solid tumours due to aberrant pro-angiogenic signaling and extracellular matrix remodeling (Madu et al., 2020). It is important to consider hypoxia in the context of tumour progression because hypoxia-inducible factor-regulated genes are involved in tumour growth, invasion, metastasis, and therapeutic resistance (Madu et al., 2020). This is particularly true of breast cancer, where studies have linked hypoxia with neovascularization, decreased susceptibility to hormonal treatment, and increases in the number of breast cancer stem cells (Madu et al., 2020). I prioritized a robust characterization of hypoxic responses of the breast cancer cells cultured in T-SLICE due to the profound implication of hypoxia in the tumour microenvironment.

I first used the Image-iT Green Hypoxia Reagent from Invitrogen™ to attempt characterizing hypoxic responses in T-SLICE. This reagent is a live cell permeable compound that becomes fluorescent in cells when oxygen tension drops below 5% O_2. I treated NIH/3T3 cells with 1.0 µM, 2.5 µM, 5.0 µM, 7.5 µM, and 10.0 µM of the Image-iT Green Hypoxia Reagent for 30 minutes at 37ºC, 5% CO_2. The medium was then refreshed, and cells were cultured for 4 hours at 1% O_2 before being imaged to assess hypoxic responses. No fluorescence was detected in cells treated with any of the concentrations of the Image-iT Green Hypoxia Reagent (Figure 3.4.1). This reagent was not used to assess the hypoxic response of breast cancer cells cultured in T-SLICE.

The ROS-ID Hypoxia Detection Reagent® from Enzo Life Sciences was the next reagent that I used to attempt characterizing hypoxic responses in T-SLICE. This reagent

takes advantage of the upregulated nitroreductase activity present in hypoxic cells to cleave the compound and release a fluorescent probe. I cultured NIH/3T3 cells at either 21% O_2 or 1% O_2 for 24 hours and subsequently treated them with 0.5 μM ROS-ID Hypoxia Detection Reagent for 30 minutes before being imaged to assess hypoxic responses. Greater fluorescent signal was detected in cells cultured at 21% O_2 than in cells cultured at 1% O_2 (Figure 3.4.2). This reagent was not used to assess the hypoxic response of breast cancer cells cultured in T-SLICE.

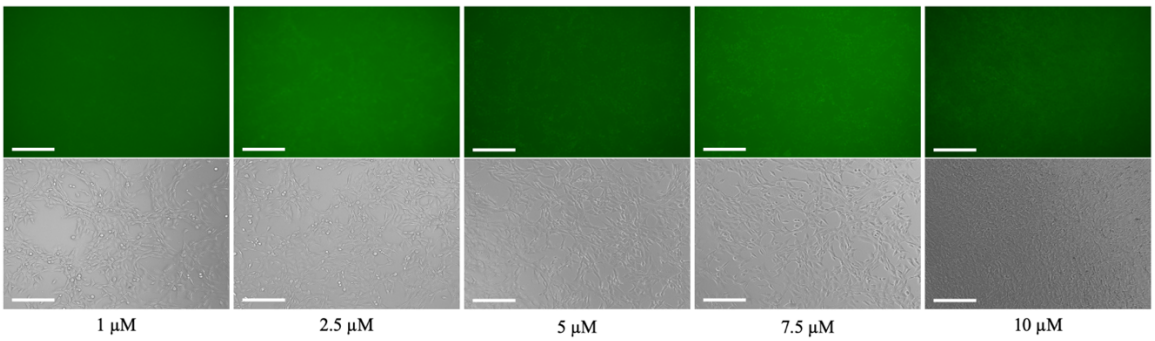

Figure 3.4.1. Determining the efficacy of Image-iT Green Hypoxia Reagent to characterize hypoxia in T-SLICE. NIH/3T3 cells were treated with a range of concentrations of Image-iT Green Hypoxia Reagent and cultured at 1% O_2 for 4 hours. Fluorescence microscopy was performed on the EVOS FL Auto 2 Cell Imaging System, Light Cube GFP 2.0 (Ex: 482 nm, Em: 524 nm). Fluorescence intensity was not strong enough to be easily detected at any of the concentrations tested and is clouded by high background fluorescence. Scale bar = 275 µm.

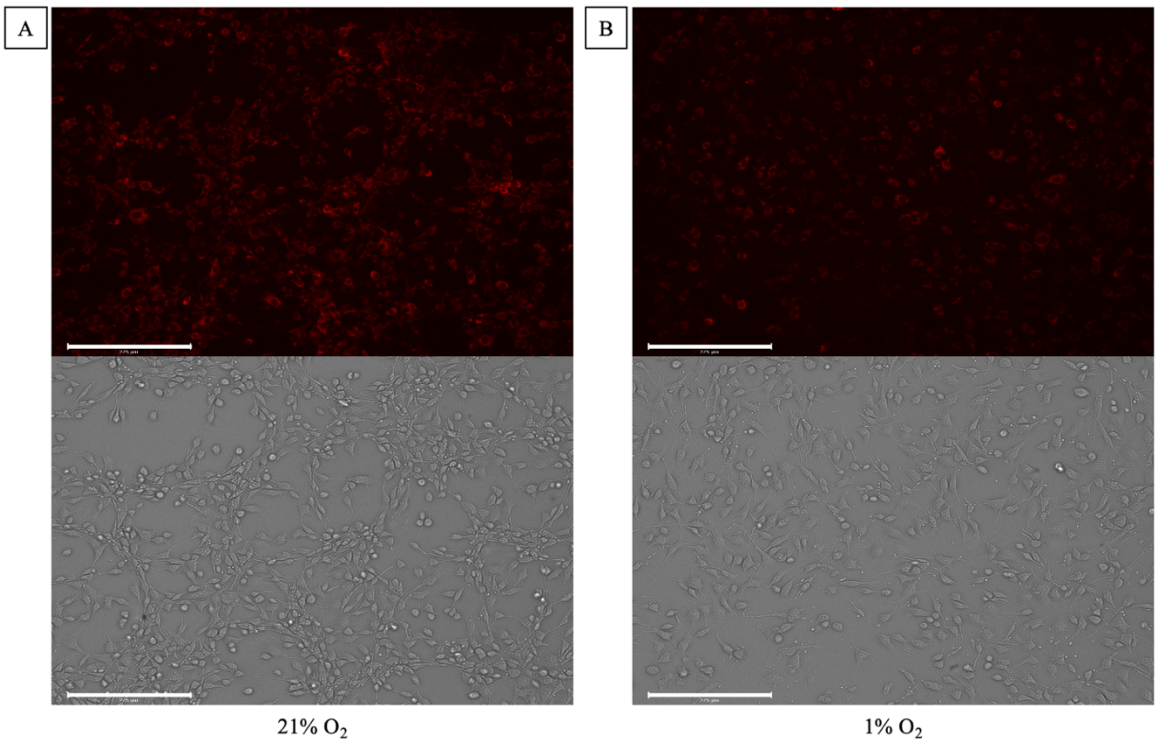

Figure 3.4.2. Determining the efficacy of Enzo Life Sciences Hypoxia/Oxidative Stress Detection Kit to characterize hypoxia in T-SLICE. NIH/3T3 cells were cultured for 24 hours at 21% O_2 (A) or 1% O_2 (B) and subsequently incubated with 0.5 µM ROS-ID Hypoxia Detection Reagent for 30 minutes. Fluorescence microscopy was performed on the EVOS FL Auto 2 Cell Imaging System, Light Cube Texas Red 2.0 (Ex: 585 nm, Em: 628 nm). Fluorescent signal was stronger in cells cultured at 21% O_2 than 1% O_2. Scale bar = 275 µm.

3.5 5HRE/GFP-transfected MCF7 breast cancer cells reveal early hypoxic response in T-SLICE

After deeming Image-iT Green Hypoxia Reagent and ROS-ID Hypoxia Detection Reagent unsuitable for characterizing hypoxic responses of breast cancer cells in T-SLICE, I created a hypoxia reporter MCF7 cell line using the 5HRE/GFP plasmid. 5HRE/GFP contains 5x hypoxia responsive elements from the human VEGF promoter and an enhanced green fluorescent protein (GFP) (Vordermark et al., 2001). Cells transfected with 5HRE/GFP will emit GFP signal when undergoing a hypoxic response mediated by hypoxia-inducible factors (Vordermark et al., 2001).

I cultured 5HRE/GFP-MCF7 spheroids (diameter <150 μm) in T-SLICE with a spacer height of 300 μm, 500 μm, and 700 μm for 24 hours and performed live-imaging for GFP expression (i.e., HIF-mediated hypoxic response). Hypoxic responses were observed in MCF7 cells cultured in T-SLICE with a 300 μm, 500 μm, and 700 μm spacer height as early as 3 hours into culture (Figure 3.5.1). Hypoxic responses were greater in MCF7 cells cultured in the middle zone of T-SLICE (0-3 mm from the centre) compared to the peripheral zone (6-9mm from the centre) in all spacer heights after 3 hours of culture (Figure 3.5.1). Hypoxic responses remained more intense in MCF7 cells cultured in the middle zone of T-SLICE after 6 hours and 12 hours of culture in all spacer heights (Figure 3.5.1). This trend was reversed after 24 hours of T-SLICE culture with 500 μm and 700 μm spacer heights and more fluorescence intensity was observed in MCF7 cells cultured in the peripheral zone of T-SLICE compared to the middle zone (Figure 3.5.1 B, C, D). Overall, fluorescence intensity decreased in MCF7 cells cultured in T-SLICE over 24 hours (Figure 3.5.1).

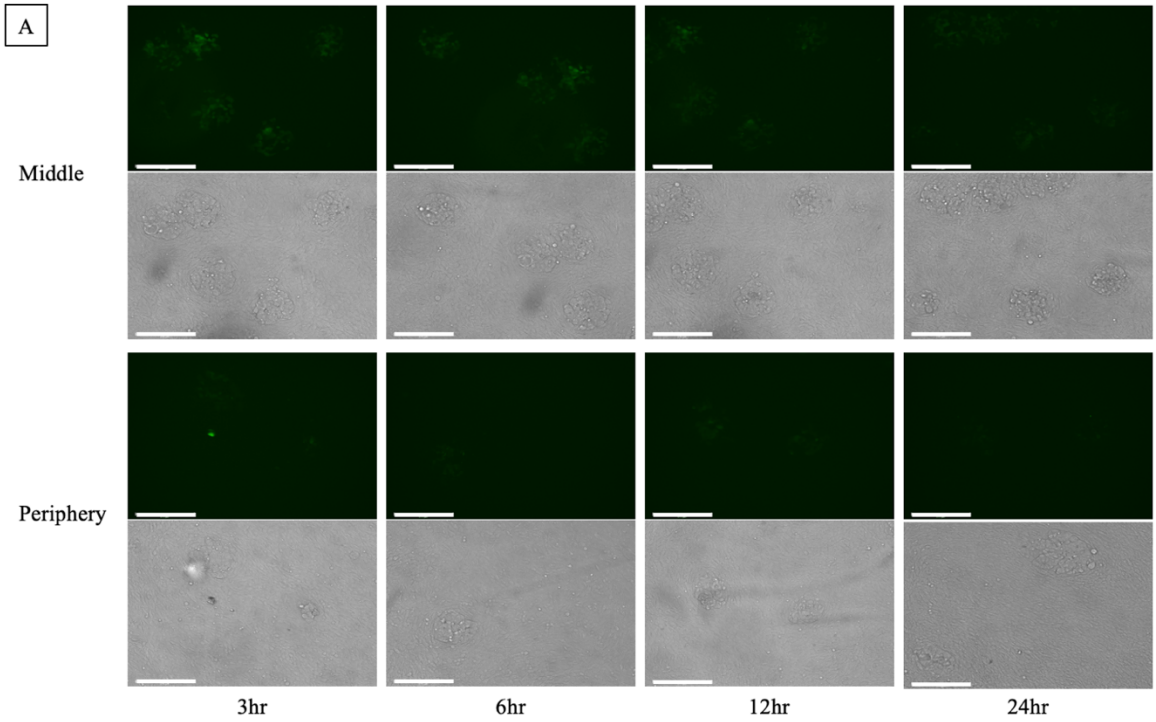
A
Middle
Periphery
3hr
6hr
12hr
24hr

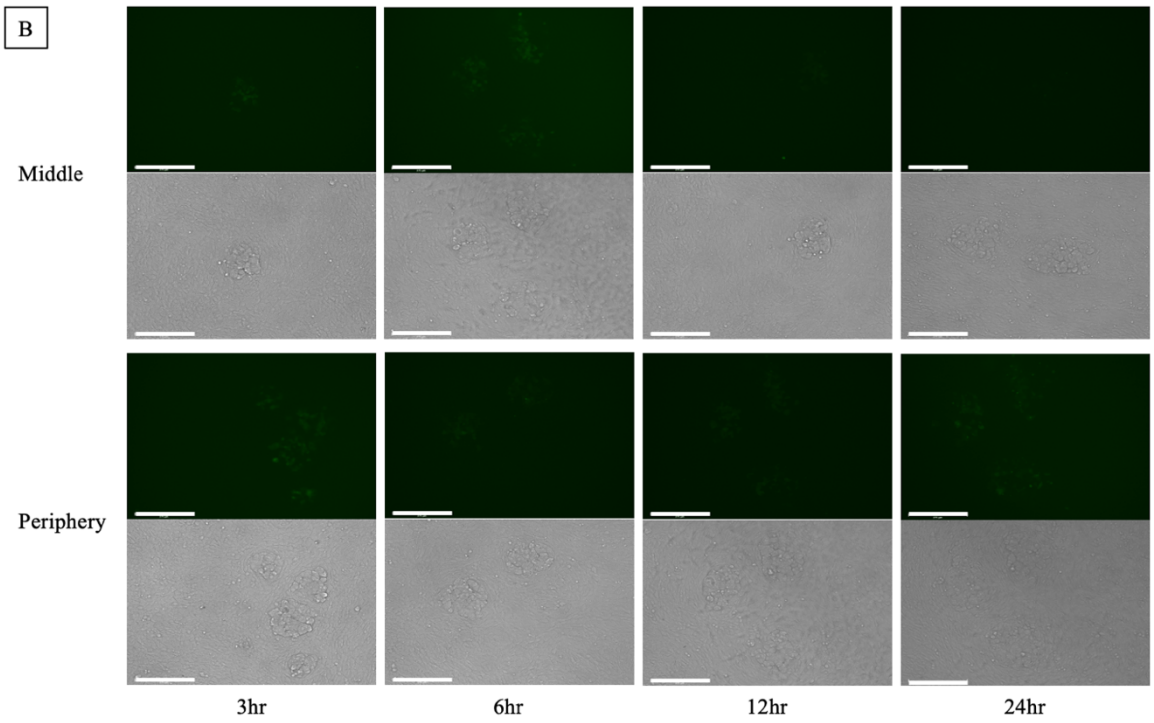
B
Middle
Periphery
3hr
6hr
12hr
24hr

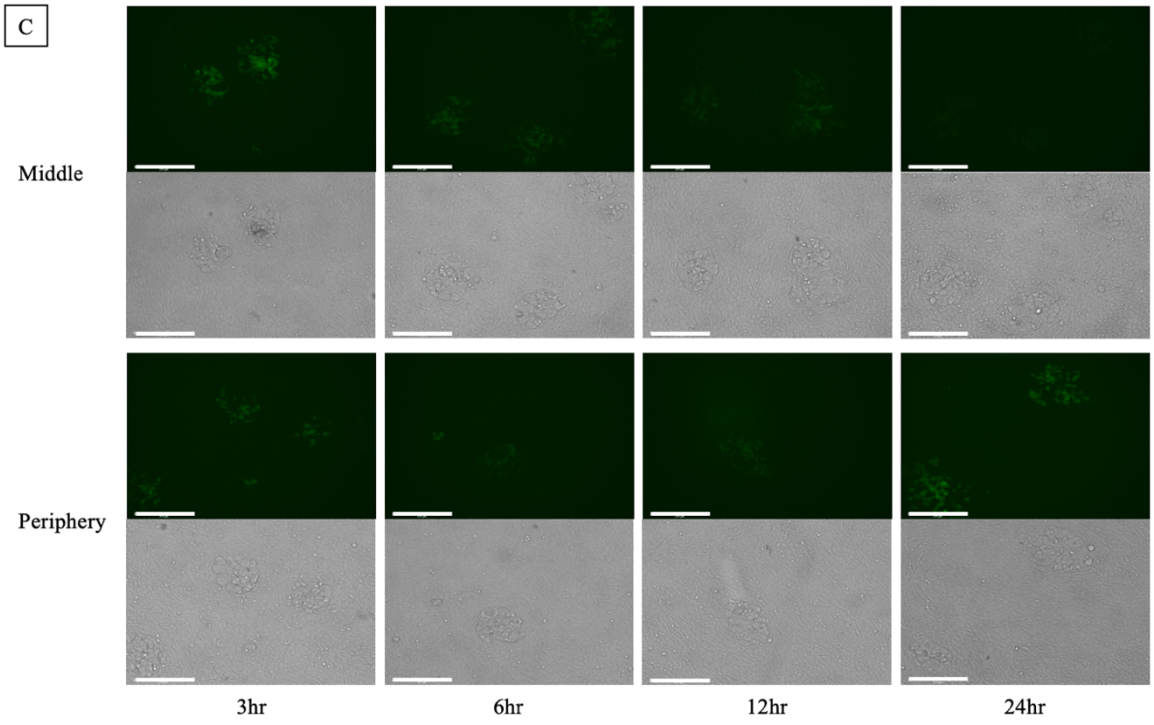

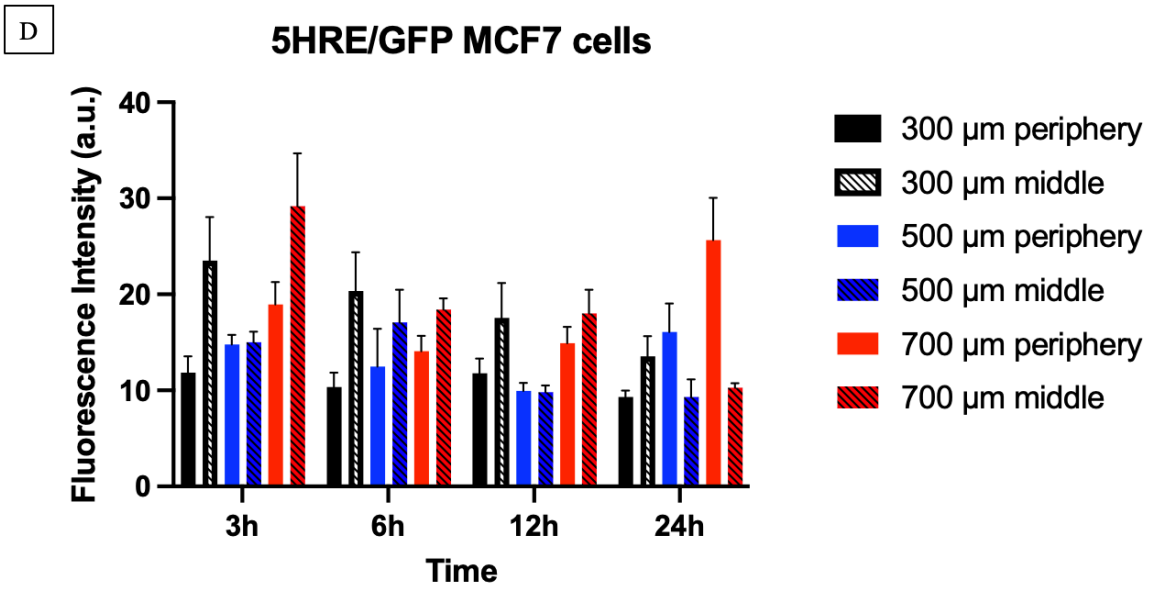

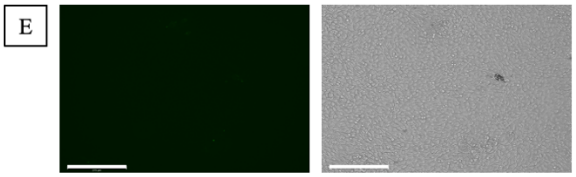

No T-SLICE control (24hr)

Figure 3.5.1. Characterizing early hypoxic cellular responses in T-SLICE using 5HRE/GFP-transfected MCF7 cells. 5HRE/GFP-transfected MCF7 cell spheroids were cultured in T-SLICE with a 300 µm, 500 µm, and 700 µm spacer height for up to 24 hours. Cells were live-imaged during T-SLICE culture at 3h, 6h, 12h, and 24h timepoints on the EVOS FL Auto 2 Cell Imaging System, Light Cube GFP 2.0 (Ex: 482 nm, Em: 524 nm). Greater fluorescence intensity was observed in cells cultured in the middle zone of T-SLICE with a 300 µm spacer height compared to cells cultured in the peripheral zone of T-SLICE (A, D). Fluorescence intensity was stronger in cells cultured in the periphery of T-SLICE with 500 µm and 700 µm spacer heights by t = 24h (B, C, D). No eGFP was detected in MCF7 cell spheroids co-cultured with fibroblasts after 24 hours (E). Data presented are representative images from three independent experiments. "Middle" = 0 – 3 mm from centre, "Periphery" = 6 – 9 mm from centre. Scale bar = 275 µm.

3.6 *EF5 staining indicates hypoxic responses are sustained in MCF7 and HCC1806 cells cultured in T-SLICE over 48 hours*

After identifying hypoxic responses are elicited in MCF7 cells after just 3 hours of culture using the hypoxia reporter cell line, I needed to confirm that hypoxic responses were maintained in T-SLICE beyond 24 hours. I used EF5 to characterize the sustained hypoxic responses that breast cancer cells display when cultured in T-SLICE for up to 48 hours. EF5 is a pentafluorinated compound that binds hypoxic cells and forms macromolecular adducts at the cell membrane when it is reduced (Koch, 2002). The EF5 adducts can then be stained with a fluorophore-conjugated antibody to selectively label cells undergoing a hypoxic response.

MCF7 and HCC1806 breast cancer cell spheroids were cultured in T-SLICE for up to 48 hours with medium supplemented with 10 μM EF5. T-SLICE cultures were fixed after 6, 12, 24, and 48 hours and EF5 adducts were labeled to characterize hypoxic responses of the MCF7 and HCC1806 cells. T-SLICE was divided into three zones for EF5 staining analysis: middle (0-3 mm from the centre), intermediate (3-6 mm from the centre), and periphery (6-9 mm from the centre).

MCF7 cells cultured in T-SLICE with a 300 μm spacer height had increasing EF5 detection in all three zones over the course of 48 hours (Figure 3.6.1). EF5 staining was greater in the intermediate and middle zones of T-SLICE compared to the periphery at matched timepoints (Figure 3.6.1). Slightly more EF5 signal was detected in the intermediate zone than the middle zone at the 12-, 24-, and 48-hour timepoints (Figure 3.6.1).

MCF7 cells cultured in T-SLICE with a 500 μm spacer height had increasing EF5 detection in all three zones over 48 hours (Figure 3.6.2). EF5 intensity was similar across all zones at matched timepoints (Figure 3.6.2).

MCF7 cells cultured in T-SLICE with a 700 μm spacer height had increasing EF5 detection in the intermediate and middle zone over 48 hours (Figure 3.6.3). EF5 intensity was similar in the intermediate and middle zone at matched timepoints and were both greater than EF5 intensity in the peripheral zone at matched timepoints (Figure 3.6.3).

HCC1806 cells cultured in T-SLICE with a 300 μm spacer height had plateaued EF5 expression after 12 hours in the intermediate and middle zones but was not detected in the periphery until 48 hours into T-SLICE culture (Figure 3.6.4). EF5 signal intensity was similar between the intermediate and middle zones (Figure 3.6.4).

HCC1806 cells cultured in T-SLICE with a 500 μm spacer height had a similar plateaued EF5 expression after 12 hours that was high and similar in the intermediate and middle zones after 12, 24, and 48 hours (Figure 3.6.5). EF5 signal intensity was not detected in the periphery until 48 hours into T-SLICE culture (Figure 3.6.5).

HCC1806 cells cultured in T-SLICE with a 700 μm spacer height also had EF5 detection plateau after 12 hours of culture in the intermediate and middle zones but was not detected in the periphery (Figure 3.6.6). EF5 signal intensity was similar in the intermediate and middle zones at matched timepoints (Figure 3.6.6).

Overall, hypoxic responses in MCF7 and HCC1806 cells are sustained and become more intense in T-SLICE over the course of 48 hours, as indicated by EF5 detection. Similar levels of EF5 detection were observed between MCF7 and HCC1806 cells cultured in the intermediate and middle zones of T-SLICE. No EF5 detection was

observed in MCF7 and HCC1806 spheroids co-cultured with NIH/3T3 fibroblasts without the T-SLICE device (Figure 3.6.7).

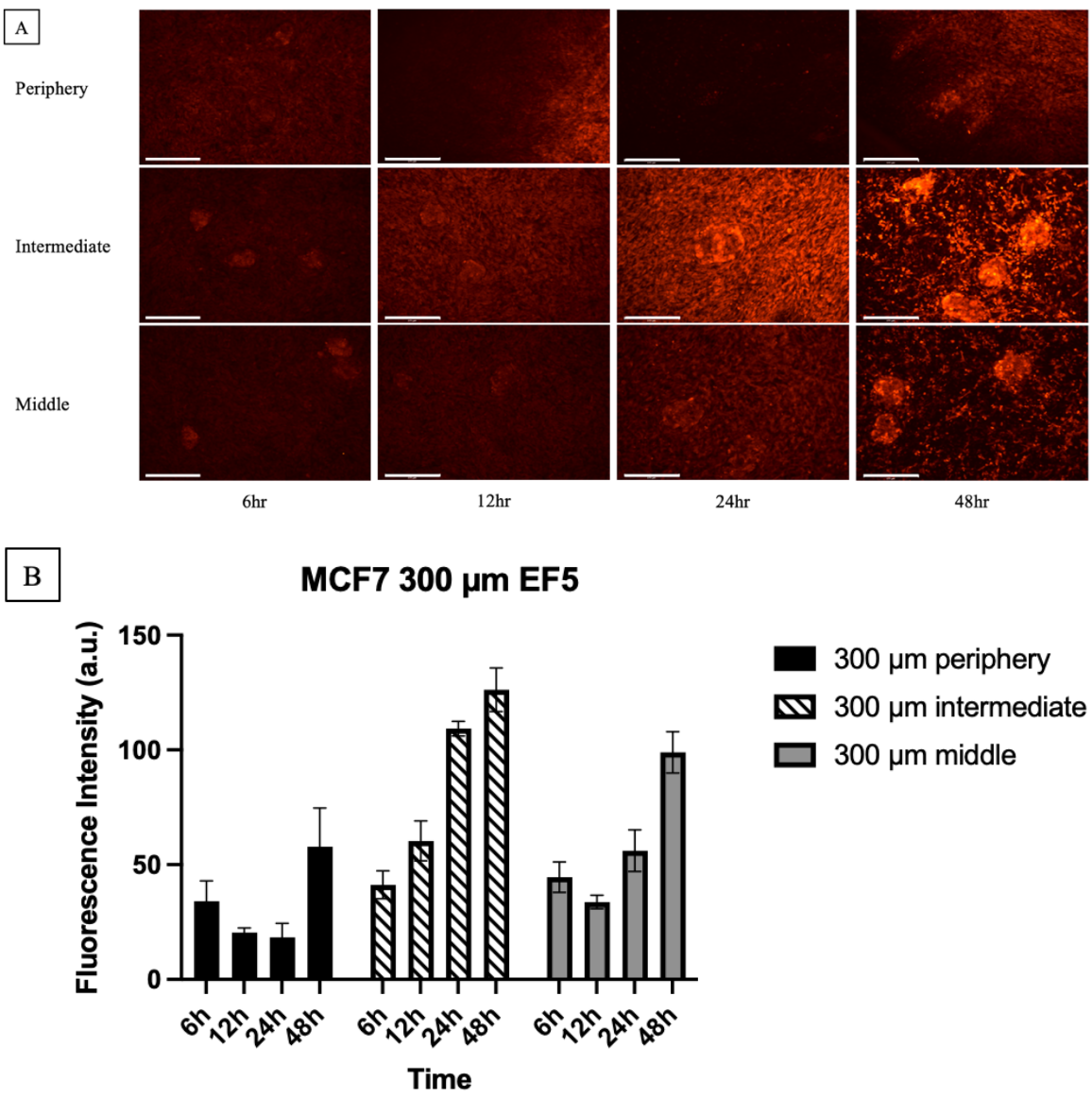

Figure 3.6.1. Characterizing MCF7 cell hypoxic response in T-SLICE with a 300 µm spacer height using EF5. MCF7 cell spheroids were cultured in T-SLICE with a 300 µm spacer height for up to 48 hours in the presence of 10 µM EF5. Cells were fixed, permeabilized, and stained with a Cy3-conjugated anti-EF5 antibody at 6h, 12h, 24h, and 48h timepoints. Images were captured on the EVOS FL Auto 2 Cell Imaging System, Light Cube RFP 2.0 (Ex: 531 nm, Em: 593 nm). Imaging data presented are representative images from three independent experiments (A). Fluorescence intensity gradually increased in all three zones over 48 hours (B). "Middle" = 0 – 3 mm from centre, "Intermediate" = 3 – 6 mm from centre, "Periphery" = 6 – 9 mm from centre. Scale bar = 275 µm.

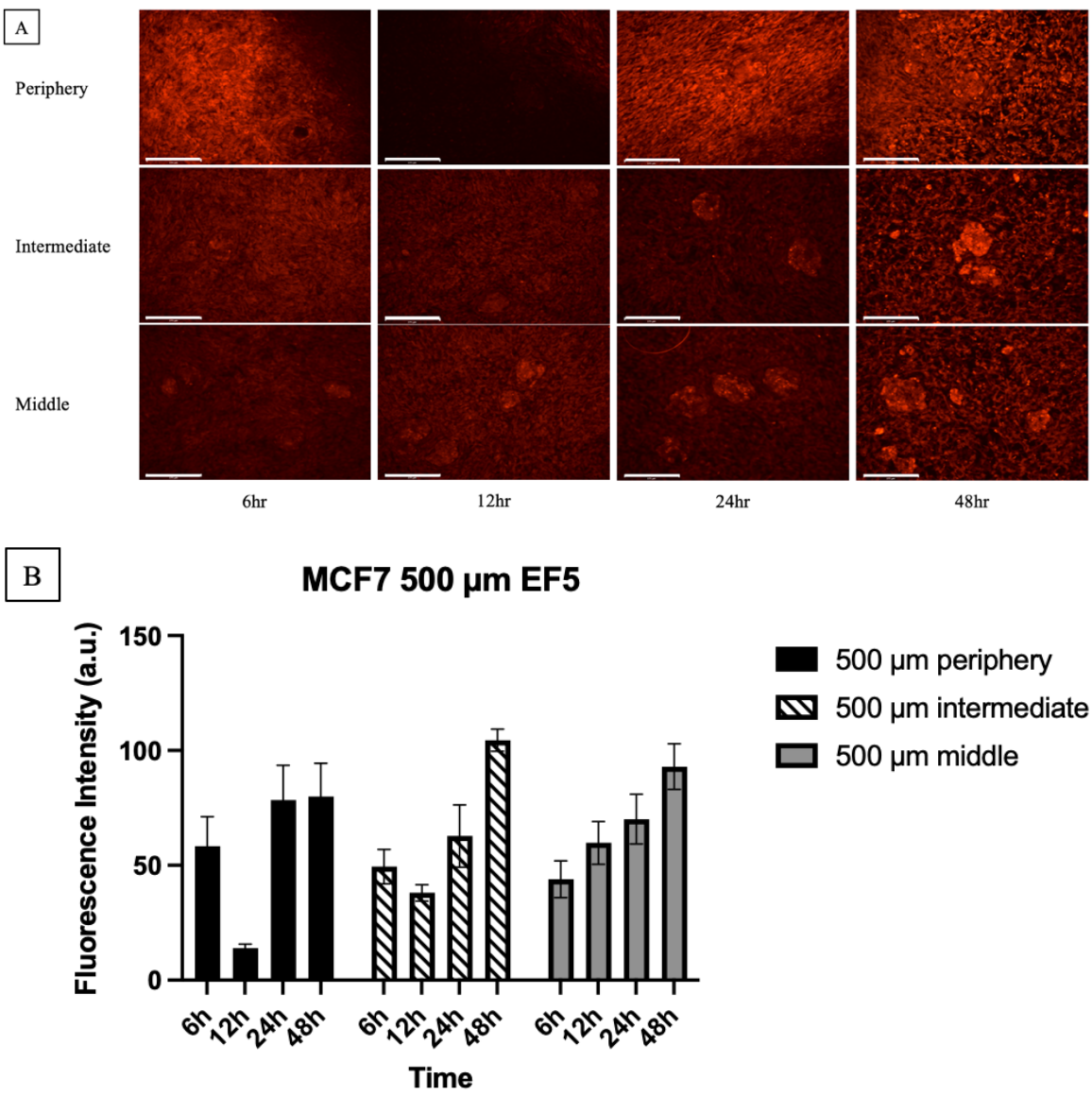

Figure 3.6.2. Characterizing MCF7 cell hypoxic response in T-SLICE with a 500 µm spacer height using EF5. MCF7 cell spheroids were cultured in T-SLICE with a 500 µm spacer height for up to 48 hours in the presence of 10 µM EF5. Cells were fixed, permeabilized, and stained with a Cy3-conjugated anti-EF5 antibody at 6h, 12h, 24h, and 48h timepoints. Images were captured on the EVOS FL Auto 2 Cell Imaging System, Light Cube RFP 2.0 (Ex: 531 nm, Em: 593 nm). Imaging data presented are representative images from three independent experiments (A). Fluorescence intensity gradually increased in all three zones over 48 hours (B). "Middle" = 0 – 3 mm from centre, "Intermediate" = 3 – 6 mm from centre, "Periphery" = 6 – 9 mm from centre. Scale bar = 275 µm.

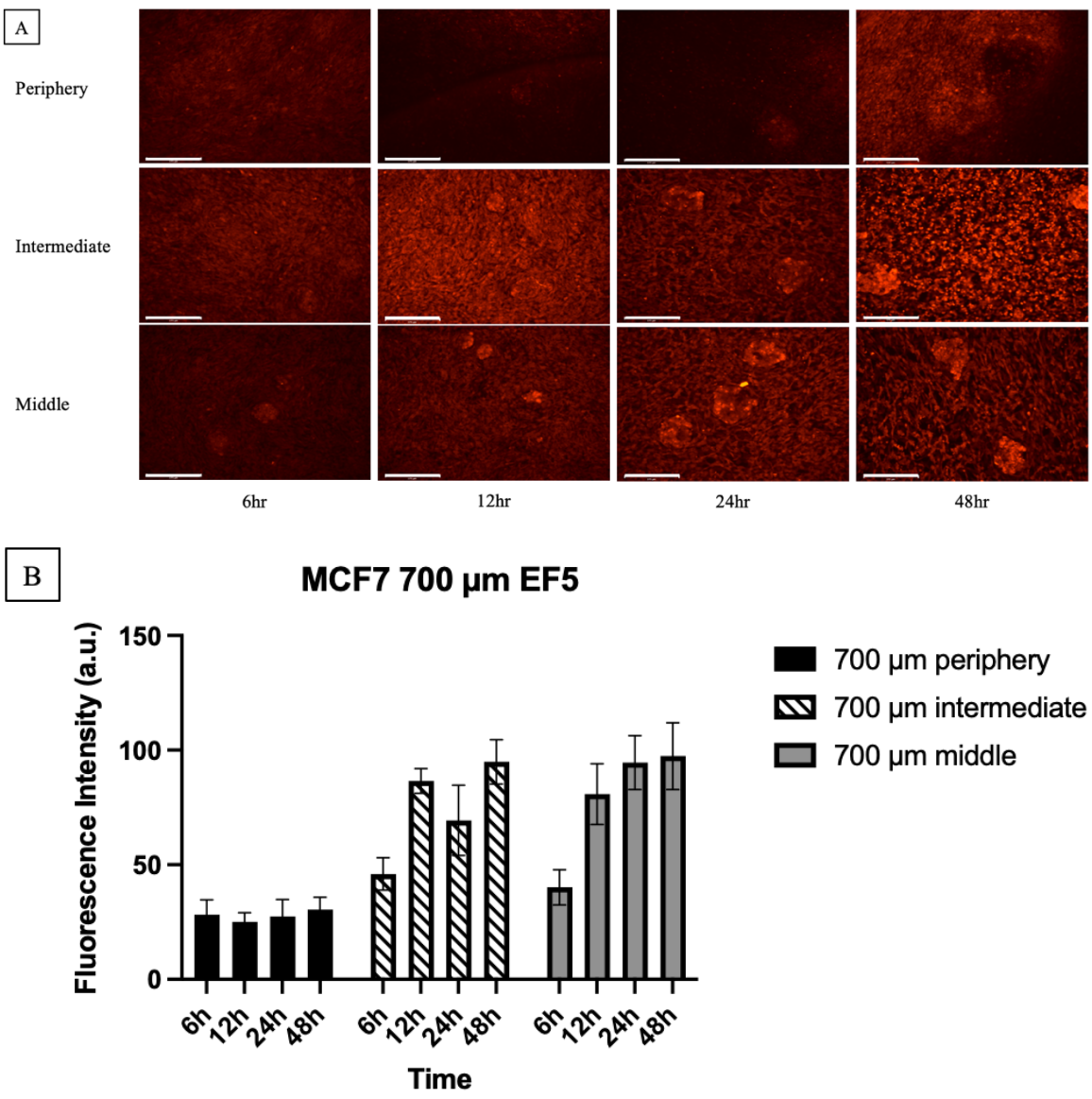

Figure 3.6.3. Characterizing MCF7 cell hypoxic response in T-SLICE with a 700 µm spacer height using EF5. MCF7 cell spheroids were cultured in T-SLICE with a 700 µm spacer height for up to 48 hours in the presence of 10 µM EF5. Cells were fixed, permeabilized, and stained with a Cy3-conjugated anti-EF5 antibody at 6h, 12h, 24h, and 48h timepoints. Images were captured on the EVOS FL Auto 2 Cell Imaging System, Light Cube RFP 2.0 (Ex: 531 nm, Em: 593 nm). Imaging data presented are representative images from three independent experiments (A). Fluorescence intensity gradually increased in all three zones over 48 hours, with little detection in the periphery (B). "Middle" = 0 – 3 mm from centre, "Intermediate" = 3 – 6 mm from centre, "Periphery" = 6 – 9 mm from centre. Scale bar = 275 µm.

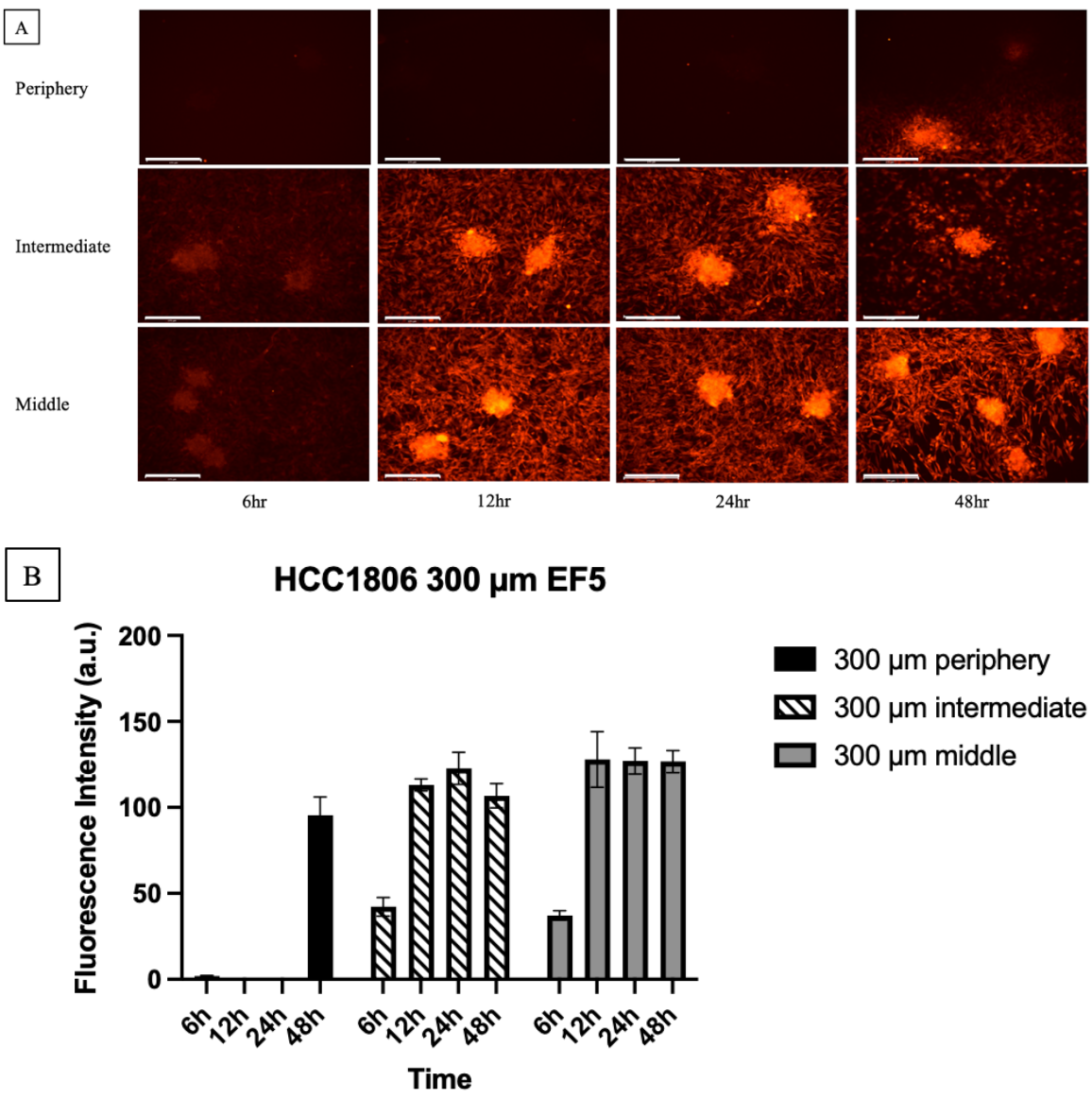

Figure 3.6.4. Characterizing HCC1806 cell hypoxic response in T-SLICE with a 300 µm spacer height using EF5. HCC1806 cell spheroids were cultured in T-SLICE with a 300 µm spacer height for up to 48 hours in the presence of 10 µM EF5. Cells were fixed, permeabilized, and stained with a Cy3-conjugated anti-EF5 antibody at 6h, 12h, 24h, and 48h timepoints. Images were captured on the EVOS FL Auto 2 Cell Imaging System, Light Cube RFP 2.0 (Ex: 531 nm, Em: 593 nm). Imaging data presented are representative images from three independent experiments (A). Fluorescence intensity increased sharply in the intermediate and middle zones at the 12-hour timepoint and was sustained over 48 hours (B). EF5 detection was nearly absent in the periphery until the 48-hour timepoint (B). "Middle" = 0 – 3 mm from centre, "Intermediate" = 3 – 6 mm from centre, "Periphery" = 6 – 9 mm from centre. Scale bar = 275 µm.

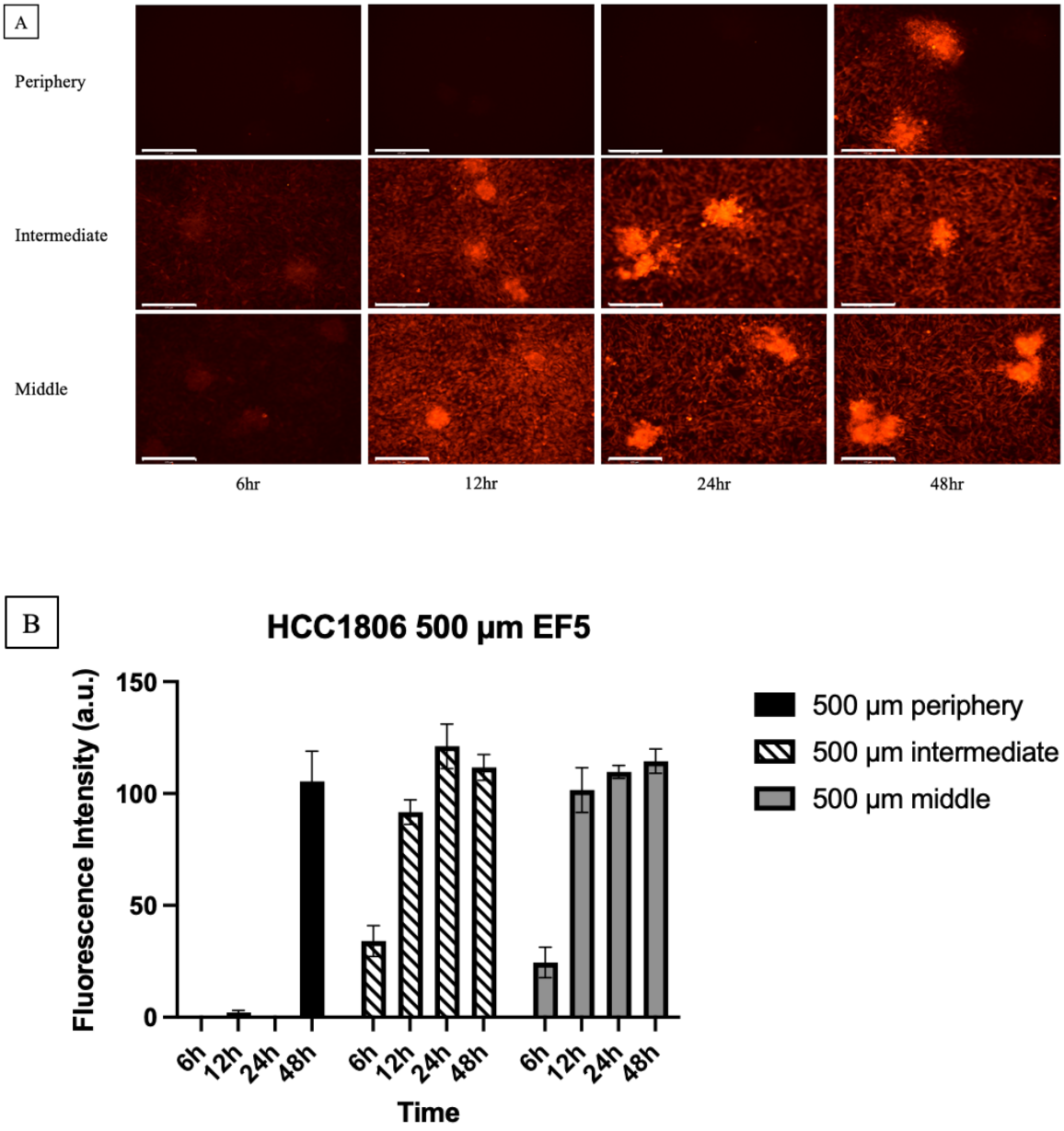

Figure 3.6.5. Characterizing HCC1806 cell hypoxic response in T-SLICE with a 500 µm spacer height using EF5. HCC1806 cell spheroids were cultured in T-SLICE with a 500 µm spacer height for up to 48 hours in the presence of 10 µM EF5. Cells were fixed, permeabilized, and stained with a Cy3-conjugated anti-EF5 antibody at 6h, 12h, 24h, and 48h timepoints. Images were captured on the EVOS FL Auto 2 Cell Imaging System, Light Cube RFP 2.0 (Ex: 531 nm, Em: 593 nm). Imaging data presented are representative images from three independent experiments (A). Fluorescence intensity increased sharply in the intermediate and middle zones at the 12-hour timepoint and was sustained over 48 hours (B). EF5 detection was nearly absent in the periphery until the 48-hour timepoint (B). "Middle" = 0 – 3 mm from centre, "Intermediate" = 3 – 6 mm from centre, "Periphery" = 6 – 9 mm from centre. Scale bar = 275 µm.

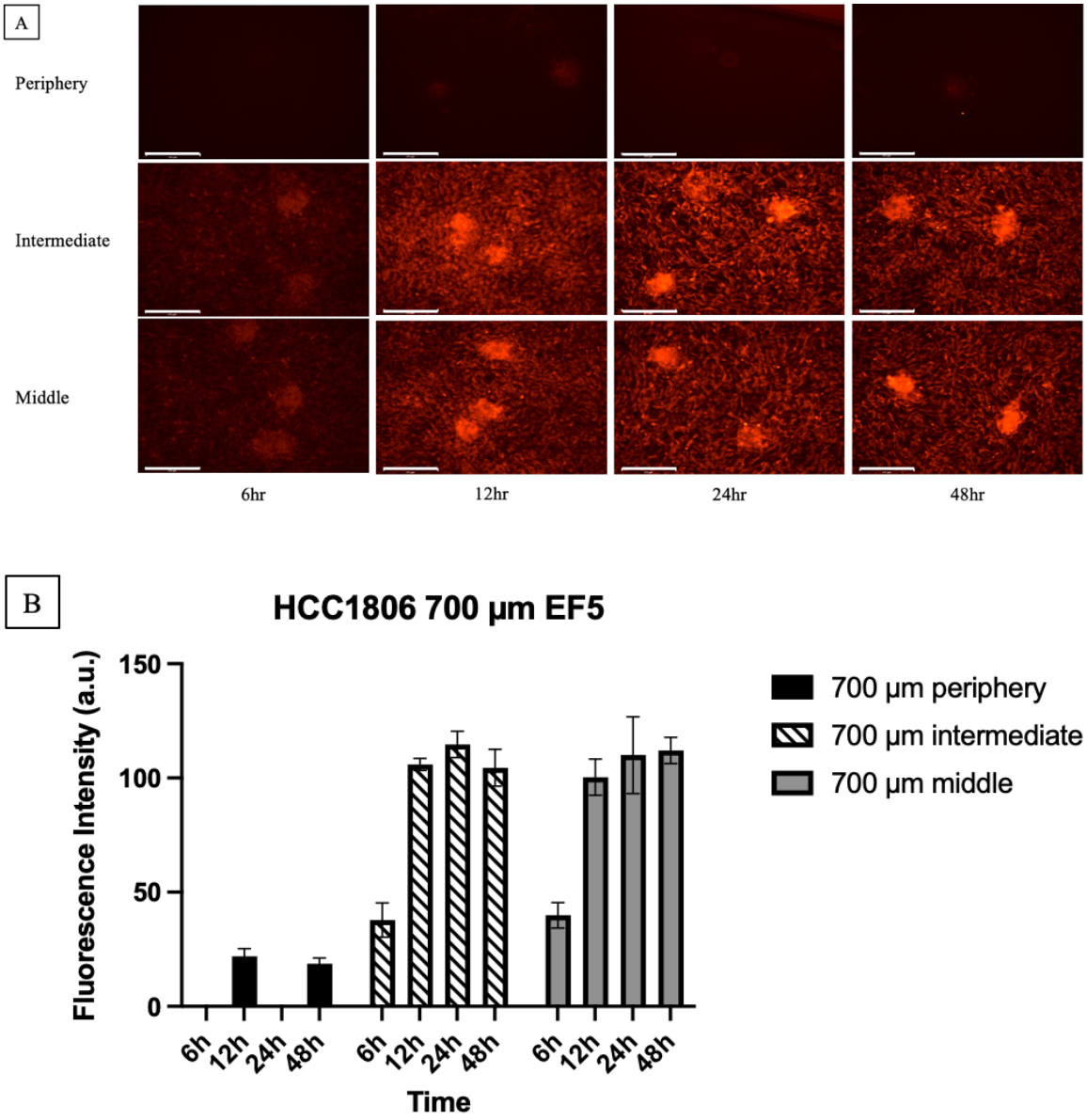

Figure 3.6.6. Characterizing HCC1806 cell hypoxic response in T-SLICE with a 700 µm spacer height using EF5. HCC1806 cell spheroids were cultured in T-SLICE with a 700 µm spacer height for up to 48 hours in the presence of 10 µM EF5. Cells were fixed, permeabilized, and stained with a Cy3-conjugated anti-EF5 antibody at 6h, 12h, 24h, and 48h timepoints. Images were captured on the EVOS FL Auto 2 Cell Imaging System, Light Cube RFP 2.0 (Ex: 531 nm, Em: 593 nm). Imaging data presented are representative images from three independent experiments (A). Fluorescence intensity increased sharply in the intermediate and middle zones at the 12-hour timepoint and was sustained over 48 hours (B). EF5 detection was nearly absent in the periphery across 48 hours (B). "Middle" = 0 – 3 mm from centre, "Intermediate" = 3 – 6 mm from centre, "Periphery" = 6 – 9 mm from centre. Scale bar = 275 µm.

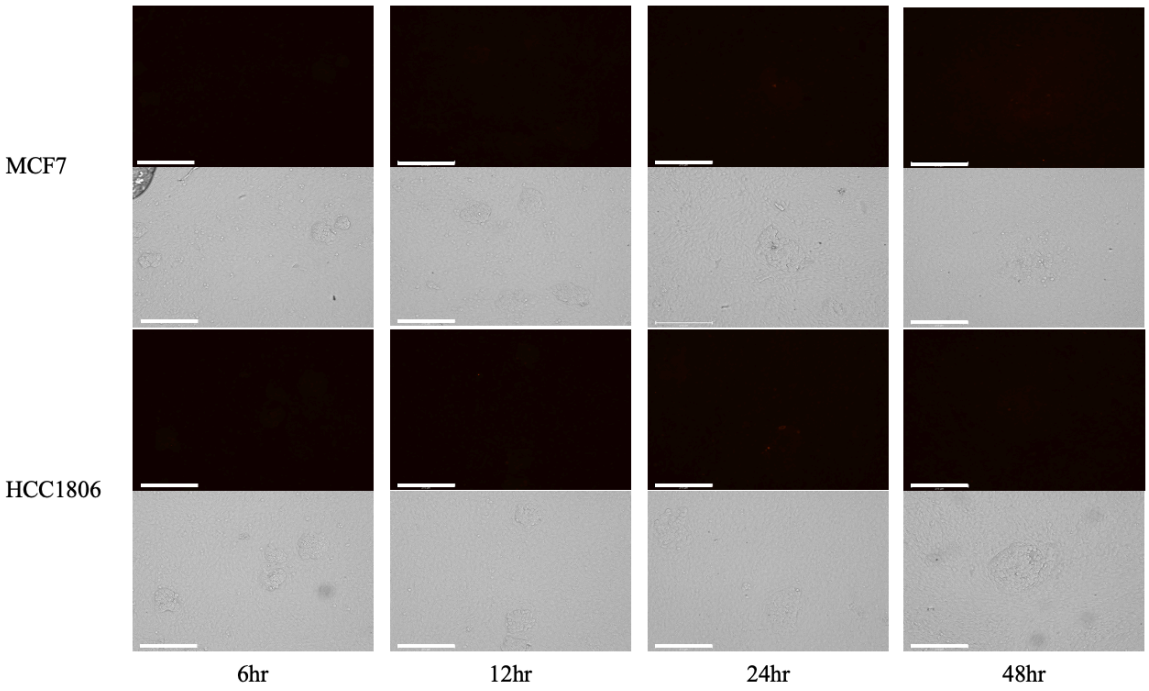

Figure 3.6.7. EF5 is not detected in MCF7 or HCC1806 cell spheroids (<150 µm diameter) co-cultured with NIH/3T3 fibroblasts without T-SLICE. MCF7 and HCC1806 cell spheroids were co-cultured with a monolayer of NIH/3T3 fibroblasts for up to 48 hours in the presence of 10 µM EF5 under standard tissue culture conditions (37ºC, 5% CO_2). Cells were fixed, permeabilized, and stained with Cy3-conjugated anti-EF5 antibody at 6h, 12h, 24h, and 48h timepoints. Images were captured on the EVOS FL Auto 2 Cell Imaging System, Light Cube RFP 2.0 (Ex: 531 nm, Em: 593 nm). EF5 detection was absent when T-SLICE devices were not added to the tissue culture.

3.7 HIF1a and HIF2a expression peak within the first 24 hours of T-SLICE culture

After demonstrating that hypoxic responses are elicited in breast cancer cells within 3 hours and sustained for 48 hours in T-SLICE, I wanted to assess hypoxia-inducible factor expression to determine how these responses were being regulated in T-SLICE. Hypoxia-inducible factor 1-alpha (HIF1a) is a transcription factor that is involved in the acute response to hypoxia (0 – 24 hours) (Zeng et al., 2015). Hypoxia-inducible factor 2-alpha (HIF2a) is also a transcription factor, but it is more involved in the chronic response to hypoxia (24 – 72 hours) (Zeng et al., 2015). Both HIF1a and HIF2a have been shown to play key roles in tumour progression (Zeng et al., 2015).

MCF7 and HCC1806 breast cancer cell spheroids were cultured in T-SLICE for up to 48 hours. T-SLICE cultures were fixed after 6, 12, 24, and 48 hours and labeled for HIF1a and HIF2a expression by immunofluorescent staining. T-SLICE was divided into three zones for HIF1a/HIF2a staining analysis: middle (0-3 mm from the centre), intermediate (3-6 mm from the centre), and periphery (6-9 mm from the centre).

MCF7 cells cultured in T-SLICE with a 300 µm spacer height had greater HIF1a expression in the intermediate and middle zones compared to the periphery (Figure 3.7.1 A). HIF1a expression was greatest in the intermediate and middle zones at the 12-hour timepoint and began to wane after 24 and 48 hours of T-SLICE culture. Similar trends in HIF2a expression were observed, with the highest expression at the 12-hour timepoint with decreasing expression after 24 and 48 hours of T-SLICE culture. HIF2a was expressed by MCF7 cells cultured in all three zones of T-SLICE (Figure 3.7.1 B).

MCF7 cells cultured in T-SLICE with a 500 µm and 700 µm spacer height also had greater HIF1a expression in the intermediate and middle zones compared to the

periphery, but expression peaked at the 24-hour timepoint before decreasing after 48 hours of T-SLICE culture (Figure 3.7.2 A) (Figure 3.7.3 A). HIF2a was expressed in MCF7 cells in all three zones of T-SLICE, with peak expression after 6 hours of T-SLICE culture and subsequent decreases in expression over the duration of 48 hours (Figure 3.7.2 B) (Figure 3.7.3 B).

HCC1806 cells cultured in T-SLICE with a 300 μm, 500 μm, and 700 μm all had similar HIF1a expression and no differences between the three zones were observed (Figure 3.7.4 A) (Figure 3.7.5 A) (Figure 3.7.6 A). HIF1a expression was minimal and remained consistent throughout the duration of the 48 hours of T-SLICE culture (Figure 3.7.4 A) (Figure 3.7.5 A) (Figure 3.7.6 A). HIF2a was expressed in HCC1806 cells equally across the 48 hours of T-SLICE culture, regardless of spacer height (Figure 3.7.4 B) (Figure 3.7.5 B) (Figure 3.7.6 B). HIF2a was most expressed in cells cultured in the peripheral zone compared to the intermediate and middle zones of T-SLICE (Figure 3.7.4 B) (Figure 3.7.5 B) (Figure 3.7.6 B).

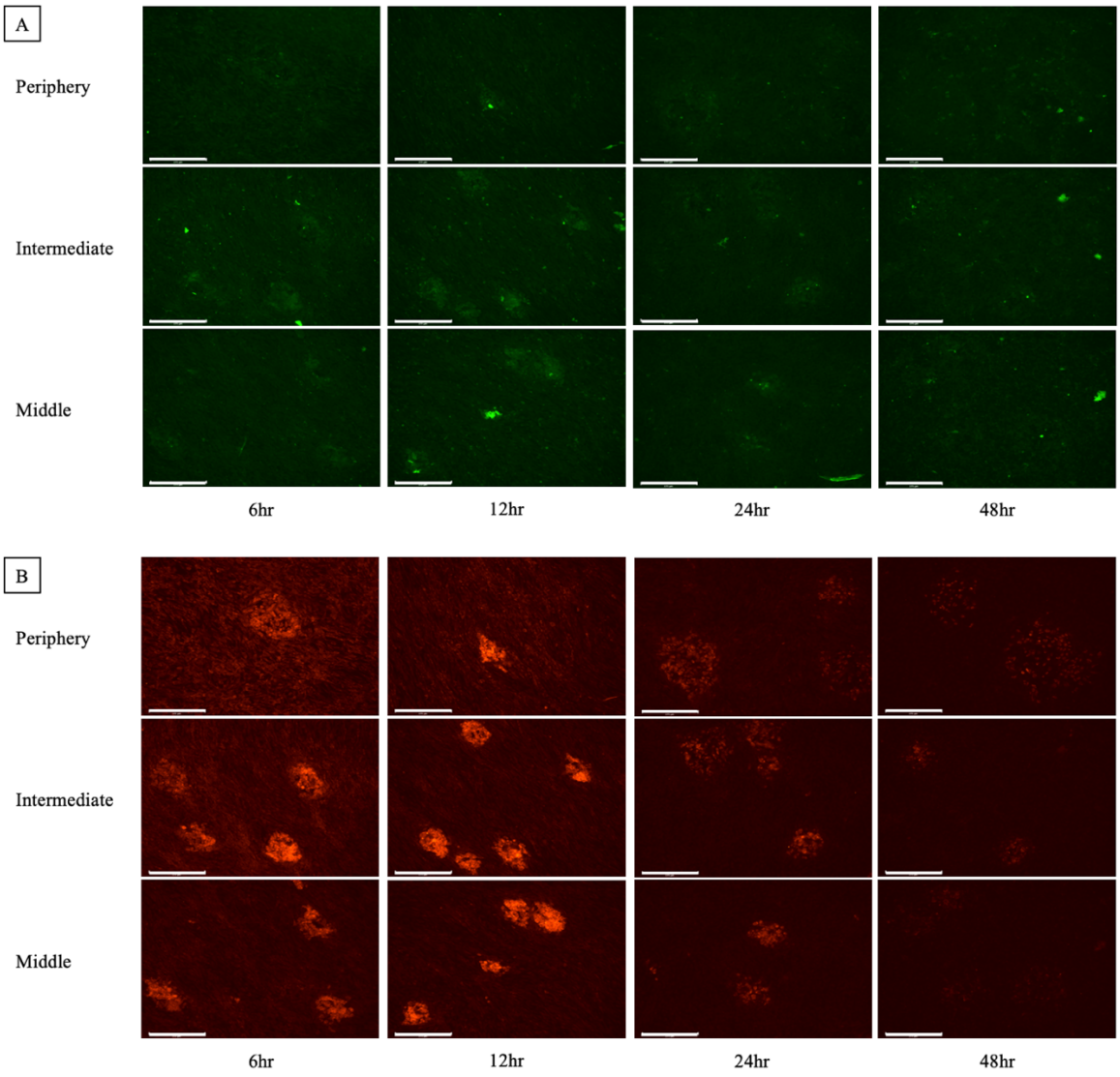

Figure 3.7.1. HIF1a/HIF2a expression in MCF7 cells cultured in T-SLICE with a 300 µm spacer height. MCF7 cell spheroids were cultured in T-SLICE with a 300 µm spacer height for up to 48 hours at 37˚C, 5% CO_2. Cells were fixed, permeabilized, and immunofluorescent labeling was performed for HIF1a/HIF2a expression at 6h, 12h, 24h, and 48h timepoints. Images were captured on the EVOS FL Auto 2 Cell Imaging System, Light Cube GFP 2.0 (Ex: 482 nm, Em: 524 nm) and Light Cube Cy5 2.0 (Ex: 635 nm, Em: 692 nm). HIF1a staining intensity peaked after 12 hours of T-SLICE culture in the intermediate and middle zones (A). HIF1a detection was nearly absent in the periphery (A). HIF2a staining intensity was most intense after 12 hours of T-SLICE culture and progressively diminished over 48 hours (B). No differences in HIF2a expression are observed between the periphery, intermediate, and middle zones (B). Data presented are representative images from three independent experiments. “Middle” = 0 – 3 mm from centre, “Intermediate” = 3 – 6 mm from centre, “Periphery” = 6 – 9 mm from centre. Scale bar = 275 µm.

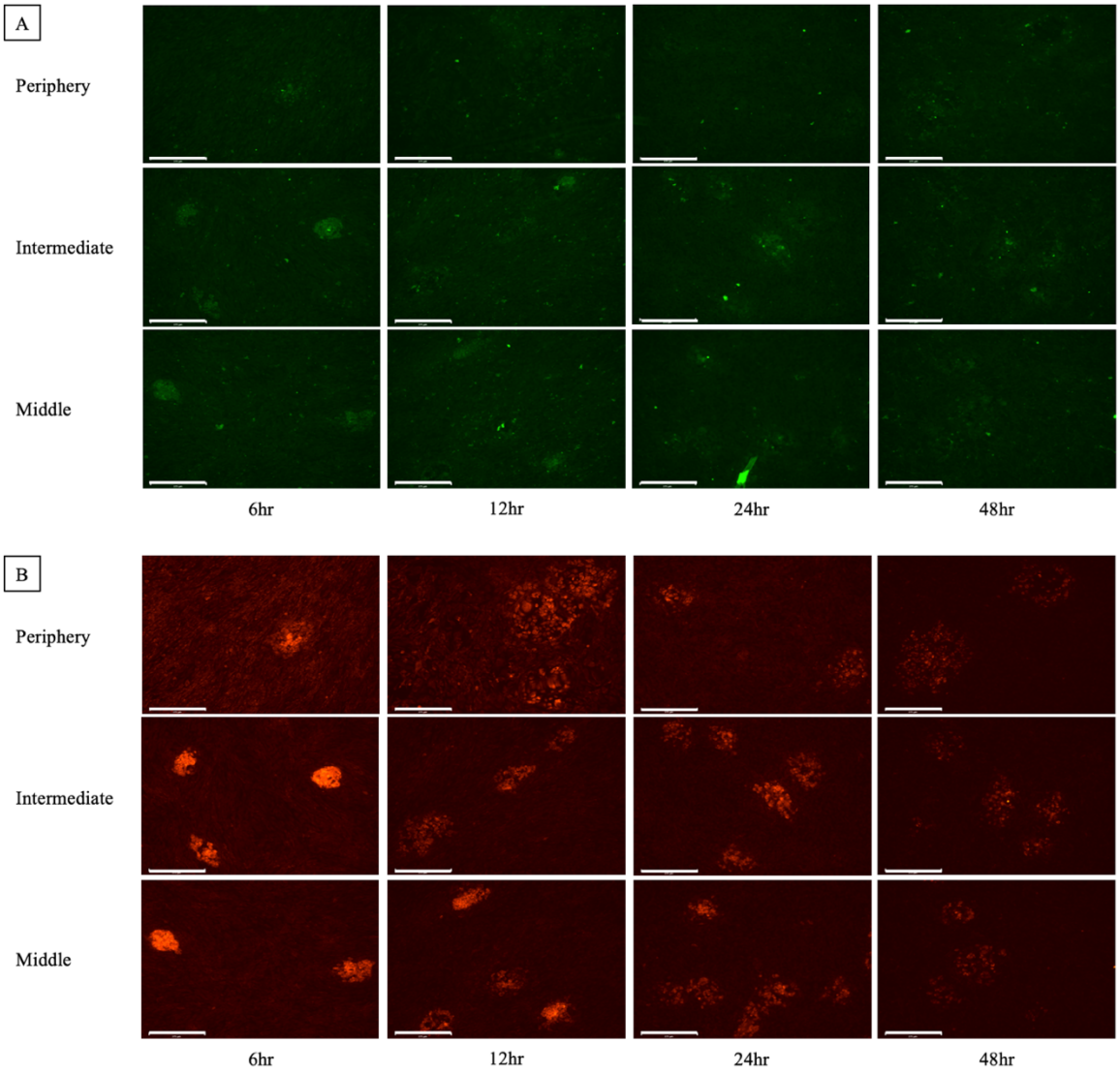

Figure 3.7.2. HIF1a/HIF2a expression in MCF7 cells cultured in T-SLICE with a 500 µm spacer height. MCF7 cell spheroids were cultured in T-SLICE with a 500 µm spacer height for up to 48 hours at 37˚C, 5% CO_2. Cells were fixed, permeabilized, and immunofluorescent labeling was performed for HIF1a/HIF2a expression at 6h, 12h, 24h, and 48h timepoints. Images were captured on the EVOS FL Auto 2 Cell Imaging System, Light Cube GFP 2.0 (Ex: 482 nm, Em: 524 nm) and Light Cube Cy5 2.0 (Ex: 635 nm, Em: 692 nm). HIF1a staining intensity peaked after 24 hours of T-SLICE culture in the intermediate and middle zones (A). HIF1a detection was nearly absent in the periphery (A). HIF2a expression was most intense after 6 hours of T-SLICE culture and progressively diminished over 48 hours (B). No differences are observed between the periphery, intermediate, and middle zones (B). Data presented are representative images from three independent experiments. “Middle” = 0 – 3 mm from centre, “Intermediate” = 3 – 6 mm from centre, “Periphery” = 6 – 9 mm from centre. Scale bar = 275 µm.

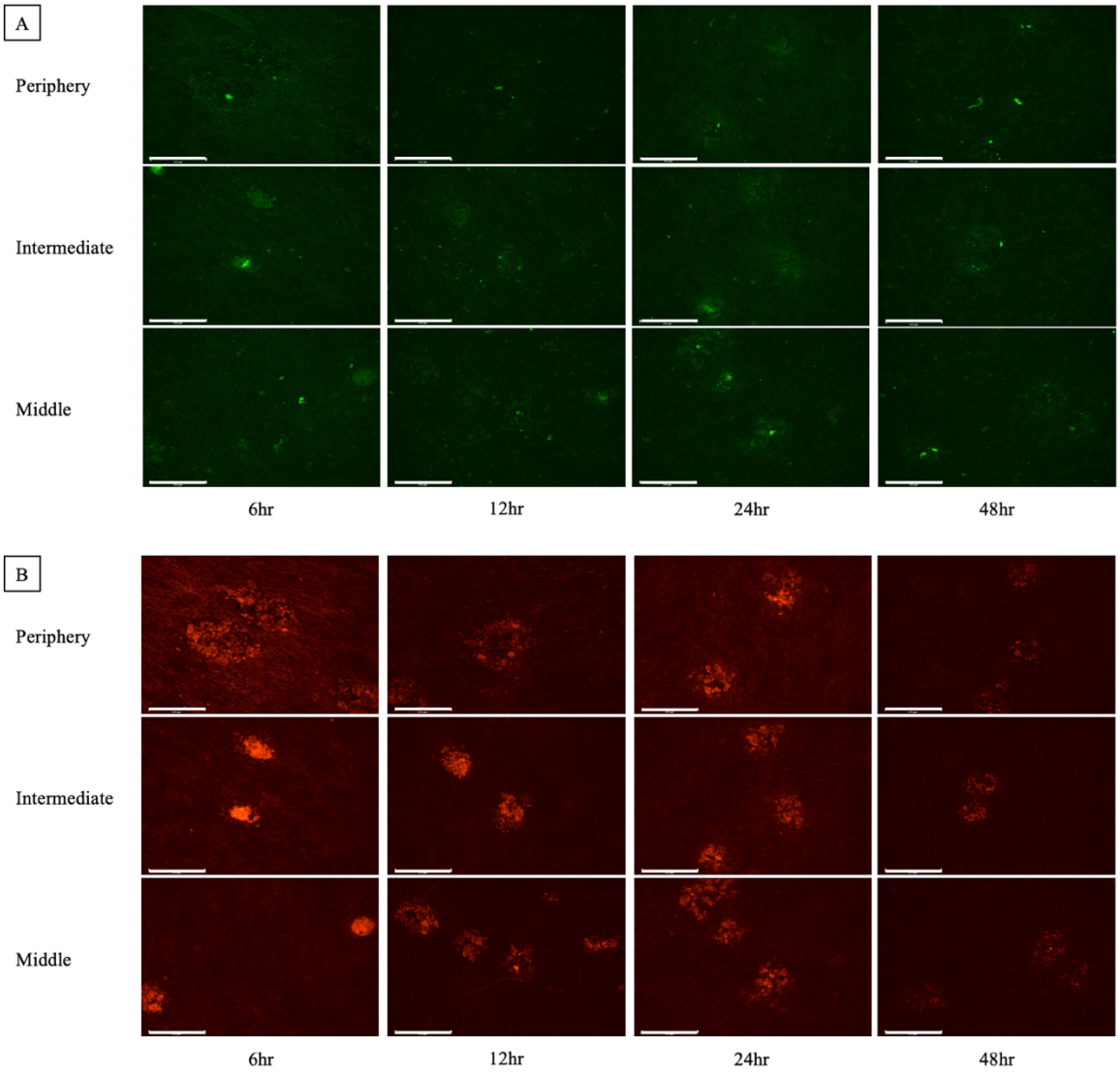

Figure 3.7.3. HIF1a/HIF2a expression in MCF7 cells cultured in T-SLICE with a 700 µm spacer height. MCF7 cell spheroids were cultured in T-SLICE with a 700 µm spacer height for up to 48 hours at 37˚C, 5% CO_2. Cells were fixed, permeabilized, and immunofluorescent labeling was performed for HIF1a/HIF2a expression at 6h, 12h, 24h, and 48h timepoints. Images were captured on the EVOS FL Auto 2 Cell Imaging System, Light Cube GFP 2.0 (Ex: 482 nm, Em: 524 nm) and Light Cube Cy5 2.0 (Ex: 635 nm, Em: 692 nm). HIF1a staining intensity peaked after 24 hours of T-SLICE culture in the intermediate and middle zones (A). HIF1a detection was nearly absent in the periphery (A). HIF2a staining intensity was most intense after 6 hours of T-SLICE culture and progressively diminished over 48 hours (B). No differences in HIF2a expression are observed between the periphery, intermediate, and middle zones (B). Data presented are representative images from three independent experiments. “Middle” = 0 – 3 mm from centre, “Intermediate” = 3 – 6 mm from centre, “Periphery” = 6 – 9 mm from centre. Scale bar = 275 µm.

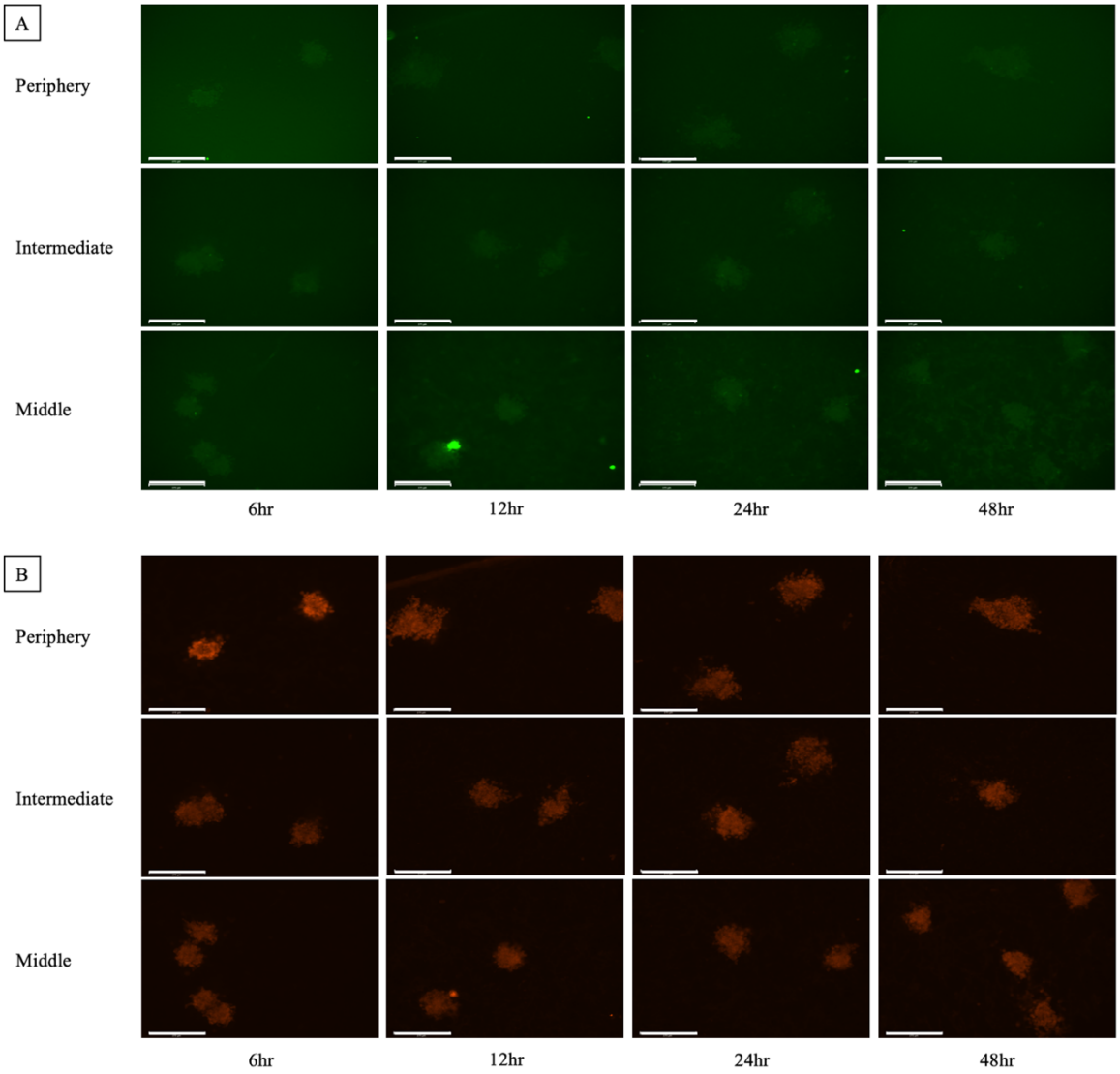

Figure 3.7.4. HIF1a/HIF2a expression in HCC1806 cells cultured in T-SLICE with a 300 µm spacer height. HCC1806 cell spheroids were cultured in T-SLICE with a 300 µm spacer height for up to 48 hours at 37˚C, 5% CO_2. Cells were fixed, permeabilized, and immunofluorescent labeling was performed for HIF1a/HIF2a expression at 6h, 12h, 24h, and 48h timepoints. Images were captured on the EVOS FL Auto 2 Cell Imaging System, Light Cube GFP 2.0 (Ex: 482 nm, Em: 524 nm) and Light Cube Cy5 2.0 (Ex: 635 nm, Em: 692 nm). HIF1a staining intensity was weak in the periphery, intermediate, and middle zones and did not vary over 48 hours (A). HIF2a staining intensity was similar in respective zones over 48 hours (B). HIF2a expression was greatest in the periphery (B). Data presented are representative images from three independent experiments. “Middle” = 0 – 3 mm from centre, “Intermediate” = 3 – 6 mm from centre, “Periphery” = 6 – 9 mm from centre. Scale bar = 275 µm.

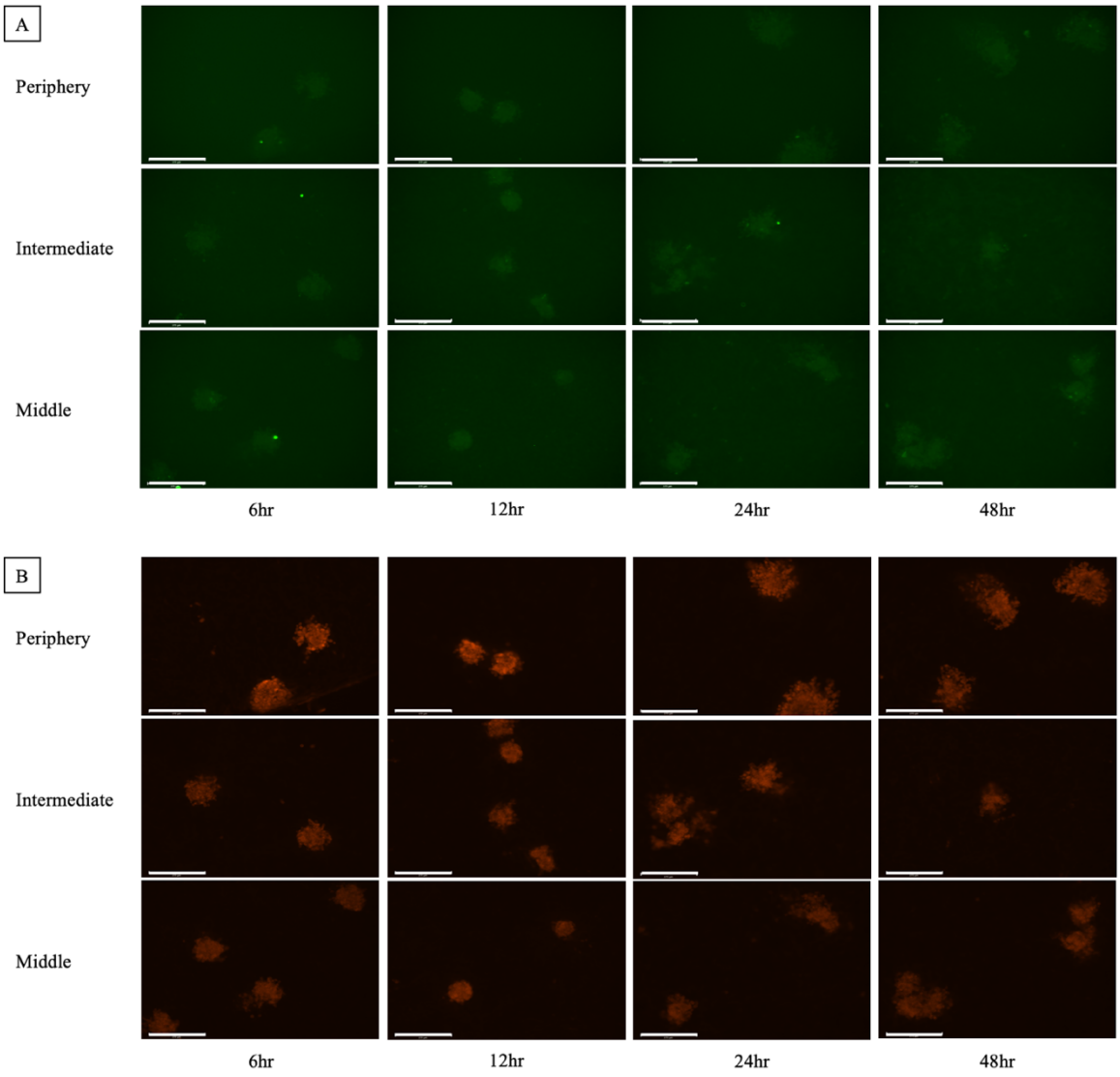

Figure 3.7.5. HIF1a/HIF2a expression in HCC1806 cells cultured in T-SLICE with a 500 µm spacer height. HCC1806 cell spheroids were cultured in T-SLICE with a 500 µm spacer height for up to 48 hours at 37˚C, 5% CO_2. Cells were fixed, permeabilized, and immunofluorescent labeling was performed for HIF1a/HIF2a expression at 6h, 12h, 24h, and 48h timepoints. Images were captured on the EVOS FL Auto 2 Cell Imaging System, Light Cube GFP 2.0 (Ex: 482 nm, Em: 524 nm) and Light Cube Cy5 2.0 (Ex: 635 nm, Em: 692 nm). HIF1a staining intensity was weak in the periphery, intermediate, and middle zones and did not vary over 48 hours (A). HIF2a staining intensity was similar in respective zones over 48 hours (B). HIF2a expression was greatest in the periphery (B). Data presented are representative images from three independent experiments. “Middle” = 0 – 3 mm from centre, “Intermediate” = 3 – 6 mm from centre, “Periphery” = 6 – 9 mm from centre. Scale bar = 275 µm.

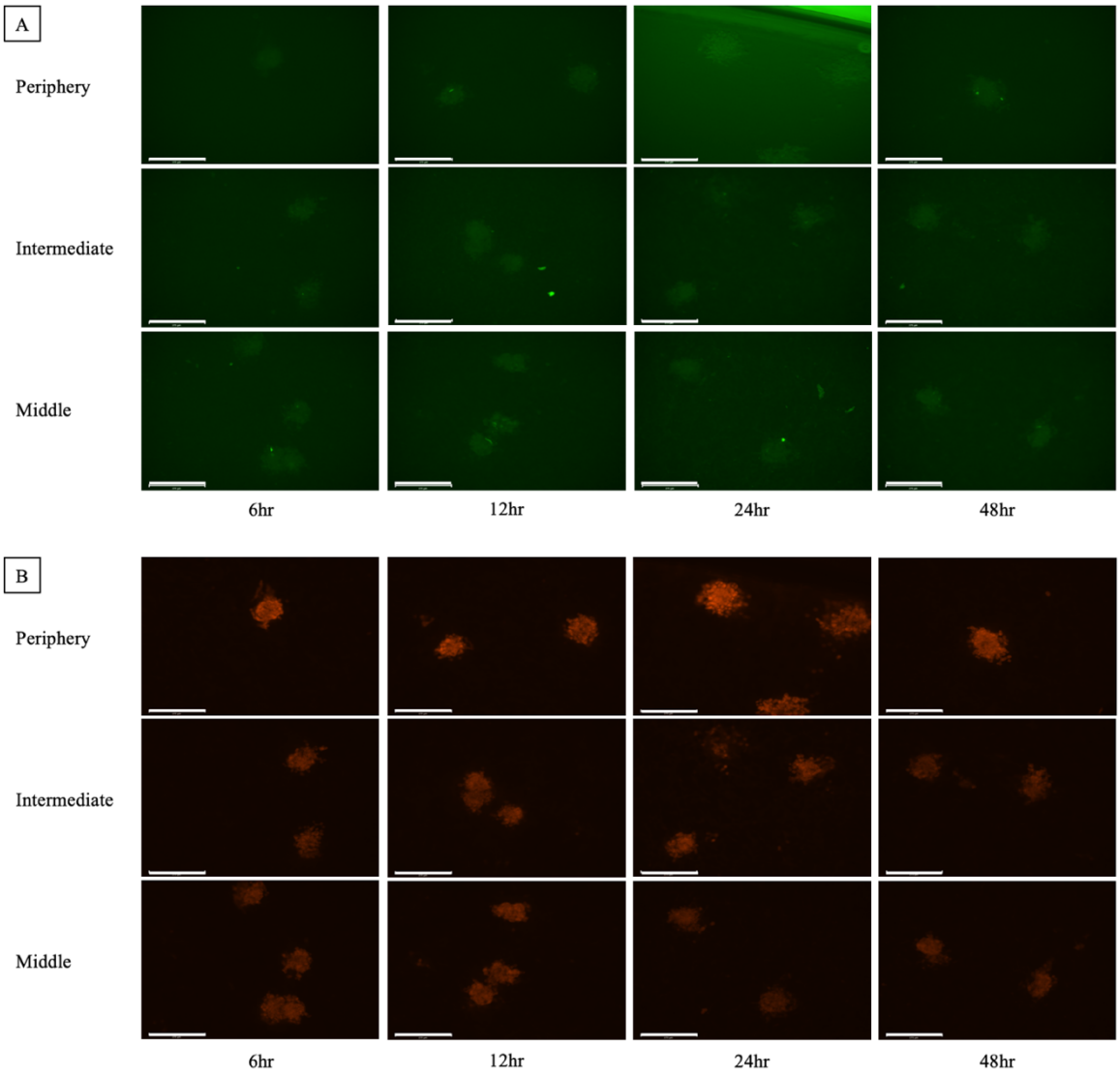

Figure 3.7.6. HIF1a/HIF2a expression in HCC1806 cells cultured in T-SLICE with a 700 µm spacer height. HCC1806 cell spheroids were cultured in T-SLICE with a 700 µm spacer height for up to 48 hours at 37˚C, 5% CO_2. Cells were fixed, permeabilized, and immunofluorescent labeling was performed for HIF1a/HIF2a expression at 6h, 12h, 24h, and 48h timepoints. Images were captured on the EVOS FL Auto 2 Cell Imaging System, Light Cube GFP 2.0 (Ex: 482 nm, Em: 524 nm) and Light Cube Cy5 2.0 (Ex: 635 nm, Em: 692 nm). HIF1a staining intensity was weak in the periphery, intermediate, and middle zones and did not vary over 48 hours (A). HIF2a staining intensity was similar in respective zones over 48 hours (B). HIF2a expression was greatest in the periphery (B). Data presented are representative images from three independent experiments. “Middle” = 0 – 3 mm from centre, “Intermediate” = 3 – 6 mm from centre, “Periphery” = 6 – 9 mm from centre. Scale bar = 275 µm.

3.8 Cell viability decreases with increasing hypoxia and is impacted more in MCF7 cells than HCC1806 cells

After demonstrating that T-SLICE generates hypoxic gradients, I wanted to investigate resulting cancer cell behaviours that occur due to oxygen and other small molecule depletion. One of the features of large solid tumours is the development of a poorly vascularized necrotic core (Nejad et al., 2021). The cell death observed in the necrotic core is attributed to various factors, including a lack of oxygen and nutrient supply (Nejad et al., 2021). I used calcein AM and ethidium homodimer-1 in tandem as a live/dead assay to assess cell viability in T-SLICE. I cultured MCF7 and HCC1806 breast cancer cell spheroids in T-SLICE for 72 hours and subsequently performed a live/dead assay. T-SLICE was divided into three zones for cell viability analysis: middle (0-3 mm from the centre), intermediate (3-6 mm from the centre), and periphery (6-9 mm from the centre).

MCF7 cells cultured in T-SLICE with a 300 μm spacer height had high cell viability in the peripheral zone, with decreasing viability in the intermediate and middle zones (Figure 3.8.1). All MCF7 cells were dead in the middle zone of T-SLICE with a 300 μm spacer height (Figure 3.8.1). It should be noted that the NIH/3T3 fibroblasts had similar viability in T-SLICE, with virtually 100% cell death found in the middle zone of T-SLICE and nearly 100% cell viability in the periphery (Figure 3.8.1). MCF7 cells cultured in T-SLICE with a 500 μm and 700 μm spacer height had good cell viability in all three zones, with no differences observed between zones (Figure 3.8.1). NIH/3T3 cell viability was also high in all three zones of T-SLICE with the larger spacer heights.

HCC1806 cells cultured in T-SLICE had high cell viability, regardless of spacer height (Figure 3.8.2). NIH/3T3 fibroblasts had lower cell viability in the middle zone of T-SLICE with a 300 μm spacer height compared to the peripheral and intermediate zones, but no differences in fibroblast cell viability were observed between zones of T-SLICE with 500 μm and 700 μm spacer heights (Figure 3.8.2).

Overall, cell viability differs between MCF7 and HCC1806 breast cancer cell lines and adjusting T-SLICE spacer height impacts fibroblast and breast cancer cell viability.

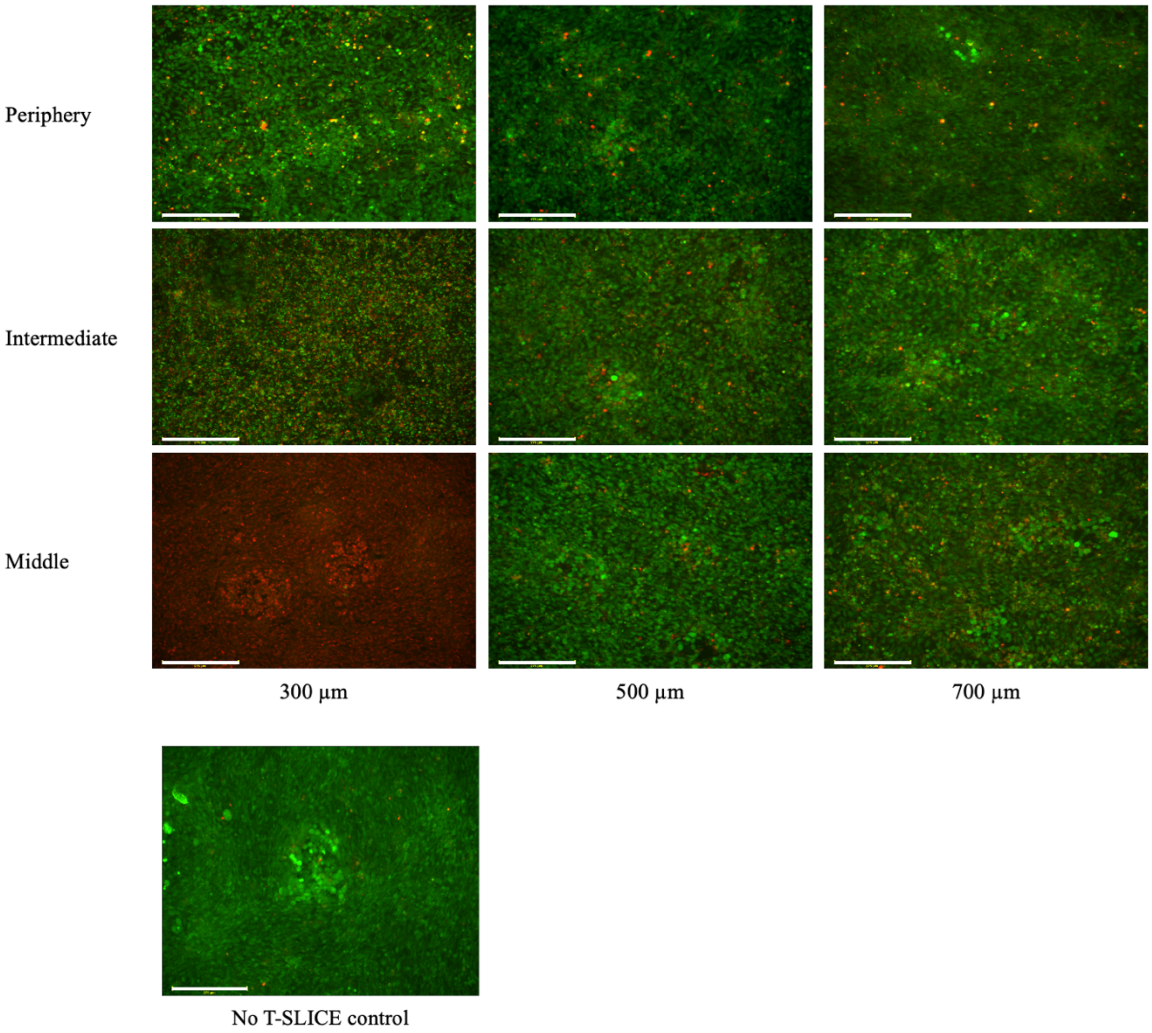

Figure 3.8.1. MCF7 cell viability decreases with increasing hypoxia in T-SLICE. **MCF7** cell spheroids were cultured in T-SLICE with a 300 µm, 500 µm, and 700 µm spacer height for 72 hours at 37˚C, 5% CO_2. Cells were stained with calcein AM/ethidium homodimer-1 live/dead assay after 72 hours of T-SLICE culture. Images were captured on the EVOS FL Auto 2 Cell Imaging System, Light Cube GFP 2.0 (Ex: 482 nm, Em: 524 nm) and RFP 2.0 (Ex: 531 nm, Em: 593 nm) and merged in ImageJ. Cell viability differed based on T-SLICE spacer height and T-SLICE zone. Data presented are representative images from three independent experiments. "Middle" = 0 – 3 mm from centre, "Intermediate" = 3 – 6 mm from centre, "Periphery" = 6 – 9 mm from centre. Scale bar = 275 µm.

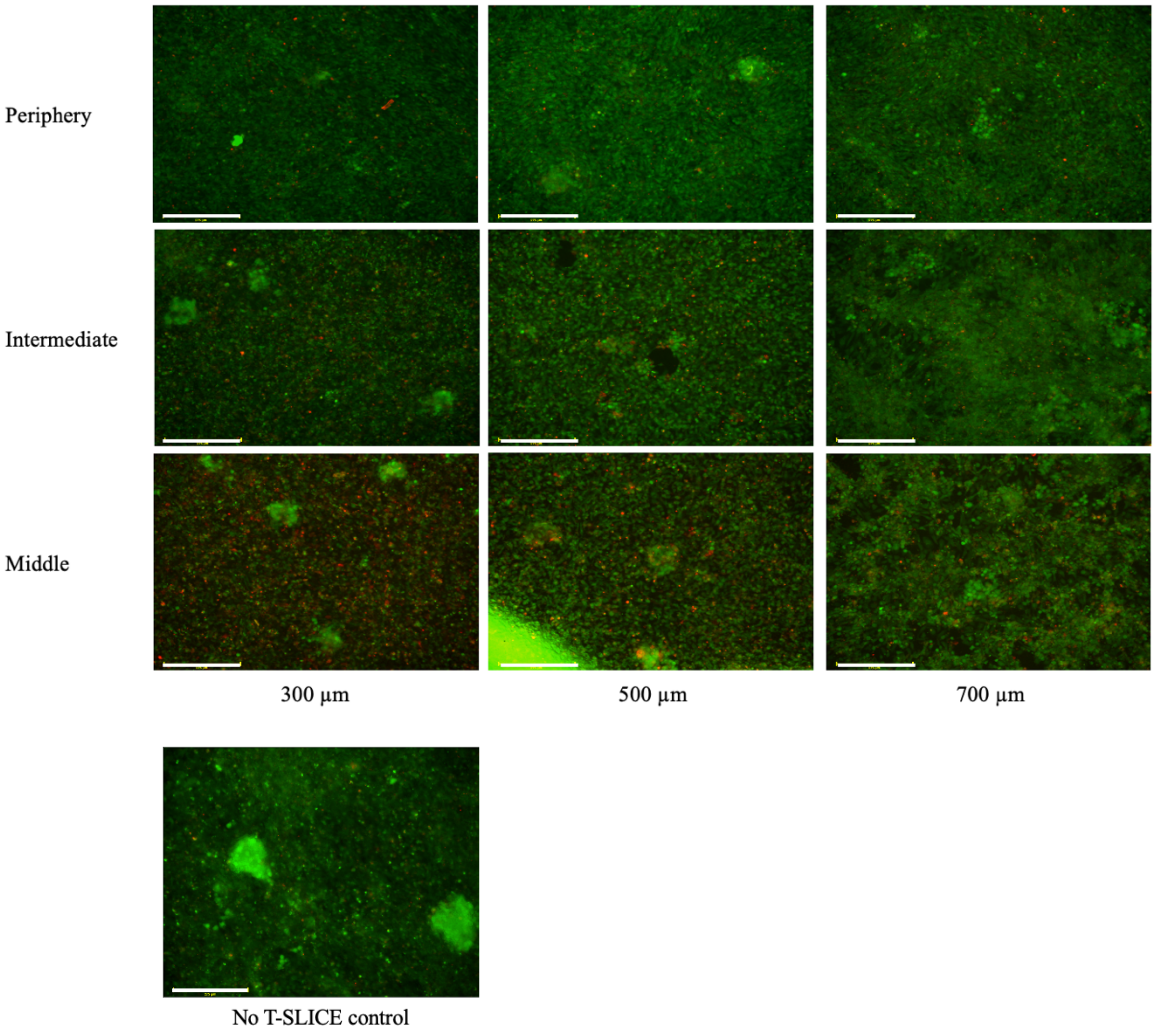

Figure 3.8.2. HCC1806 cell viability remains stable across all three zones of T-SLICE. HCC1806 cell spheroids were cultured in T-SLICE with a 300 µm, 500 µm, and 700 µm spacer height for 72 hours at 37˚C, 5% CO_2. Cells were stained with calcein AM/ethidium homodimer-1 live/dead assay after 72 hours of T-SLICE culture. Images were captured on the EVOS FL Auto 2 Cell Imaging System, Light Cube GFP 2.0 (Ex: 482 nm, Em: 524 nm) and RFP 2.0 (Ex: 531 nm, Em: 593 nm) and merged in ImageJ. HCC1806 cell viability remained high in all zones of T-SLICE regardless of spacer height. NIH/3T3 cell viability differed based on T-SLICE spacer height and T-SLICE zone. Data presented are representative images from three independent experiments. "Middle" = 0 – 3 mm from centre, "Intermediate" = 3 – 6 mm from centre, "Periphery" = 6 – 9 mm from centre. Scale bar = 275 µm.

3.9 Hypoxia generated in T-SLICE inhibits MCF7 and HCC1806 cell proliferation

Decreased cell proliferation rate is a characteristic cell response in hypoxic regions of tumours (Zhang et al., 2018). I wanted to investigate how MCF7 and HCC1806 breast cancer cell proliferation was impacted by the hypoxia generated in T-SLICE. To do this, I cultured MCF7 and HCC1806 breast cancer cell spheroids in T-SLICE for 72 hours with medium containing EdU, a thymidine analog that can then be labeled in a click-chemistry reaction. EdU detection serves as a direct measure of newly synthesized DNA and thus newly proliferated cells. T-SLICE was divided into two zones for cell proliferation analysis: middle (0-3 mm from the centre) and periphery (6-9 mm from the centre).

MCF7 and HCC1806 cells cultured in the periphery of T-SLICE with a 300 µm, 500 µm, and 700µm spacer height had high expression of EdU after 72 hours (Figure 3.9.1) (Figure 3.9.2). NIH/3T3 cells had greatest expression of EdU in the periphery of T-SLICE with a 700 µm spacer height, with decreasing expression as spacer height gets smaller (Figure 3.9.1) (Figure 3.9.2). EdU detection was absent in the middle zone of T-SLICE in all spacer heights tested (Figure 3.9.1) (Figure 3.9.2). Overall, cell proliferation rates are similar in the periphery of T-SLICE compared to the no-T-SLICE control, but no cell proliferation was observed in the middle zone of T-SLICE after 72 hours in either cell line tested.

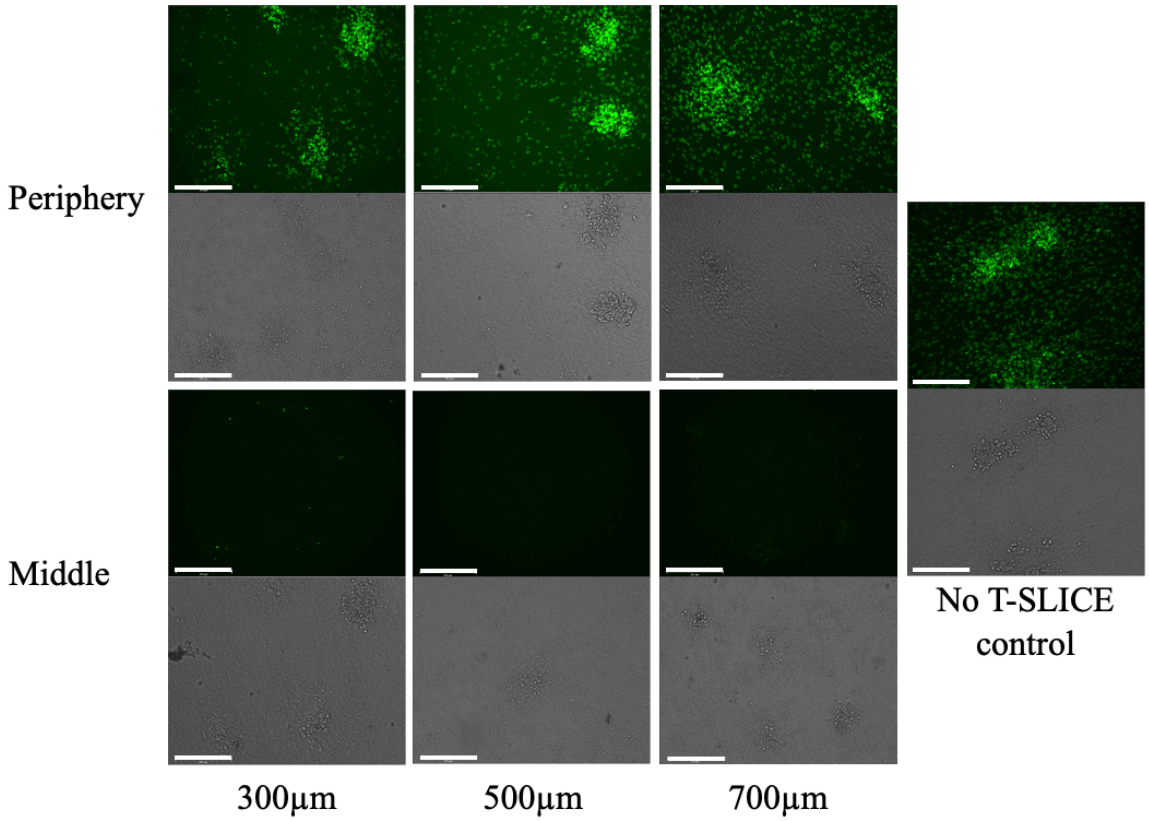

Figure 3.9.1. MCF7 cell proliferation is inhibited in the most hypoxic zone of T-SLICE. MCF7 cell spheroids were cultured with 10 µM EdU in T-SLICE with a 300 µm, 500 µm, and 700 µm spacer height for 72 hours at 37˚C, 5% CO_2. Cells were then fixed, permeabilized, and labeled for EdU detection. Images were captured on the EVOS FL Auto 2 Cell Imaging System, Light Cube GFP 2.0 (Ex: 482 nm, Em: 524 nm). Cell proliferation was absent in the middle of all T-SLICE devices. Cell proliferation in the periphery increased with T-SLICE spacer height. Control represents a NIH/3T3-MCF7 co-culture without the addition of T-SLICE. Data presented are representative images from three independent experiments. "Middle" = 0 – 3 mm from centre, "Periphery" = 6 – 9 mm from centre. Scale bar = 275 µm.

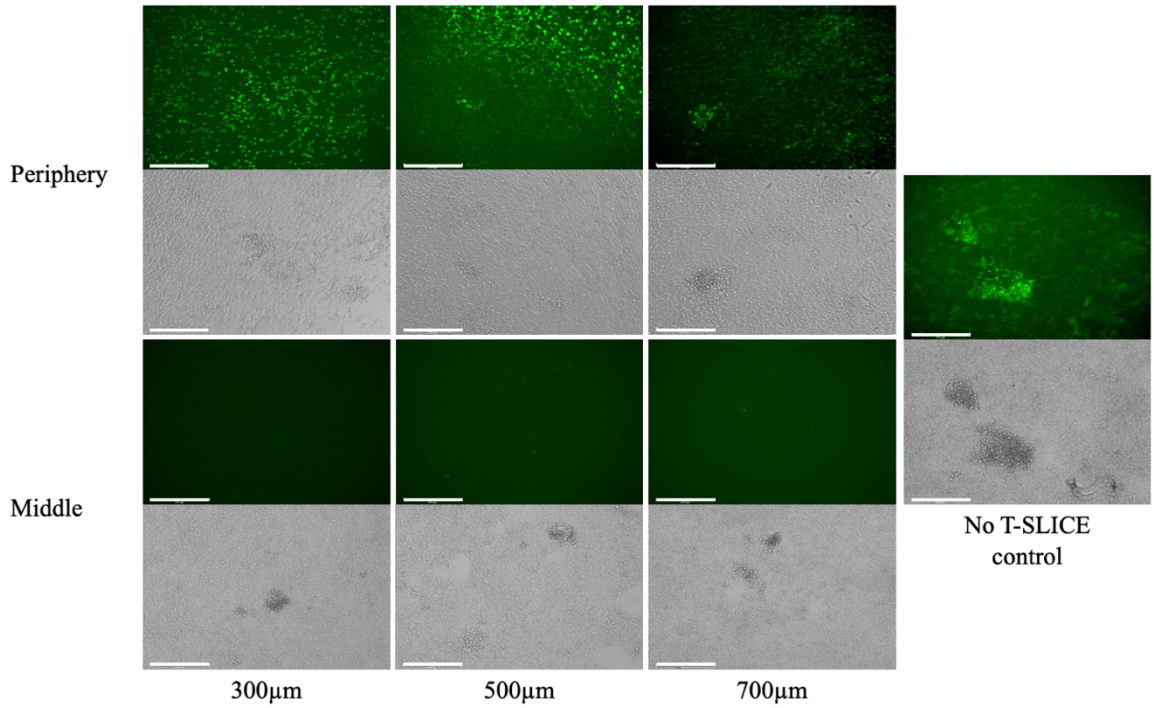

Figure 3.9.2. HCC1806 cell proliferation is inhibited in the most hypoxic zone of T-SLICE. HCC1806 cell spheroids were cultured with 10 µM EdU in T-SLICE with a 300 µm, 500 µm, and 700 µm spacer height for 72 hours at 37˚C, 5% CO_2. Cells were then fixed, permeabilized, and labeled for EdU detection. Images were captured on the EVOS FL Auto 2 Cell Imaging System, Light Cube GFP 2.0 (Ex: 482 nm, Em: 524 nm). Cell proliferation was absent in the middle of all T-SLICE devices. Cell proliferation in the periphery was similar in all T-SLICE devices, regardless of spacer height. Data presented are representative images from three independent experiments. "Middle" = 0 – 3 mm from centre, "Periphery" = 6 – 9 mm from centre. Scale bar = 275 µm.

3.10 Mitochondrial membrane potential decreases with increasing hypoxia and is lost to a greater degree in MCF7 cells than HCC1806 cells

Mitochondrial membrane potential (M.M.P.) is lost when cells are undergoing bioenergetic stress and prepare for apoptosis (Zhao et al., 2018). Correlations have been found between higher M.M.P. and cell survival and invasiveness in breast cancer and is becoming increasingly investigated as a prognostic marker and therapeutic target (Zhao et al., 2018). To assess M.M.P. of MCF7 and HCC1806 breast cancer cells in T-SLICE, I cultured cells for 72 hours with Mitoview 633 Dye added to the medium. Mitoview 633 Dye is potential-dependent and accumulates in mitochondria in proportion to electron gradient. Cells were live-imaged in T-SLICE every 24 hours to investigate how M.M.P. is impacted by the biochemical gradients generated in T-SLICE. T-SLICE was divided into three zones for M.M.P. analysis: middle (0-3 mm from the centre), intermediate (3-6 mm from the centre), and periphery (6-9 mm from the centre).

MCF7 cells cultured in T-SLICE with a 300 μm spacer height had high Mitoview 633 accumulation in the periphery with sustained but decreasing accumulation in the intermediate and middle zones of T-SLICE through 48 hours of culture (Figure 3.10.1). Mitoview 633 detection was sustained in the periphery and intermediate zones of T-SLICE with a 300 μm spacer height after 72 hours but was lost in the middle zone (Figure 3.10.1). NIH/3T3 fibroblasts suffered greater loss of M.M.P. in the intermediate and middle zones of T-SLICE compared to the periphery (Figure 3.10.1). MCF7 cells cultured in T-SLICE with a 500 μm and 700 μm spacer height had high Mitoview 633 accumulation in the periphery with sustained but decreasing accumulation in the intermediate and middle zones of T-SLICE over the entire 72-hour culture period (Figure

3.10.2) (Figure 3.10.3). NIH/3T3 fibroblasts suffered greater loss of M.M.P. in the intermediate and middle zones of T-SLICE with a 500 μm spacer height than a 700 μm spacer height after 72 hours (Figure 3.10.2) (Figure 3.10.3).

HCC1806 cells cultured in T-SLICE with a 300 μm, 500 μm, and 700 μm spacer height had sustained Mitoview 633 accumulation throughout the 72-hour culture period (Figure 3.10.4) (Figure 3.10.5) (Figure 3.10.6). There were little to no differences observed in Mitoview 633 accumulation in HCC1806 cells across the periphery, intermediate, and middle zones of T-SLICE. NIH/3T3 fibroblasts had lower Mitoview 633 accumulation in the intermediate and middle zones of T-SLICE of all spacer heights (Figure 3.10.4) (Figure 3.10.5) (Figure 3.10.6).

Overall, M.M.P. decreased in the breast cancer cells in the zones of T-SLICE previously shown to display greater hypoxic responses. M.M.P. was lost to a greater extent in MCF7 cells than HCC1806 cells after 72 hours of T-SLICE culture.

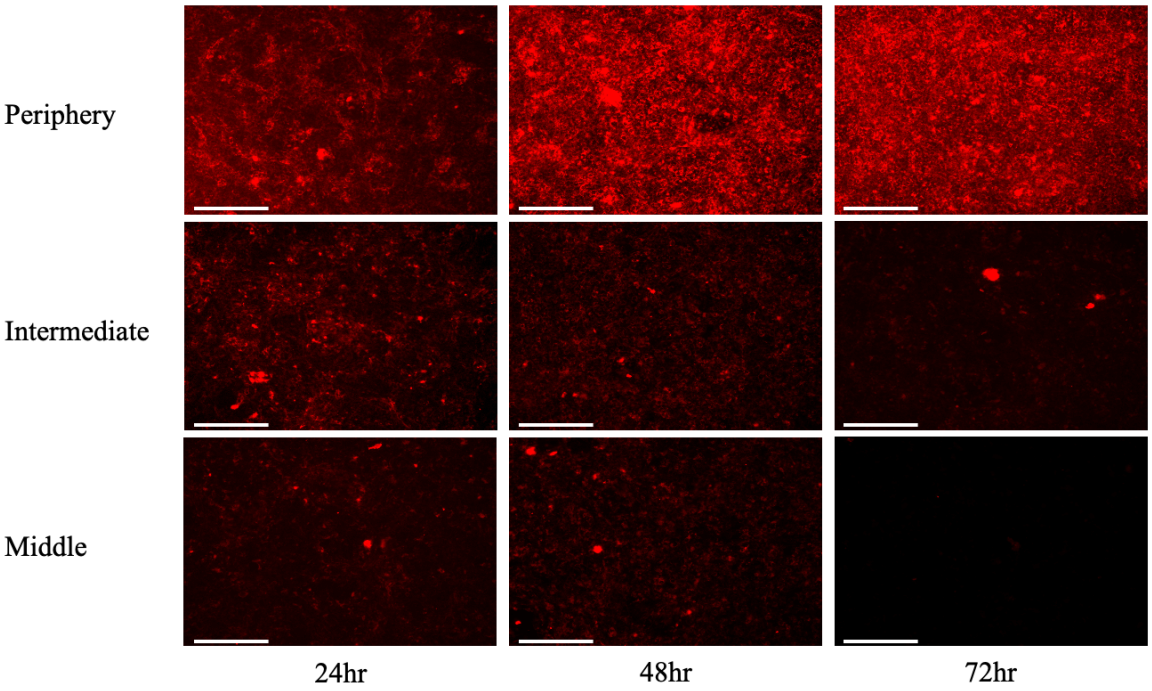

Figure 3.10.1. MCF7 mitochondrial membrane potential was lost over 72 hours in T-SLICE with a 300 µm spacer height. MCF7 cell spheroids were cultured with 100 nM Mitoview 633 Dye in T-SLICE with a 300 µm spacer height for up to 72 hours at 37˚C, 5% CO_2. Cells were live-imaged at 24-, 48-, and 72-hour timepoints. Images were captured on the EVOS FL Auto 2 Cell Imaging System, Light Cube Cy5 2.0 (Ex: 635 nm, Em: 692 nm). Mitoview 633 dye had the highest levels of accumulation in the peripheral zone and decreased across the intermediate and middle zones of T-SLICE. Data presented are representative images from three independent experiments. "Middle" = 0 – 3 mm from centre, "Intermediate" = 3 – 6 mm from centre, "Periphery" = 6 – 9 mm from centre. Scale bar = 275 µm.

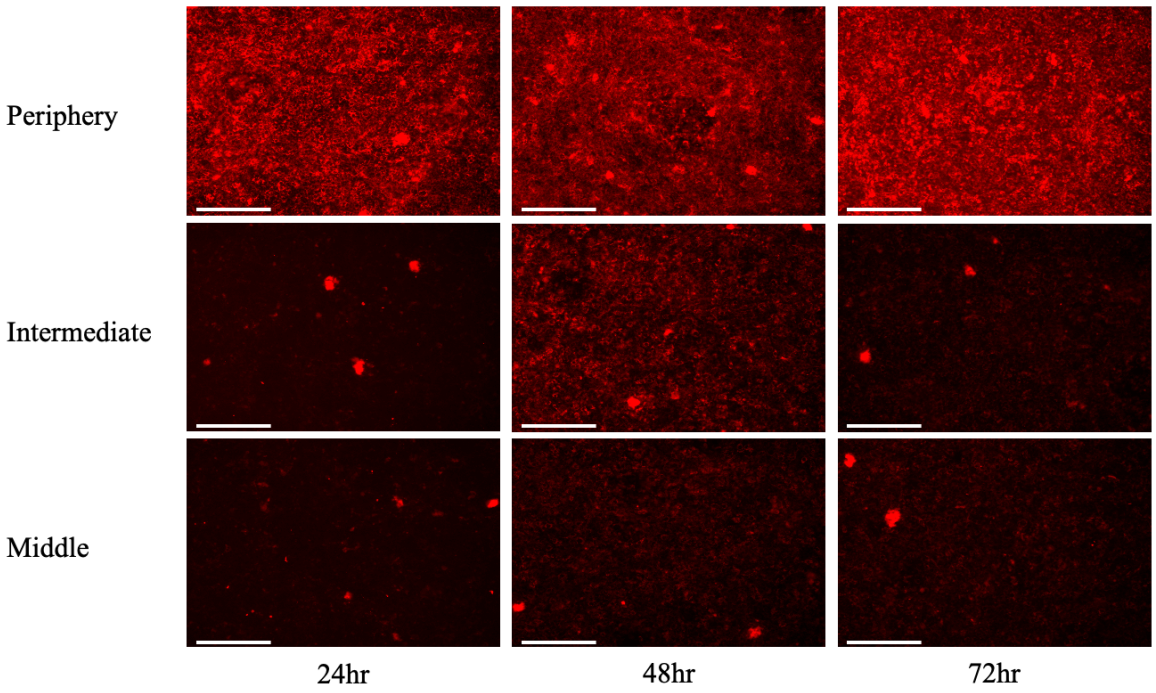

Figure 3.10.2. MCF7 mitochondrial membrane potential was sustained over 72 hours in T-SLICE with a 500 µm spacer height. MCF7 cell spheroids were cultured with 100 nM Mitoview 633 Dye in T-SLICE with a 500 µm spacer height for up to 72 hours at 37˚C, 5% CO_2. Cells were live-imaged at 24-, 48-, and 72-hour timepoints. Images were captured on the EVOS FL Auto 2 Cell Imaging System, Light Cube Cy5 2.0 (Ex: 635 nm, Em: 692 nm). Mitoview 633 dye had the highest levels of accumulation in the peripheral zone and decreased across the intermediate and middle zones of T-SLICE. NIH/3T3 fibroblasts suffered greater loss of M.M.P. than MCF7 cells. Data presented are representative images from three independent experiments. "Middle" = 0 – 3 mm from centre, "Intermediate" = 3 – 6 mm from centre, "Periphery" = 6 – 9 mm from centre. Scale bar = 275 µm.

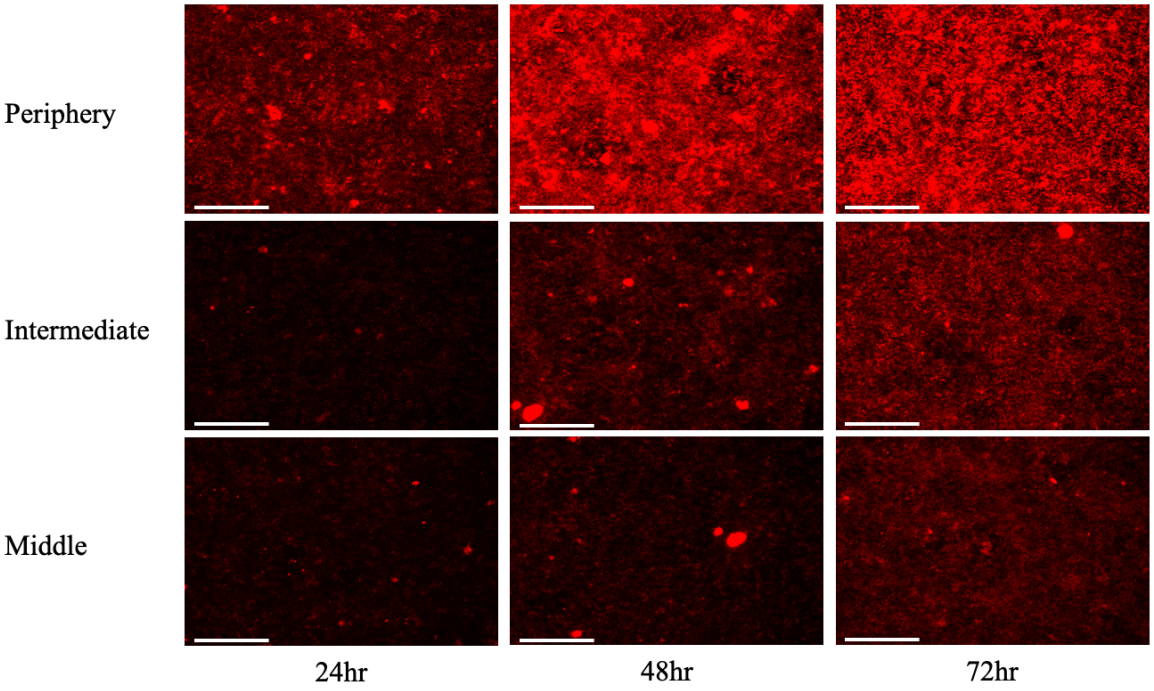

Figure 3.10.3. MCF7 mitochondrial membrane potential was sustained over 72 hours in T-SLICE with a 700 µm spacer height. MCF7 cell spheroids were cultured with 100 nM Mitoview 633 Dye in T-SLICE with a 700 µm spacer height for up to 72 hours at 37˚C, 5% CO_2. Cells were live-imaged at 24-, 48-, and 72-hour timepoints. Images were captured on the EVOS FL Auto 2 Cell Imaging System, Light Cube Cy5 2.0 (Ex: 635 nm, Em: 692 nm). Mitoview 633 dye had the highest levels of accumulation in the peripheral zone and decreased across the intermediate and middle zones of T-SLICE. NIH/3T3 fibroblasts suffered greater loss of M.M.P. than MCF7 cells. Data presented are representative images from three independent experiments. "Middle" = 0 – 3 mm from centre, "Intermediate" = 3 – 6 mm from centre, "Periphery" = 6 – 9 mm from centre. Scale bar = 275 µm.

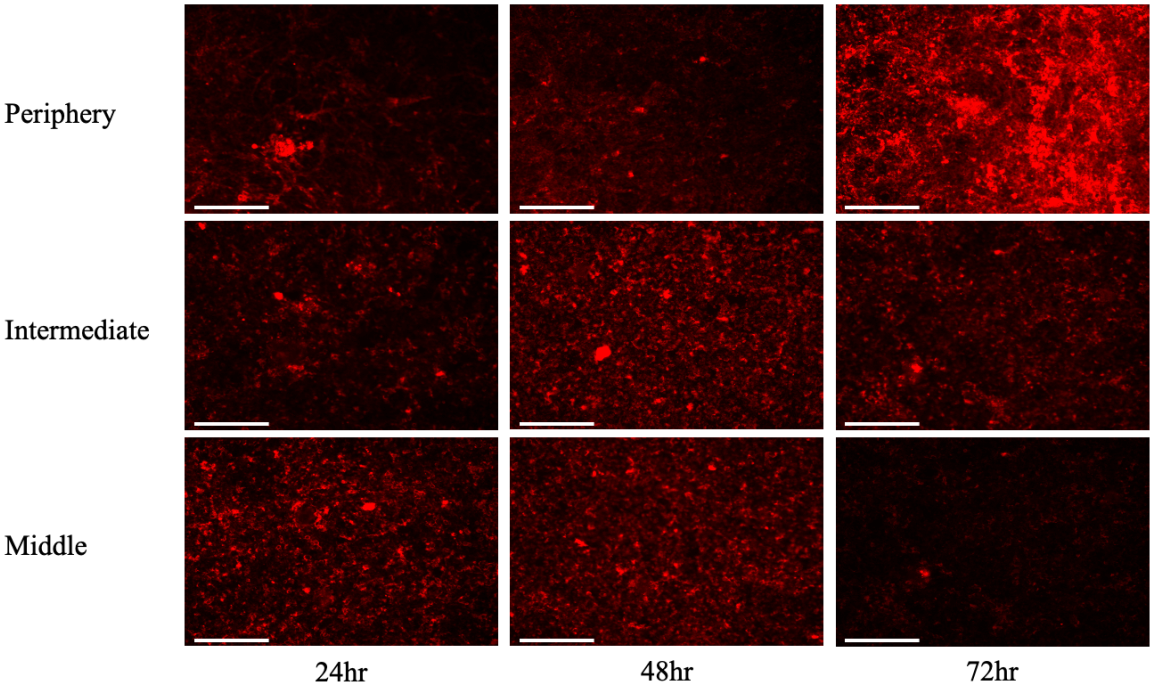

Figure 3.10.4. HCC1806 mitochondrial membrane potential was sustained over 72 hours in T-SLICE with a 300 µm spacer height. HCC1806 cell spheroids were cultured with 100 nM Mitoview 633 Dye in T-SLICE with a 300 µm spacer height for up to 72 hours at 37˚C, 5% CO_2. Cells were live-imaged at 24-, 48-, and 72-hour timepoints. Images were captured on the EVOS FL Auto 2 Cell Imaging System, Light Cube Cy5 2.0 (Ex: 635 nm, Em: 692 nm). Mitoview 633 dye had similar levels of accumulation in the periphery, intermediate, and middle zones of T-SLICE at matched timepoints. NIH/3T3 fibroblasts suffered greater loss of M.M.P. than HCC1806 cells in the intermediate and middle zones. Data presented are representative images from three independent experiments. “Middle” = 0 – 3 mm from centre, “Intermediate” = 3 – 6 mm from centre, “Periphery” = 6 – 9 mm from centre. Scale bar = 275 µm.

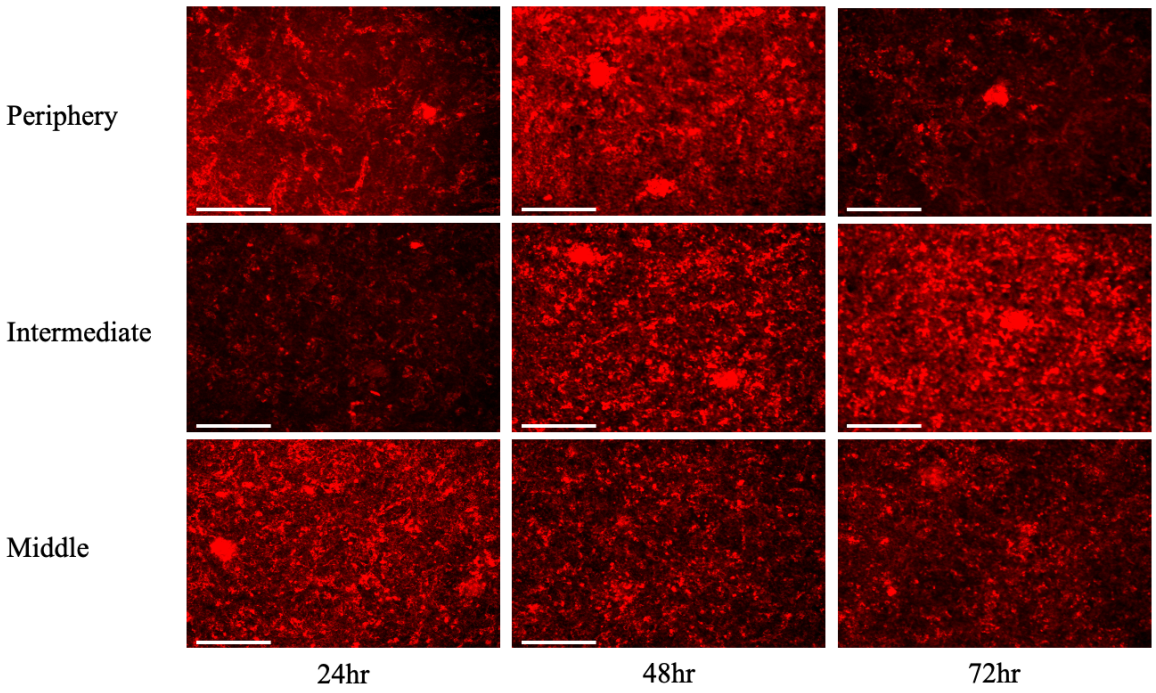

Figure 3.10.5. HCC1806 mitochondrial membrane potential was sustained over 72 hours in T-SLICE with a 500 µm spacer height. HCC1806 cell spheroids were cultured with 100 nM Mitoview 633 Dye in T-SLICE with a 500 µm spacer height for up to 72 hours at 37˚C, 5% CO_2. Cells were live-imaged at 24-, 48-, and 72-hour timepoints. Images were captured on the EVOS FL Auto 2 Cell Imaging System, Light Cube Cy5 2.0 (Ex: 635 nm, Em: 692 nm). Mitoview 633 dye had similar levels of accumulation in the periphery, intermediate, and middle zones of T-SLICE at matched timepoints. NIH/3T3 fibroblasts suffered greater loss of M.M.P. than HCC1806 cells in the intermediate and middle zones. Data presented are representative images from three independent experiments. “Middle” = 0 – 3 mm from centre, “Intermediate” = 3 – 6 mm from centre, “Periphery” = 6 – 9 mm from centre. Scale bar = 275 µm.

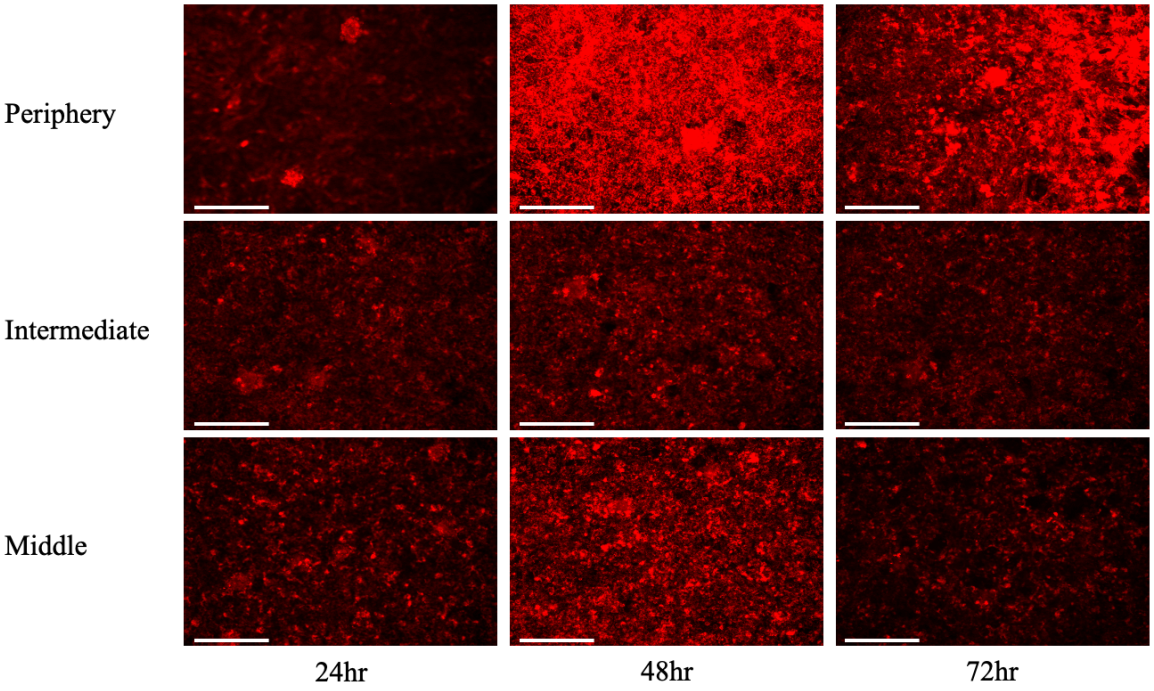

Figure 3.10.6. HCC1806 mitochondrial membrane potential was sustained over 72 hours in T-SLICE with a 700 µm spacer height. HCC1806 cell spheroids were cultured with 100 nM Mitoview 633 Dye in T-SLICE with a 700 µm spacer height for up to 72 hours at 37˚C, 5% CO_2. Cells were live-imaged at 24-, 48-, and 72-hour timepoints. Images were captured on the EVOS FL Auto 2 Cell Imaging System, Light Cube Cy5 2.0 (Ex: 635 nm, Em: 692 nm). Mitoview 633 dye had similar levels of accumulation in the periphery, intermediate, and middle zones of T-SLICE at matched timepoints. NIH/3T3 fibroblasts suffered greater loss of M.M.P. than HCC1806 cells in the intermediate and middle zones. Data presented are representative images from three independent experiments. “Middle” = 0 – 3 mm from centre, “Intermediate” = 3 – 6 mm from centre, “Periphery” = 6 – 9 mm from centre. Scale bar = 275 µm.

3.11 HIF-regulated gene expression differs between MCF7 and HCC1806 breast cancer cell lines cultured in T-SLICE

Hypoxia in the tumour microenvironment plays a major role in shaping tumour biology through the stabilization of hypoxia-inducible factors, which are transcription factors that control a large set of genes with various functions including metabolism, cell survival, and extracellular matrix remodeling (Ye et al., 2018). Changes in HIF-regulated gene expression in response to the hypoxic TME facilitate the invasion, metastasis, and therapeutic resistance of cancer cells (Ye et al., 2018). To assess changes in HIF-regulated gene expression in MCF7 and HCC1806 breast cancer cells cultured in T-SLICE, I selected a set of 25 HIF-regulated genes with established roles in breast cancer progression (Appendix A) to investigate how the hypoxic gradients generated in T-SLICE alters their expression compared to 2D tissue culture in different zones of T-SLICE. I designed sets of primers suitable for qRT-PCR to amplify the genes of interest. *In silico* analysis found that all sets of primers (25 HIF-regulated genes of interest, 2 housekeeping genes) were human-specific. To validate their specificity, I isolated RNA from three separate NIH/3T3 murine fibroblast and MCF7 human breast cancer cell cultures, synthesized cDNA, and performed qRT-PCR to confirm that only genes from the human MCF7 cells were amplified. I found that only eight of the HIF-regulated genes of interest and one housekeeping gene were human-specific and could be used for qRT-PCR analysis in T-SLICE (Figure 3.11.1).

MCF7 and HCC1806 cells were cultured in T-SLICE with a 500 μm spacer height for 6 and 24 hours. I isolated RNA from MCF7 and HCC1806 cells from the middle (0 – 5 mm from the centre) and the edge (5 – 9 mm from the centre) of T-SLICE.

I isolated RNA from MCF7 and HCC1806 cells cultured in 2D tissue culture at matched timepoints. Fold change is normalized to 2D tissue culture at matched timepoints, and gene expression is reported relative to housekeeping gene beta actin.

Glyceraldehyde 3-phosphate dehydrogenase (GAPDH) is a glycolytic enzyme regulated by HIFs and has emerging roles in cancer progression being discovered (Zhang et al., 2015). GAPDH expression was significantly upregulated in MCF7 cells cultured in both zones of T-SLICE after 6 hours and in the middle zone after 24 hours (Figure 3.11.2 A). GAPDH was significantly upregulated in HCC1806 cells cultured in the middle zone of T-SLICE after 6 hours, but no significant differences were found after 24 hours (Figure 3.11.3 A).

Lactate dehydrogenase-A (LDHA) catalyzes the conversion of pyruvate into lactate, which has been shown to increase breast cancer cell proliferation rate, migration, and invasion (Martinez-Ordonez et al., 2021). LDHA expression was significantly upregulated in MCF7 cells in all areas of T-SLICE after 6 and 24 hours (Figure 3.11.2 B). LDHA expression was only significantly higher in the HCC1806 cells cultured in the middle zone of T-SLICE after 6 and 24 hours (3.11.3 B).

Fucosyltransferase 11 (FUT11) is HIF-regulated and stabilizes PDK1 under hypoxic conditions to promote cancer cell proliferation and metastasis (Cao et al., 2021). FUT11 expression was significantly higher in MCF7 cells cultured in all areas of T-SLICE after 6 hours and 24 hours (Figure 3.11.2 C). The only significant change in FUT11 expression in HCC1806 cells cultured in T-SLICE was in the middle zone after 24 hours (3.11.3 C).

MGAT2 is responsible for N-glycosylation and plays a role in oncogenesis. MGAT2 expression was significantly upregulated in MCF7 cells cultured in all zones of T-SLICE after 6 hours, but no significant differences were found after 24 hours (Figure 3.11.2 D). The only significant change in MGAT2 expression in HCC1806 cells was in the middle zone of T-SLICE after 6 hours (Figure 3.11.3 D).

UGT1A1 is involved in estradiol glucuronidation, and studies suggest it may play a role in the etiology of breast cancer (Guillemette et al., 2001). UGT1A1 was significantly upregulated in MCF7 cells cultured around the edge of T-SLICE after 6 hours, but no other significant differences were found in MCF7 or HCC1806 cells (Figure 3.11.2 E) (Figure 3.11.3 E).

Tissue inhibitor matrix metalloproteinase 1 (TIMP1) is an inhibitory molecule that regulates enzymes involved in extracellular matrix remodeling (Cheng et al., 2016). High TIMP1 expression in triple-negative breast cancer has been found to correlate with poor prognosis (Cheng et al., 2016). No significant differences in TIMP1 expression were found in MCF7 cells cultured in T-SLICE after 6 or 24 hours (Figure 3.11.2 F). TIMP1 expression was significantly higher in HCC1806 cells cultured in the middle zone of T-SLICE after 6 and 24 hours (Figure 3.11.3 F).

Urokinase-type plasminogen activator (PLAU) plays important roles in cell-substrate adhesion, tissue migration, and extracellular matrix binding (Chen et al., 2021). No significant differences in PLAU expression in MCF7 cells cultured in T-SLICE were found (Figure 3.11.2 G). PLAU expression was significantly higher in HCC1806 cells cultured in the middle zone of T-SLICE after 6 and 24 hours (Figure 3.11.3 G).

Transforming growth factor beta-3 (TGFB3) is involved in controlling cell proliferation, differentiation, motility, and apoptosis and has been linked with poor breast cancer prognosis (Ghellal et al., 2000). No significant differences in TGFB3 expression were found in MCF7 cells cultured in T-SLICE (Figure 3.11.2 H). TGFB3 was significantly upregulated in HCC1806 cells in the middle zone of T-SLICE after 6 hours (Figure 3.11.3 H).

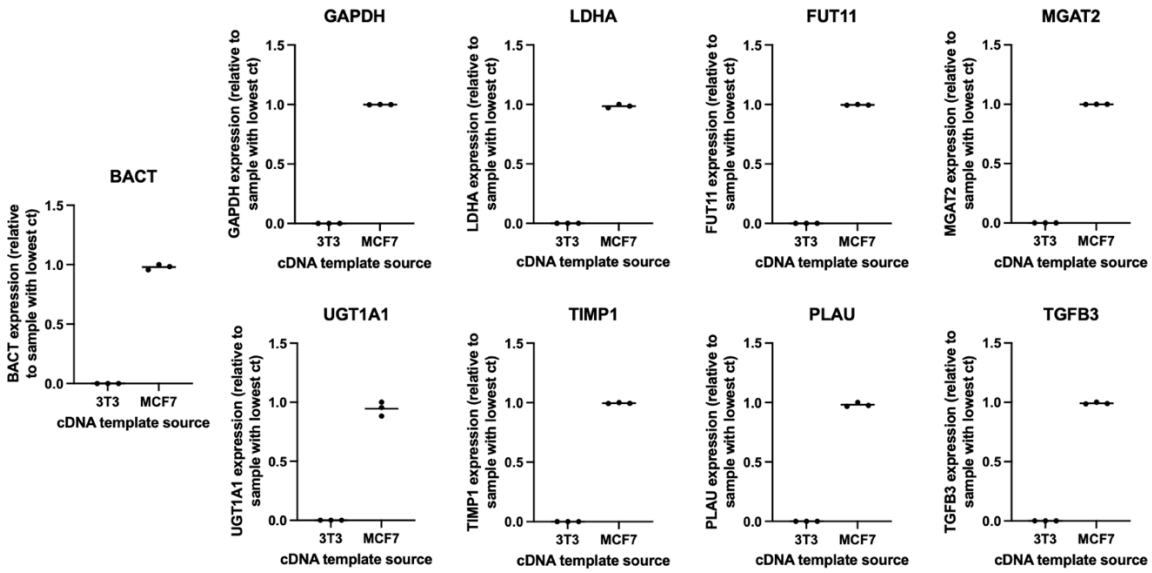

Figure 3.11.1. Validation that primers to investigate HIF-regulated gene expression in T-SLICE are human-specific. A total of 27 sets of primers were tested for their human specificity. NIH/3T3 (murine) and MCF7 (human) cells were cultured for 24 hours at 37°C, 5% CO_2 and had RNA isolated for cDNA synthesis and qRT-PCR analysis to validate human-specificity of the primer sets. 9 of 27 primer sets tested were validated to be human-specific (BACT, GAPDH, LDHA, FUT11, MGAT2, UGT1A1, TIMP1, PLAU, TGFB3).

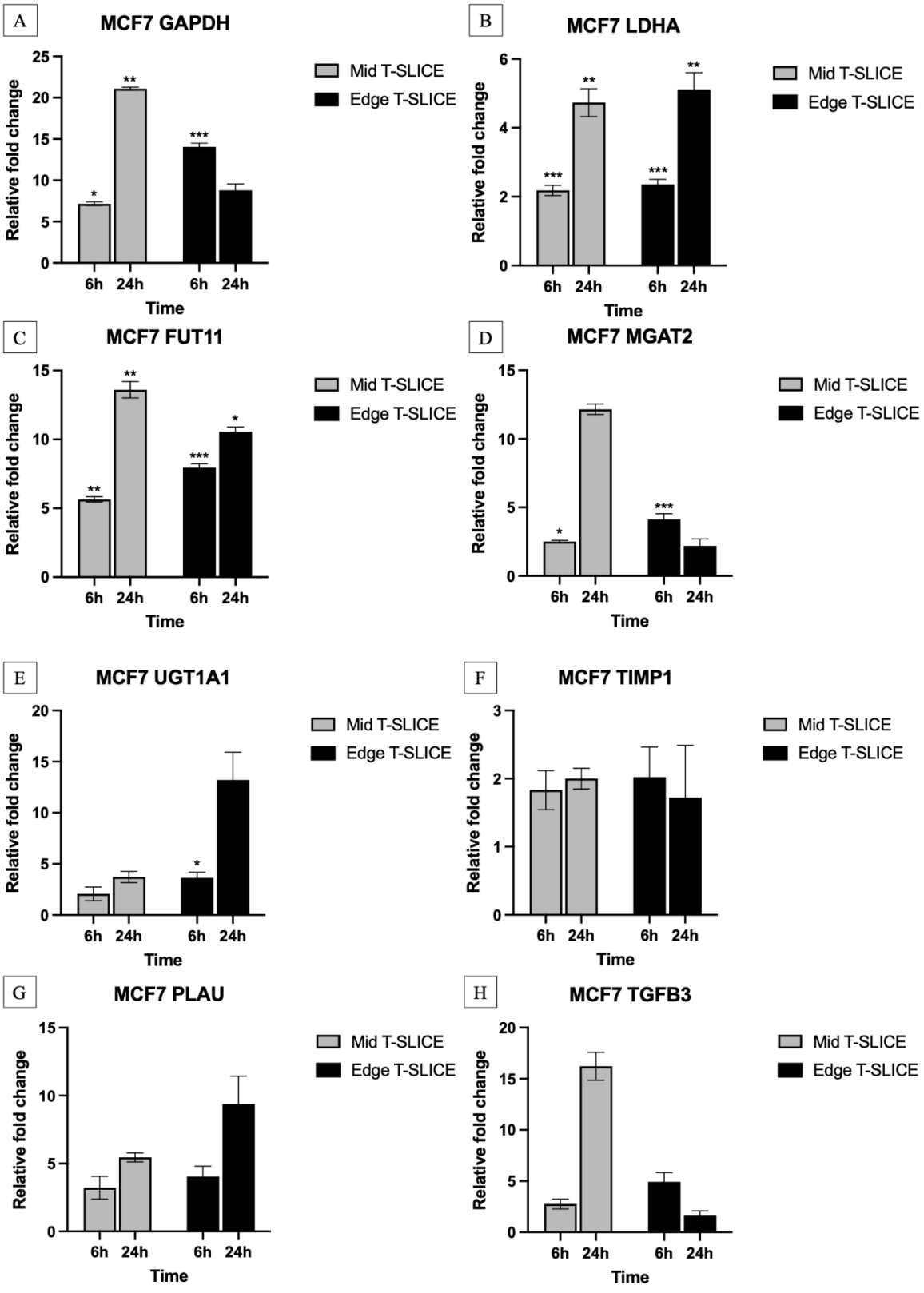
A
MCF7 GAPDH
Relative fold change
Time
6h 24h 6h 24h
Mid T-SLICE
Edge T-SLICE
B
MCF7 LDHA
C
MCF7 FUT11
D
MCF7 MGAT2
E
MCF7 UGT1A1
F
MCF7 TIMP1
G
MCF7 PLAU
H
MCF7 TGFB3

Figure 3.11.2. qRT-PCR analysis of HIF-regulated gene expression in MCF7 cells cultured in T-SLICE with a 500 µm spacer height. MCF7 cell spheroids were cultured in T-SLICE with a 500 µm spacer height for 6 and 24 hours followed by RNA isolation and cDNA synthesis for quantitative Real Time-PCR gene expression analysis. Relative gene expression of GAPDH (A), LDHA (B), FUT11 (C), MGAT2 (D), UGT1A1 (E), TIMP1 (F), PLAU (G), and TGFB3 (H) relative to housekeeping gene BACT in the middle (0-5 mm from centre) and edge of T-SLICE (5-9 mm from centre). Data is normalized to 2D culture at matched timepoints. P-values were obtained with one-way analysis of variance (ANOVA), Dunnett post-test. *$p<0.05$, **$p<0.01$, ***$p<0.001$, ****$p<0.0001$.

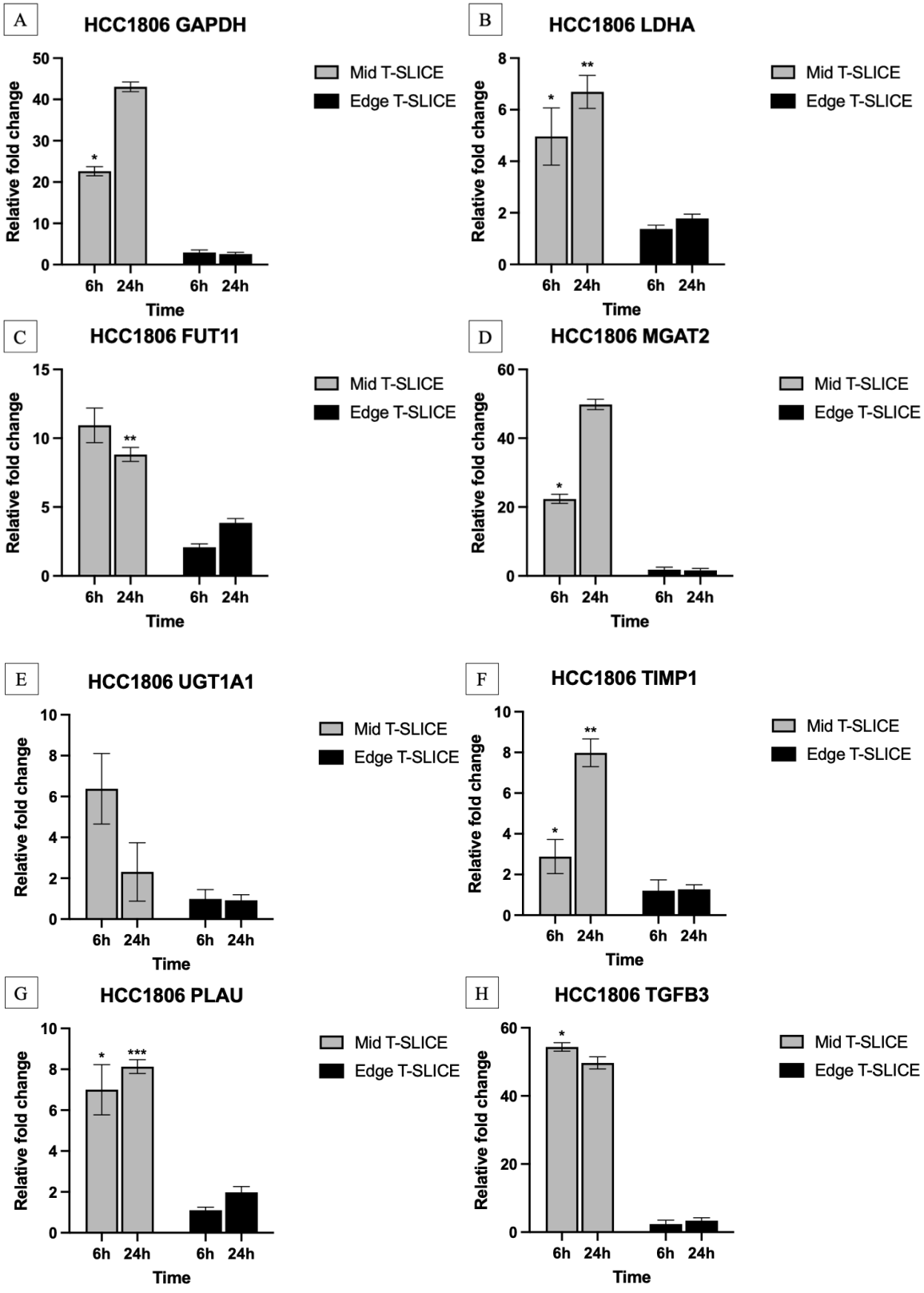
A
HCC1806 GAPDH
Relative fold change
Time
6h 24h 6h 24h
Mid T-SLICE
Edge T-SLICE
B
HCC1806 LDHA
C
HCC1806 FUT11
D
HCC1806 MGAT2
E
HCC1806 UGT1A1
F
HCC1806 TIMP1
G
HCC1806 PLAU
H
HCC1806 TGFB3

Figure 3.11.3. qRT-PCR analysis of HIF-regulated gene expression in HCC1806 cells cultured in T-SLICE with a 500 µm spacer height. HCC1806 cell spheroids were cultured in T-SLICE with a 500 µm spacer height for 6 and 24 hours followed by RNA isolation and cDNA synthesis for quantitative Real Time-PCR gene expression analysis. Relative gene expression of GAPDH (A), LDHA (B), FUT11 (C), MGAT2 (D), UGT1A1 (E), TIMP1 (F), PLAU (G), and TGFB3 (H) relative to housekeeping gene BACT in the middle (0-5 mm from centre) and edge of T-SLICE (5-9 mm from centre). Data is normalized to 2D culture at matched timepoints. P-values were obtained with one-way analysis of variance (ANOVA), Dunnett post-test. *$p<0.05$, **$p<0.01$, ***$p<0.001$, ****$p<0.0001$.

Chapter 4: Discussion

4.1 General overview

Cancer is the leading cause of death in Canada and the number of new cancer diagnoses and deaths continues to rise each year (Brenner et al., 2022). Breast cancer is the most diagnosed cancer in the Canadian female population and is projected to account for 6.5% of all cancer deaths in 2022 (Brenner et al., 2022). Part of what makes breast cancer so difficult to treat is its high level of heterogeneity and development of chemotherapeutic resistance. The tumour microenvironment plays a large role in driving tumour heterogeneity and should be considered when modeling cancer disease *in vitro*. Unfortunately, the commonly used *in vitro* disease modeling methods fail to incorporate important features of the TME, making them unreliable for certain applications such as drug testing. Tumour-on-a-chip (TOAC) devices have made significant progress in modeling the TME *in vitro*, but are often hindered due to their inability to be imaged, tuned, scaled, or used by researchers outside of the laboratory that they were developed in. This research project designed a TOAC device, T-SLICE, to mimic important features of the tumour microenvironment while circumventing common limitations faced in the field of cancer disease modeling.

4.2 T-SLICE overcomes common limitations faced with tumour-on-a-chip devices

Tumour-on-a-chip and microfluidic devices often face one or more of the following limitations: incompatible with live-imaging techniques, inability to be tuned to mimic various physiological environments, poor usability due to high cost or the need for user expertise, low throughput, and low content. These factors were all considered when designing T-SLICE to overcome barriers currently faced in cancer disease modeling.

Table 3.1.1 highlights how these limitations were overcome, which will be discussed in detail in this section.

Optically transparent materials had to be selected to fabricate T-SLICE to maintain its imageability. Glass coverslips are well established cell growth surfaces when downstream staining and imaging analysis is required (Rodig, 2020). Fibronectin is an abundant glycoprotein found in the ECM and is frequently used to make surfaces cell adherent (Ruoslahti, 1984). Integrins on the cell surface bind the RGD (arginine-glycine-aspartic acid) groups of fibronectin and create strong points of attachment (McCarthy et al., 1990). Polydimethylsiloxane (PDMS) is a silicon elastomer that is frequently used in microfluidic device assembly for its desirable cytocompatibility, ease of use, and optical transparency (Borok et al., 2021). I chose to design T-SLICE using two parallel closely spaced glass coverslips separated using PDMS to culture cells in the space between the glass coverslips. This was achieved by PDMS soft lithography in 3D-printed molds followed by attaching a glass coverslip to the underside of the PDMS to make the device oxygen impermeable. I used plasma oxidation to bond the glass coverslip to the PDMS, which occurs by generating reactive chemical groups on the surface of the PDMS and glass coverslip to form irreversible covalent bonds between the two substrates (Borok et al., 2021). Creating T-SLICE using PDMS soft lithography makes the fabrication process easily and rapidly tunable. The spacer height or dimensions of T-SLICE can be adjusted by editing the design of the 3D-printed mold in CAD software, which can be accomplished in a matter of minutes for a user who is familiar with the CAD software.

High cost and the need for user expertise limits the widespread use of many TOAC and microfluidic devices. T-SLICE was designed using readily accessible,

inexpensive materials to give other life sciences laboratories the opportunity to use it in the future. The total cost to make one T-SLICE device is approximately $1.50; the breakdown of this cost is $0.10 of resin is used to make the 3D-printed mold, $0.10 for a circular glass coverslip, and between $1.00 - $1.30 of PDMS. The 3D-printed molds and the T-SLICE devices have been reused for up to 6 months. Any laboratory interested in using T-SLICE will need to invest in a MSLA 3D resin printer, which can be purchased for $300 - $500. The only additional costs are 6-well plates, reagents for the desired experiments, and a CO_2 incubator, all of which are already required for any cell culture technique. T-SLICE was also designed to be user friendly by incorporating commonly used 2D and 3D cell culture techniques (Imamura et al., 2015; Imparato et al., 2015). The combination of cost effectiveness with usability makes T-SLICE highly accessible, giving it the potential to be used to model cancer and other hypoxic conditions in many life sciences laboratories.

The final main design considerations for T-SLICE were to make it high content and high throughput. As discussed previously, the optical transparency of T-SLICE offers the ability to perform live-cell imaging. This design feature can be useful in terms of being high content. Researchers can make similar reporter cell lines to the hypoxia reporter 5HRE/GFP-MCF7 cell line used in this study (Section 3.5) to investigate spatiotemporal dynamics of cancer progression. Imaging-based assay modalities can be paired with biochemical -omic assays (e.g., transcriptomic, metabolomic) to collect a large amount of information from a single T-SLICE culture. Performing qRT-PCR (Section 3.11) was the first non-imaging-based assay performed in T-SLICE. Harvesting cells from T-SLICE was more technically challenging than cell staining followed by

microscopy, but future research will be directed at optimizing these protocols and identifying compatible biochemical assays. One of the ways that T-SLICE is high throughput is due to its low cell number requirement. Only 1.0 – 2.0 x 10^4 breast cancer cells were needed to generate enough spheroids (i.e., 192) for T-SLICE. This number is significantly lower than similar TOAC devices capable of generating the same biochemical gradients, which require 1.5-10 x 10^6 cells per construct (Rodenhizer et al., 2016). This research group acknowledged the high cell number requirement of their device and was able to reduce it by 66%, however this still requires a minimum of 0.5 x 10^6 cancer cells per construct (Landon-Brace et al., 2021). The low number of cancer cells required for T-SLICE culture make it favourable for studying primary tumour samples that may only be available in very limited quantities.

4.3 5HRE/GFP-MCF7 cells demonstrate that hypoxia gradients are generated in T-SLICE as early as 3 hours into culture

Given the biological significance of hypoxia in the TME influencing cancer cell behaviours, I prioritized a robust characterization of cellular hypoxic response in T-SLICE in this research project. The aberrant vascularization within the TME results in the generation of hypoxic regions within solid tumours, which are often observed in their core (Petrova et al., 2018). Cancerous and non-cancerous stromal cells undergo HIF-mediated transcriptional responses to adapt their metabolism and growth rate to suit the stressful environmental conditions (Petrova et al., 2018). I created a hypoxia reporter 5HRE/GFP-MCF7 cell line in this project to assess MCF7 hypoxic response in T-SLICE (section 3.5). I also used EF5 to demonstrate hypoxia gradients were sustained in T-SLICE for extended periods of culture (section 3.6). I finalized hypoxia characterization

in T-SLICE by performing HIF1a/HIF2a immunofluorescent staining of MCF7 and HCC1806 cells cultured in T-SLICE (Section 3.7).

5HRE/GFP MCF7 cells were cultured in T-SLICE with spacer heights ranging from 300 µm to 700 µm for up to 24 hours to assess the generation of hypoxic gradients in T-SLICE. Vordermark et al. (2001) created the 5HRE/GFP plasmid with an enhanced green fluorescent protein (eGFP) that does not have the same oxygen requirement for chromophore formation as standard GFP. The plasmid contains the hypoxia-responsive 5HRE-hCMVmp promoter to drive eGFP expression when cells undergo a hypoxic response (Vordermark et al., 2001). I detected fluorescence in the 5HRE/GFP-MCF7 cells as early as three hours into T-SLICE culture, which indicates hypoxia. Fluorescence intensity was strongest in MCF7 cells cultured in the middle zones of T-SLICE for the first 12 hours of culture (Figure 3.5.1). These findings were expected since T-SLICE was predicted to generate a diffusion-limited hypoxia gradient with the greatest depletion of oxygen in the middle of the device. Unexpectedly, fluorescence intensity became greater in the periphery of T-SLICE with a 500 µm and 700 µm spacer height compared to the middle zone after 24 hours (Figure 3.5.1). Fluorescence intensity also gradually decreased over 24 hours, suggesting hypoxia gradients were not being sustained in T-SLICE. One possible explanation for this is that despite the lower O_2 requirement for chromophore formation of eGFP compared to GFP, it still requires approximately 0.02% oxygen for efficient formation (Vordermark et al., 2001). If T-SLICE generates zones of anoxia this could explain why fluorescence is lost after 24 hours. This is unlikely given that MCF7 cells remain viable in the middle zone of T-SLICE with a 500 µm and 700 µm spacer height for up to 72 hours (section 3.8). Tumour lactic acidosis is frequently

observed in the TME of solid tumours as lactate accumulates, dropping the pH below 6.5 (Fischbeck et al., 2020). Green Fluorescent Protein (and eGFP) has a pK_a of ~6.0 and is considered acid-sensitive since its fluorescent signal is quenched when pH drops below 6.0 (Shinoda et al., 2018). It is possible that the most hypoxic zones of T-SLICE become acidic over 24 hours, which could help explain why a loss of eGFP signal is observed in 5HRE/GFP-MCF7 cells over 24 hours. The qRT-PCR data presented in section 3.11 (Figure 3.11.2) supports this reasoning since LDHA expression was significantly increased compared to 2D cell culture after 6h and 24h of T-SLICE culture. Lactate dehydrogenase A converts pyruvate to lactate, leading to acidification (Martinez-Ordonez et al., 2021). The idea that fluorescence quenching is occurring is more plausible than the hypoxia gradients being lost over just 24 hours. A solution to this problem is to clone an acid-tolerant fluorescent protein (e.g., Sirius (pK_a <3.0), pLSSmKate2 (pK_a 2.7)) into the 5HRE backbone to prevent signal quenching as pH decreases (Shinoda et al., 2018). The 5HRE/GFP-MCF7 cell line was useful in this project for analyzing initial cellular hypoxic response in T-SLICE, but an alternate method was required to confirm hypoxia gradients were sustained over extended culture periods.

4.4 EF5 assay confirms that hypoxia gradients are sustained in T-SLICE over 48 hours

EF5 is a 2-nitroimidazole compound that can be used to detect cellular hypoxic response (Lord et al., 1996). It is frequently used *in vivo* to detect tissue hypoxia in animal studies but has been used *in vitro* to quantify O_2 partial pressure in TOAC devices (Rodenhizer et al., 2016). EF5 can be used *in vitro* by adding the compound to cell culture medium and culturing cells in its presence for the duration of culture. EF5 is reduced in hypoxic cells to form adducts at the cell membrane, which can then be labeled

with a fluorophore conjugated anti-EF5 antibody (Koch, 2002). I cultured MCF7 and HCC1806 breast cancer cell spheroids in T-SLICE in the presence of 10 μM EF5 for up to 48 hours and assessed EF5 adduct formation after 6, 12, 24, and 48 hours. EF5 adducts were labeled with a Cy3 conjugated anti-EF5 antibody and imaged on the EVOS FL Auto 2 Cell Imaging System to assess hypoxia gradients in T-SLICE.

EF5 fluorescence intensity in MCF7 cells increased gradually in the intermediate and middle zone of T-SLICE with a spacer height of 300 μm, 500 μm, and 700 μm over 48 hours (Figures 3.6.1 – 3.6.3). EF5 detection in MCF7 cells was lower in the periphery compared to the intermediate and middle zones of T-SLICE. These findings were expected since the intermediate and middle zones of T-SLICE were predicted to become hypoxic as oxygen is unable to diffuse into the centremost regions of the device. One unexpected finding was that the EF5 detection in the intermediate and middle zones of T-SLICE were similar at matched timepoints, indicating equal degrees of hypoxia in these two zones. This could be explained by the linear relationship that exists between O_2 tension and EF5 binding over 0.1% - 10% O_2 tension (Koch, 2002). EF5 binding no longer fits this linear relationship when O_2 tension drops below 0.1%. It is possible that steep O_2 gradients are generated in T-SLICE with the centremost regions nearing anoxia. Our findings differ from those of Rodenhizer and colleagues (2016), who were able to demonstrate a gradual increase in EF5 binding in their TOAC device.

EF5 fluorescence intensity in HCC1806 cells increased sharply in the intermediate and middle zone of T-SLICE with a spacer height of 300 μm, 500 μm, and 700 μm after 12 hours and were sustained over 48 hours (Figures 3.6.4 – 3.6.6). EF5 detection in HCC1806 cells in the periphery was nearly absent until 48 hours into T-

SLICE culture. These findings differ from those in MCF7 cells that had a more gradual increase in hypoxic response. Another interesting finding is that EF5 fluorescence intensity was stronger in HCC1806 cells compared to MCF7 cells cultured in T-SLICE with matched spacer heights at matched timepoints (Figures 3.6.1 – 3.6.6). Studies have found that basal-like breast cancer expresses a different set of genes and at different levels of expression than luminal breast cancers, which could explain why we observe a more intense hypoxic response in the HCC1806 cells compared to MCF7 cells in T-SLICE (Ye et al., 2018). Regardless, EF5 demonstrated that hypoxia gradients were being generated and sustained in T-SLICE over 48 hours, which was ultimately the goal of this assay. The next step was to characterize how these hypoxic responses were being mediated over the course of 48 hours.

4.5 The dynamics of HIF expression were not captured using immunofluorescence staining, but discrete changes were detected

Cellular hypoxic responses are mainly attributed to hypoxia-inducible factors (HIFs) (Semenza, 2012). Hypoxia-inducible factors are transcription factors that contain an oxygen-sensitive alpha subunit that is transiently activated when cells are exposed to a low oxygen environment, and a beta subunit (HIF1b) that is constitutively expressed (Semenza, 2012). HIFa and HIF1b subunits dimerize when cells are under hypoxic stress to help the cells adjust to the stressful environment. HIF1a and HIF2a are important alpha subunits in the cellular response to hypoxic stress. HIF1a is typically involved in the acute response to hypoxia (0 - 24 hours) and HIF2a is involved in the chronic response to hypoxia (24 - 72 hours). I cultured MCF7 and HCC1806 breast cancer cell spheroids in T-SLICE for up to 48 hours and performed immunofluorescent staining to investigate

how HIF1a and HIF2a expression fluctuates over time. I predicted that HIF1a would have highest expression in the first 24 hours of T-SLICE culture and HIF2a would have highest expression after 24 and 48 hours.

HIF1a expression peaked in the first 12 – 24 hours in MCF7 cells cultured in T-SLICE depending on the spacer height of the device (Figures 3.7.1 – 3.7.3). Higher levels of expression were observed in the middle and intermediate zones of T-SLICE than around the periphery. HIF2a expression also peaked in MCF7 cells in the first 12 hours of T-SLICE culture (Figures 3.7.1 – 3.7.3). It should also be noted that HIF2a expression was similar among the periphery, intermediate, and middle zones of T-SLICE. These findings were both unexpected since HIF2a is reported to be involved in the chronic response to hypoxia and the EF5 assay did not detect hypoxia in the periphery of T-SLICE, especially within the first 12 hours.

HIF1a expression was relatively absent in HCC1806 cells cultured in T-SLICE, irrespective of spacer height or region within the device (Figures 3.7.4 – 3.7.6). HCC1806 HIF2a expression was highest in the periphery of T-SLICE and remained constant over 48 hours. These findings were unexpected since the EF5 assay suggested the most robust hypoxic response in HCC1806 cells cultured in the intermediate and middle zones of T-SLICE compared to the periphery. One of the difficulties associated with immunostaining HIF1a and HIF2a is their transient nature. A 2014 study by Bagnall et al. cultured HeLa cells under continuous hypoxic conditions to investigate the temporal dynamics of HIF1a and HIF2a expression. They found that HIF1a and HIF2a are both transiently expressed in 3-hour pulses (Bagnall et al., 2014). They concluded that these transient bursts of HIF1a/HIF2a signaling have important roles in cell survival under

hypoxic conditions in diseases such as cancer. The transient bursts of HIF1a and HIF2a signaling could explain the difficulty detecting their expression in T-SLICE. Detection methods could be optimized in the future to better characterize how hypoxic responses are being mediated in cells cultured in T-SLICE. Given the results from the 5HRE/GFP-MCF7 and EF5 assays, I concluded that hypoxia gradients were generated and sustained in T-SLICE and investigated tumour cell behaviours in response to hypoxia.

4.6 Cell viability, cell proliferation, and mitochondrial membrane potential are impacted by hypoxia gradients generated in T-SLICE

After demonstrating that hypoxia gradients are generated and sustained in T-SLICE, I assessed how they impact cell viability, cell proliferation, and mitochondrial membrane potential in MCF7 and HCC1806 breast cancer cell lines. Tumour cells adapt to hypoxia to upregulate pro-survival genes, but if O_2 tension is too low the cancer cells are unable to compensate for such a lack of oxygen and die, resulting in the generation of a necrotic core in some poorly vascularized tumours (Nejad et al., 2021). One of the hypoxic responses of cancer cells is to decrease their proliferation rate (Zhang et al., 2018). Hypoxia also leads to the loss of mitochondrial membrane potential, which is a hallmark of cells preparing to undergo apoptosis (Zhao et al., 2018).

MCF7 and HCC1806 cells were cultured in T-SLICE with 300 µm, 500 µm, and 700 µm spacer heights for 72 hours and subsequently stained with a live/dead assay. Very high MCF7 and HCC1806 cell viability was observed in the periphery, intermediate, and middle zones of T-SLICE with a 500 µm and 700 µm spacer height (Figures 3.8.1 – 3.8.2). MCF7 cell spheroids cultured in the middle zone of T-SLICE with a 300 µm spacer height were all dead after 72 hours (Figure 3.8.1). HCC1806 cell spheroids were

able to better resist the steep hypoxia gradients generated in the middle of T-SLICE with a 300 μm spacer height and survived despite high levels of cell death in surrounding fibroblasts (Figure 3.8.2). Studies have identified differences in hypoxic responses of basal-like (e.g., HCC1806) and luminal-type (e.g., MCF7) breast cancer cell lines, which could help explain the differences that we observe in their ability to survive under steep oxygen gradients (Ye et al., 2018).

MCF7 and HCC1806 cells were cultured in T-SLICE with 300 μm, 500 μm, and 700 μm spacer heights for 72 hours in the presence of EdU and subsequently labeled for EdU detection. MCF7 and HCC1806 cell proliferation was inhibited in the middle, most hypoxic zone of T-SLICE regardless of spacer height (Figures 3.9.1 – 3.9.2). MCF7 cell proliferation rate in the periphery of T-SLICE increased with spacer height (Figure 3.9.1), indicating that by simply adjusting spacer height to modify the steepness of the hypoxia gradients is sufficient to have an impact on cell response. Similar results were found in a study by Zhang and colleagues (2018) that assessed how simulated hypoxia in MCF7 cells impacts cell proliferation rate. They determined that hypoxia inhibits MCF7 cell proliferation and promotes migration (Zhang et al., 2018). In a primary tumour, this would allow breast cancer cells to escape the stressful TME of the primary tumour site and metastasize. Many systemic chemotherapeutics take advantage of the increased cell proliferation rate of cancer cells than healthy cells, but their effectiveness is limited when hypoxia in the TME decreases cell proliferation rate. The ability to recapitulate this tumour cell response in T-SLICE will be important for anti-cancer drug testing in T-SLICE in the future.

MCF7 and HCC1806 cells were cultured in T-SLICE with 300 μm, 500 μm, and 700 μm spacer heights for 72 hours in the presence of 100 nM Mitoview 633 Dye. Mitoview 633 accumulates in mitochondria in a membrane potential-dependent mechanism and loss of mitochondrial membrane potential (M.M.P.) leads to the loss of dye accumulation in the mitochondria. In general, MCF7 cells suffered a loss of M.M.P. in the intermediate and middle zones of T-SLICE over 72 hours, which correlate with the areas of most intense hypoxia (Figures 3.10.1 – 3.10.3). Other studies investigating M.M.P. in MCF7 cells have found that loss of M.M.P. correlates with MCF7 cells entering apoptosis (Shahali et al., 2018). The loss of M.M.P. in MCF7 cells under hypoxic stress is indicative of a shift in metabolism to adapt to their nutrient- and oxygen-limited surroundings. HCC1806 cells had sustained M.M.P. over 72 hours regardless of T-SLICE spacer height (Figures 3.10.4 – 3.10.6). Studies investigating different breast cancer subtypes have found that TNBC have increased expression of HIF-regulated genes relative to luminal-type breast cancers, many of which are involved in cell metabolism (Chaturvedi et al., 2014; Ye et al., 2018). This could help explain why M.M.P. appears to be more impacted in MCF7 cells compared to HCC1806 cells. Another interesting observation is that NIH/3T3 fibroblast M.M.P. was lost over 72 hours in T-SLICE culture, regardless of the breast cancer cell line that they were cultured with (Figures 3.10.1 – 3.10.6). Hypoxia has been shown to deplete mitochondrial membrane potential in human uterosacral ligament fibroblasts (Zhao et al., 2018). This is important to note because it demonstrates that the biochemical gradients generated in T-SLICE impact all cells cultured within the device, which is similar to what is observed in a natural tumour with a stromal cell compartment. It is important to analyze all assays

collectively to gain an understanding of how the biochemical gradients generated in T-SLICE impact breast cancer cell responses. This will be discussed further in the conclusion of this thesis.

4.7 HIF-regulated gene expression varies between MCF7 and HCC1806 cell lines

I assessed differences in HIF-regulated gene expression between MCF7 and HCC1806 cells cultured in T-SLICE with a 500 μm spacer height as the final experiment in this research project. MCF7 and HCC1806 cells were cultured in T-SLICE for 6 and 24 hours prior to RNA isolation for downstream qRT-PCR analysis. RNA was isolated from the middle (0 – 5 mm from centre) and the edge of T-SLICE (5 – 9 mm from centre). Eight target genes were analyzed for changes in relative expression normalized against beta-actin from cells cultured in 2D cell culture at matched timepoints.

Glyceraldehyde-3-phosphate dehydrogenase (GAPDH) is a glycolytic enzyme that is regulated by HIFs and nitric oxide (Zhang et al., 2015). Emerging roles of GAPDH in breast cancer progression are being discovered. GAPDH was significantly upregulated in MCF7 cells cultured around the edge and middle of T-SLICE after 6 hours, with greater expression around the edge than the middle, but only in the middle after 24 hours (Figure 3.11.2 A). This was different in HCC1806 cells, which only had a significant increase in the middle zone of T-SLICE after 6 hours (Figure 3.11.3 A). It should be noted that the relative fold change of GAPDH in HCC1806 cells was roughly a 40-fold increase relative to 2D culture, but this value was insignificant due to high variation among replicates. A study by Higashimura and colleagues (2011) also observed a hypoxia-induced upregulation of GAPDH in MCF7 cells, supporting the findings in this study. The higher baseline expression of glycolytic enzymes (e.g., GAPDH) in TNBC

relative to luminal-type breast cancer could explain why the change in GAPDH expression in HCC1806 cells cultured in T-SLICE for 24 hours is not significant relative to 2D cell culture (Chaturvedi et al., 2014; Ye et al., 2018).

Lactate dehydrogenase-A (LDHA) catalyzes the conversion of pyruvate into lactate, which has been shown to increase breast cancer cell proliferation rate, migration, and invasion (Martinez-Ordonez et al., 2021). It is also implicated in the conversion of stromal fibroblasts to CAFs in the TME. LDHA was significantly upregulated in MCF7 cells cultured in the middle and edge of T-SLICE after 6 and 24 hours (Figure 3.11.2 B). HCC1806 cells only had a significant increase in LDHA expression in the middle zone of T-SLICE after 6 and 24 hours (Figure 3.11.3 B). These findings support the EF5 assay data that found MCF7 cells cultured around the periphery displayed a slight hypoxic response, but HCC1806 cells in the periphery of T-SLICE did not display a hypoxic response in the first 24 hours. This could explain why there is no significant increase in LDHA expression in HCC1806 cells cultured around the edge of T-SLICE.

Fucosyltransferase 11 (FUT11) is a HIF1a-regulated gene that stabilizes PDK1 under hypoxic conditions to promote proliferation and metastasis (Cao et al., 2021). FUT11 expression in MCF7 cells was significantly increased in the middle and edge zones of T-SLICE after 6 and 24 hours but was only significantly upregulated in HCC1806 cells cultured in the middle of T-SLICE after 24 hours (Figures 3.11.2 C, 3.11.3 C). Like LDHA, this finding correlates with the EF5 data that did not observe hypoxic responses in HCC1806 cells cultured around the periphery of T-SLICE within the first 24 hours. Ye and colleagues (2018) were the first group to identify changes in FUT11 expression in a HIF-dependent manner and research has since shifted to assess its

potential to be a clinical biomarker of hypoxia in breast cancer. This group also demonstrated that MCF7 cells cultured under hypoxia increase FUT11 expression more than several other breast cancer cell lines (Ye et al., 2018).

Tissue inhibitor of metalloproteinases-1 (TIMP1) regulates the function of enzymes involved in ECM remodeling. (Cheng et al., 2016). TIMP1 expression correlates with poor prognosis in TNBC (Cheng et al., 2016). No significant differences were found in TIMP1 expression in MCF7 cells cultured in the middle or edge zones of T-SLICE compared to 2D culture (Figure 3.11.2 F). HCC1806 cells had significantly increased expression of TIMP1 in the middle zone of T-SLICE after 6 and 24 hours relative to 2D culture (Figure 3.11.3 F). These findings are supported in the literature that have reported higher levels of TIMP1 expression in TNBC cell lines compared to hormone receptor positive breast cancer cell lines (Cheng et al., 2016).

Urokinase-type plasminogen activator (PLAU) plays important roles in cell-substrate adhesion, tissue migration, and extracellular matrix binding (Chen et al., 2021). No significant differences in expression were found between MCF7 cells cultured in T-SLICE and 2D culture (Figure 3.11.2 G). HCC1806 cells cultured in T-SLICE were found to have significantly increased expression of PLAU in the middle zone of T-SLICE after 6 and 24 hours relative to 2D culture (Figure 3.11.3 G). PLAU has not been heavily investigated in breast cancer but has been shown to be upregulated in head and neck squamous cell carcinoma and lung cancer (Chen et al., 2021). PLAU is necessary for tumour progression and metastasis and further studies into its role in breast cancer may be warranted. Given its upregulation in HCC1806 cells cultured in the most hypoxic

regions of T-SLICE, it is plausible that PLAU could be facilitating the migration of cells from the hypoxic TME to a more oxygenated area with less environmental stressors.

Transforming growth factor beta 3 (TGFB3) controls cell proliferation, differentiation, and motility and is associated with poor breast cancer prognosis (Ghellal et al., 2000). The only statistically significant difference in TGFB3 expression was in HCC1806 cells cultured in the middle of T-SLICE for 6 hours (Figure 3.11.3 H). Despite this, increased expression is observed in both MCF7 and HCC1806 cells cultured in the middle zone of T-SLICE for 6 and 24 hours compared to 2D culture (Figures 3.11.2 H, 3.11.3 H). These increases in gene expression were likely not statistically significant due to large variation among replicates. A 2009 study by Dunn et al. identified a synergistic relationship between hypoxia and TGFB3 signaling to promote bone metastasis in breast cancer. Future studies could investigate if breast cancer cells cultured in the middle of T-SLICE also upregulate the expression of metastatic markers along with TGFB3 to further elucidate tumour cell responses to hypoxia.

The HIF-regulated gene expression analysis in T-SLICE demonstrates that breast cancer cell lines derived from different breast cancer subtypes can have different responses to environmental stimuli in the TME. This is similar to what is observed *in vivo* between basal-like and luminal breast cancers, which have different propensities to invade, metastasize, and become resistant to therapy. Isolating cells from distinct locations in T-SLICE was technically challenging and could explain some of the large variation observed in the expression of certain genes among biological replicates. Future work will focus on refining biochemical assays to facilitate the integration of -omics-

based data into T-SLICE assay modalities. This will be further discussed under the current limitations of T-SLICE.

4.8 Limitations

This research project was largely focused on the design and fabrication of T-SLICE and characterizing breast cancer cell responses to biochemical gradients analogous to those observed in the TME. T-SLICE generates cell-driven hypoxia gradients analogous to those observed *in vivo* and other TOAC and microfluidic devices designed to generate hypoxia gradients (Rodenhizer et al., 2016; Grist et al., 2019; Ayuso et al., 2016). The cell responses to the hypoxia gradients in T-SLICE match those observed in these TOAC and microfluidic devices, too. One of the limitations of this study is that it did not incorporate many biophysical features of the TME into its design. Culturing the MCF7 and HCC1806 breast cancer cells as spheroids in T-SLICE captured some 3D cell-cell interaction that is absent in 2D tissue culture. Biophysical cues in the TME shape tumour progression and metastasis and should be a focus of future work on optimizing T-SLICE to be as biomimetic as possible of the *in vivo* TME (Emon et al., 2018). One of the other limitations in the current design of T-SLICE is that it uses fibroblasts and cancer cell spheroids isolated from different species. This was useful for qRT-PCR analysis by enabling the selective amplification of human templates but does not capture the full spectrum of fibroblast-cancer cell communication. Given the importance of fibroblast-cancer cell communication in the TME, a single species version of T-SLICE (i.e., fibroblasts and cancer cells both derived from human) should be developed in the near future. This should not have much impact on the biochemical gradients generated within T-SLICE.

A hydrogel could be developed and incorporated into T-SLICE to be more representative of the biophysical environment in the TME. To model breast cancer in T-SLICE, the hydrogel should be collagenous and stiff to match the mechanical properties of the fibrotic ECM in cancerous breast tissue (Jiang et al., 2022). In addition to stiffness, the porosity and biochemistry of the hydrogel should be considered and matched to that of the ECM *in vivo*. Fisher et al. (2015) used hyaluronan-based hydrogels to study cell-substrate adhesion and ECM remodeling in breast cancer. Incorporating MMP-sensitive sequences in the hydrogel is important to permit the investigation of ECM remodeling by the cancer cells and their invasive and metastatic phenotypes (Park et al., 2018). Adding a hydrogel to T-SLICE will facilitate the investigation of other cell types (e.g., endothelial cells, immune cells) and their responses to the biochemical gradients generated in the device. This could include endothelial cell migration and organization into tubules to vascularize the hypoxic zones of T-SLICE or assessing immune cell infiltration and function under different biochemical pressures. Incorporating a hydrogel to mimic the ECM in T-SLICE will also enable research into how the biochemical gradients established in T-SLICE impact cancer cell invasion.

Despite the widespread use of PDMS in microfluidic device fabrication, it still faces several drawbacks. One of the main disadvantages of using PDMS for microfluidic device fabrication is its ability to absorb hydrophobic small molecules (Toepke & Beebe, 2006). This is an important issue to consider when conducting drug testing in microfluidic devices made using PDMS since approximately 40% of drugs on the market are hydrophobic (Larraneta et al., 2018). T-SLICE will be used for anti-cancer drug testing in the future, so investigation into alternate materials for device design could be

warranted. Substantial research efforts have been put forth in the last few years to find substitute polymers for microfluidic device fabrication. Polyester elastomers, tetrafluoroethylene-propylene elastomers, and thermoplastic elastomers are all optically transparent and have far lower absorption of hydrophobic small molecules compared to PDMS (Campbell et al., 2021). These alternative materials are faced with their own set of limitations, including high cost, inability to scale, and difficulty to assemble (Campbell et al., 2021). Future design considerations will be discussed in subsection 4.9 (future directions).

4.9 Future directions

It is important to consider the results in this research project before rejecting PDMS as a suitable polymer for drug testing in T-SLICE. One finding that supports the use of PDMS in T-SLICE is the characterization of hypoxia using EF5 (Figures 3.6.1 – 3.6.6). EF5 is pentafluoronated and highly hydrophobic, suggesting it could be absorbed by PDMS and have difficulty diffusing into T-SLICE to assess hypoxia gradients (Koch, 2002). Fortunately, the highest levels of EF5 detection were in the centremost regions of T-SLICE, indicating that it was able to fully diffuse into the device from surrounding cell culture medium. A 2017 study by van Meer and colleagues tested the absorption of four cardiac drugs by PDMS and found that the hydrophobicity of the PDMS did not determine the absorption of the drugs into the polymer. They also suggested the use of surface coatings on PDMS to limit the absorption of drugs and proteins. Gokaltun and colleagues (2019) developed a smart copolymer of poly(ethylene) glycol (PEG) and PDMS to create PDMS-PEG segments that are mixed into the PDMS elastomer during manufacture, which segregate to the external surfaces of the PDMS chip to decrease its

hydrophobicity. This method significantly improved the wettability of the device and maintains its increased hydrophilicity for up to 20 months (Gokaltun et al., 2019). Poly(ethylene) glycol is commonly used in our research lab and this method of PDMS surface modification could be used if drug absorption is an issue in future drug testing applications using T-SLICE.

Another future design consideration of T-SLICE is to optimize the ability to perform biochemical assays (e.g., -omic analyses) due to difficulties isolating cells from specific regions in the device. Crude isolation from two large areas was achieved in this study for qRT-PCR analysis of HIF-regulated genes, but it is highly probable that cells had different gene expression profiles within a single zone. Having to restrict cell isolation to two zones (i.e., edge and middle) leads to the loss of spatial resolution and should be addressed in the future. This is technically challenging, but techniques exist to combat this issue. Fluorescence *in situ* hybridization (FISH) can be used to identify the presence of specific genes in cells or tissues using fluorophore-coupled nucleotides that bind complementary sequences of the gene of interest (Cui et al., 2016). FISH assays are currently used clinically to determine copy number of Her2 when classifying breast cancers (Petroni et al., 2016). Using FISH in combination with T-SLICE culture offers the opportunity to assess how the biochemical gradients generated in the device impact breast cancer biomarker expression. Another genomic method that can be used in T-SLICE is single-cell RNA-sequencing (scRNA-seq), which can profile the transcriptome of individual cells within a tissue or large population of cells (Haque et al., 2017). A single cell suspension would need to be isolated from T-SLICE, which could be achieved using flow cytometry, and subsequently undergo RNA isolation, cDNA synthesis and

library construction, and sequence the libraries (Haque et al., 2017). Incorporating scRNA-seq into T-SLICE analysis would allow researchers to identify sub-clonal populations of cancer cells and determine if T-SLICE is capable of recapitulating intratumour heterogeneity. One of the limiting factors to performing scRNA-seq is its high cost, which can easily total tens of thousands of dollars depending on the number of samples being analyzed. As with other genomic technologies, hopefully scRNA-seq becomes more accessible to all life sciences researchers as time passes and new genomic technologies are developed. This also presents an opportunity to develop a technique to precisely harvest cells from pinpoint locations within T-SLICE. Focus should be placed on engineering a technique to harvest cells from distinct loci in T-SLICE in the near future.

One of the next experiments that should be performed in T-SLICE is anti-cancer drug testing to assess how the hypoxia gradients impact drug susceptibility in the breast cancer cell lines. It is well established that poor vascularization in solid tumours impairs systemic drug delivery to the tumour (van Loo et al., 2002; Jing et al., 2019). The hypoxia in the TME resulting from aberrant vascularization impacts the efficacy of chemotherapy, endocrine therapy, and radiation therapy in breast cancer (van Loo et al., 2002; Jing et al., 2019). Investigating drug response in different biochemical environments will provide insight into which therapeutic regimen will work to treat a specific cancer. This will be particularly important upon validation that T-SLICE can recapitulate ITH.

The most important future direction of this research project, and the overarching goal behind the development of T-SLICE, is to validate that it can recapitulate ITH. This

can be achieved using patient-derived xenografts as the validation target. Patient-derived xenografts are the current gold standard for maintaining tumour heterogeneity. To perform this validation, PDX-derived single-cell suspensions will be seeded into T-SLICE and transcriptomic profiles of the tumour before and after T-SLICE culture will be compared. It is hypothesized that the biochemical gradients generated in T-SLICE will be similar enough to those in the native tumour TME to support all sub-clonal populations of cancer cells present in the *in vivo* tumour. Upon validation, T-SLICE could potentially offer researchers a reliable *in vitro* method of modeling breast cancer to study tumour biology and therapeutic response. This technology could be used to create patient avatars and determine which therapeutic regimen can be used to treat an individual patient's tumour, which will fit nicely into the growing field of precision medicine.

4.10 Conclusions

The findings of this research project demonstrate that T-SLICE generates cell-driven hypoxia gradients, which impact breast cancer cell responses similar to those observed *in vivo*. Furthermore, T-SLICE overcomes many of the limitations frequently faced in the field of *in vitro* cancer modeling; it is imageable, easily tunable, cost-effective, user-friendly, high content, and relatively high throughput. It is important to analyze all the assays collectively when determining the effects of hypoxia in T-SLICE on the breast cancer cells. Culturing breast cancer cells in T-SLICE is advantageous over culturing cells in constant low oxygen (e.g., 1% O_2) conditions because it is more representative of the range of biochemical pressures faced in the *in vivo* TME. There is a relationship between spacer height and size of the T-SLICE that can be manipulated to

drive different biochemical gradients within the device. Decreasing spacer height while keeping the diameter of the device the same will generate steeper hypoxia gradients, and vice versa. Alternatively, increasing the diameter of the device while keeping spacer height constant will generate steeper gradients, and vice versa. This simple tuning strategy will enable researchers to generate a wide range of biochemical gradients in T-SLICE to model many different types of cancer, and potentially model cancers on an individualized basis upon validation. The high tunability of T-SLICE will also lend itself to modeling hypoxic tissues and diseases other than cancer, such as cartilage, infarct, ischemia-reperfusion injury, and chronic obstructive pulmonary disorder. The next steps of this research project should focus on the development of a more biomimetic biophysical environment in T-SLICE and assessing how the biochemical gradients impact therapeutic efficacy. Future goals of this project should focus on validating T-SLICE's ability to recapitulate ITH to offer cancer biologists and oncologists a new tool to investigate tumour biology and therapeutic response. Finally, correlating gene expression profiles of distinct tumour cell populations with chemotherapeutic response will help link gene expression patterns to tumour phenotype. The ability to pair transcriptomic data with other assay modalities, which is made possible by the imageability of T-SLICE, to guide clinical treatment offers potential major advances in cancer patient treatment and, therefore, cancer patient prognosis.

References

Acerbi, I., Cassereau, L., Dean, I., Shi, Q., Au, A., Park, C., Chen, Y. Y., Liphardt, J., Hwang, E. S., & Weaver, V. M. (2015). Human breast cancer invasion and aggression correlates with ECM stiffening and immune cell infiltration. *Integrative Biology: Quantitative Biosciences from Nano to Macro, 7*(10), 1120-1134.

Ayuso, J. M., Virumbrales-Muñoz, M., Lacueva, A., Lanuza, P. M., Checa-Chavarria, E., Botella, P., Fernández, E., Doblare, M., Allison, S. J., Phillips, R. M., Pardo, J., Fernandez, L. J., & Ochoa, I. (2016). Development and characterization of a microfluidic model of the tumour microenvironment. *Scientific reports, 6,* 36086.

Bagnall, J., Leedale, J., Taylor, S. E., Spiller, D. G., White, M. R., Sharkey, K. J., Bearon, R. N., &Sée, V. (2014). Tight control of hypoxia-inducible factor-α transient dynamics is essential for cell survival in hypoxia. *The Journal of Biological Chemistry, 289*(9), 5549-5564.

Bajaj, J., Diaz, E., & Reya, T. (2020). Stem cells in cancer initiation and progression. *The Journal of Cell Biology, 219*(1), e201911053.

Black, J. C., Atabakhsh, E., Kim, J., Biette, K. M., Van Rechem, C., Ladd, B., Burrowes, P. D., Donado, C., Mattoo, H., Kleinstiver, B. P., et al. (2015). Hypoxia drives transient site-specific copy gain and drug-resistant gene expression. *Genes & Development, 29*(10), 1018-1031.

Brenner, D. R., Poirier, A., Woods, R. R., Ellison, L. F., Billette, J. M., Demers, A. A., Zhang, S. X., Yao, C., Finley, C., Fitzgerald, N., Saint-Jacques, N., Shack, L., Turner, D., & Holmes, E. (2022). Projected estimates of cancer in Canada in 2022. *Canadian Medical Association Journal, 194*(17), E601-E607.

Brenner, D. R., Weir, H. K., Demers, A. A., Ellison L. F., Louzado, C., Shaw, A., Turner, D., Woods, R. R., & Smith L. M. (2020). Projected estimates of cancer in Canada in 2020. *Canadian Medical Association Journal, 192*(9), E199-E205.

Campbell, S. B., Wu, Q., Yazbeck, J., Liu, C., Okhovatian, S., & Radisic, M. (2021). Beyond Poyldimethylsiloxane: Alternative Materials for Fabrication of Organ-on-a-Chip Devices and Microphysiological Systems. *ACS Biomaterials and Science Engineering, 7*(7), 2880-2899.

Canadian Cancer Society. (2022). *Stages of breast cancer*. https://cancer.ca/en/cancer-information/cancer-types/breast/staging.

Cancer.Net. (2022). *Breast Cancer – Metastatic: Statistics* https://www.cancer.net/cancer-types/breast-cancer metastatic/statistics#:~:text=The%205%2Dyear%20survival%20rate, metastatic%20breast%20cancer%20is%2022%25.

Cao, W., Zeng, Z., Pan, R., Wu, H., Zhang, X., Chen, H., Nie, Y., Yu, Z., & Lei, S. (2021). Hypoxia-Related Gene FUT11 Promotes Pancreatic Cancer Progression by Maintaining the Stability of PDK1. *Frontiers in Oncology, 11*, 675991.

Cha, Y. J., & Koo, J. S. (2020). Role of Tumor-Associated Myeloid Cells in Breast Cancer. *Cells, 9*(8), 1785.

Chatterjee, N., & Bivona, T. G. (2019). Polytherapy and Targeted Cancer Drug Resistance. *Trends in Cancer, 5*(3), 170-182.

Chaturvedi, P., Gilkes, D. M., Takano, N., & Semenza, G. L. (2014). Hypoxia-inducible factor-dependent signaling between triple-negative breast cancer cells and mesenchymal stem cells promotes macrophage recruitment. *Proceeding of the National Academy of Sciences of the United States of America, 111*(20), E2120-2129.

Chen, C. L., Chu, J. S., Su, W. C., Huang, S. C., & Lee, W. Y. (2010). Hypoxia and metabolic phenotypes during breast carcinogenesis: expression of HIF-1alpha, GLUT1, and CAIX. *Virchows Archiv: an international journal of pathology, 457*(1), 53-61.

Chen, G., Sun, J., Xie, M., Yu, S., Tang, Q., & Chen, L. (2021). PLAU Promotes Cell Proliferation and Epithelial-Mesenchymal Transition in Head and Neck Squamous Cell Carcinoma. *Frontiers in Genetics, 12,* 651882.

Cheng, G., Fan, X., Hao, M., Wang, J., Zhou, X., & Sun, X. (2016). Higher levels of TIMP-1 expression are associated with a poor prognosis in triple-negative breast cancer. *Molecular cancer, 15*(1), 30.

Choi, J., Gyamfi, J., Jang, H., & Koo, J. S. (2018). The role of tumor-associated macrophage in breast cancer biology. *Histology and Histopathology, 33*(2), 133-145.

Cohen, N., Shani, O., Raz, Y., Sharon, Y., Hoffman, D., Abramovitz, L., & Erez, N. (2017). Fibroblasts drive an immunosuppressive and growth promoting microenvironment in breast cancer via secretion of Chitinase 3-like 1. *Oncogene, 36*(31), 4457-4468.

Colpaert, C. G., Vermeulen, P. B., Fox, S. B., Harris, A. L., Dirix, L. Y., & Van Marck, E. A. (2003). The presence of a fibrotic focus in invasive breast carcinoma correlates with the expression of carbonic anhydrase IX and is a marker of hypoxia and poor prognosis. *Breast Cancer Research and Treatment, 81*(2), 137-147.

Cui, C., Shu, W., & Li, P. (2016). Fluorescence In situ Hybridization: Cell-Based Genetic Diagnostic and Research Applications. *Frontiers in Cell Development and Biology, 4,* 89.

Cui, Y. & Guo, G. (2016). Immunomodulatory Function of the Tumor Supressor p53 in Host Immune Response and the Tumor Microenvironment. *International Journal of Molecular Science, 17*(11), 1942.

Dagogo-Jack, I., & Shaw, A. T. (2018). Tumour heterogeneity and resistance to cancer therapies. *Nature Reviews. Clinical Oncology, 15*(2), 81-94.

Dunn, L. K., Mohammad, K. S., Fournier, P. G., McKenna, C .R., Davis, H. W., Niewolna, M., Peng, X. H., Chirgwin, J. M., & Guise, T. A. (2009). Hypoxia and TGF-beta drive breast cancer bone metastases through parallel signaling pathways in tumor cells and the bone microenvironment. *PLoS One, 4*(9), e6896.

Elwakeel, E., 7 Weigert, A. (2021). Breast Cancer CAFs: Specttrum of Phenotypes and Promising Targeting Avenues. *International Journal of Molecular Sciences, 22*(21), 11636.

Emami Nejad, A., Najafgholian, S., Rostami, A., Sistani, A., Shojaeifar, S., Esparvarinha, M., Nedaeinia, R., Haghjooy Javanmard, S., Taherian, M., Ahmadlou, M., Salehi, R., Sadeghi, B., & Manian, M. (2021). The role of hypoxia in the tumor microenvironment and development of cancer stem cell: a novel approach to developing treatment. *Cancer cell international, 21*(1), 62.

Emon, B., Bauer, J., Jain, Y., Jung, B., & Saif, T. (2018). Biophysics of Tumor Microenvironment and Cancer Metastasis – A Mini Review. *Computational and Structural Biotechnology Journal, 16*, 279-287.

Evans, J. J., Alkaisi, M. M., & Sykes, P. H. (2019). Tumour Initiation: a Discussion on Evidence for a "Load-Trigger" Mechanism. *Cell Biochemistry and Biophysics, 77*(4), 293-308.

Fischbeck, A. J., Reuhland, S., Ettinger, A., Paetzold, K., Masouris, I., Noessner, E., & Mendler, A. N. (2020). Tumor Lactic Acidosis: Protecting Tumor by Inhibiting Cytotoxic Activity Through Motility Arrest and Bioenergetic Silencing. *Frontiers in Oncology, 10*, 589434.

Fisher, S. A., Anandakumaran, P. N., Owen, S. C., & Shoichet, M. S. (2015). *Advanced Functional Materials, 25*(46), 7162-7172.

Gao, J., Guo, Z., Cheng, J., Sun, B., Yang, J., Li, H., Wu, S., Dong, F., & Yan, X. (2020). Differential metabolic responses in breast cancer cell lines to acidosis and lactic acidosis revealed by stable isotope assisted metabolomics. *Scientific Reports, 10*(21967).

Garaszczuk, R., Yong, J. H. E., Sun, Z., & de Oliveira, C. (2022). The Economic Burden of Cancer in Canada from a Societal Perspective. *Current Oncology, 29*(4), 2735-2748.

Ghellal, A., Li, C., Hayes, M., Byrne, G., Bundred, N., & Kumar, S. (2000). Prognostic significance of TGF beta 1 and TGF beta 3 in human breast carcinoma. *Anticancer Research, 20*(6B), 4413-4418.

Gioiella, F., Urciuolo, F., Imparato, G., Brancato, V., & Netti, P. A. (2016). An Engineered Breast Cancer Model on a Chip to Replicate ECM-Activation In Vitro during Tumor Progression. *Advanced healthcare materials, 5*(23), 3074-3084.

Gökaltun, A., Kang, Y. B. A., Yarmush, M. L., Usta, O. B., & Asatekin, A. (2019). Simple Surface Modification of Poly(dimethylsiloxane) via Surface Segregating Smart Polymers for Biomicrofluidics. *Scientific Reports, 9*(1), 7377.

Grimes, D. R., Kannanm P., Warren, D. R., Markelc, B., Bates, R., Muschel, R., & Partridge, M. (2016). Estimating oxygen distribution from vasculature in three-dimensional tumour tissue. *Journal of The Royal Society Interface, 13*(116), 20160070.

Grist, S. M., Nasseri, S. S., Laplatine, L., Schmok, J. C., Yao, D., Hua, J., Chrostowski, L., & Cheung, K. C. (2019). Long-term monitoring in a microfluidic system to study tumour spheroid response to chronic and cycling hypoxia. *Scientific reports, 9*(1), 17782.

Hanahan, D. (2022). Hallmarks of Cancer: New Dimensions. *Cancer Discovery, 12*(1), 31-46.

Hanahan, D., & Weinberg, R. A. (2000). The hallmarks of cancer. *Cell, 100*(1), 57-70.

Hanahan, D., & Weinberg, R. A. (2011). Hallmarks of cancer: the next generation. *Cell, 144*(5), 646-674.

Hansen, J. M., Coleman, R. L., & Sood, A. K. (2016). Targeting the tumour microenvironment in ovarian cancer. *European Journal of Cancer, 56*, 131-143.

Haque, A., Engel, J., Teichmann, S. A., & Lönnberg, T. (2017). A practical guide to single-cell RNA-sequencing for biomedical research and clinical applications. *Genome Medicine, 9*(1), 75.

Higashimura, Y., Nakajima, Y., Yamaji, R., Harada, N., Shibasaki, F., Nakano, Y., & Inui, H. (2011). Up-regulation of glyceraldehyde-3-phosphate dehydrogenase gene expression by HIF-1 activity depending on Sp1 in hypoxic breast cancer cells. *Archives of biochemistry and biophysics, 509*(1), 1-8.

Huang, Y., Huang, Z., Tang, Z., Chen, Y., Huang, M., Liu, H., Huang, W., Ye, Q., & Jia, B. (2021). Research Progress, Challenges, and Breakthroughs of Organoids as Disease Models. *Frontiers in Cell and Developmental Biology, 9,* 740574.

Imamura, Y., Mukohara, T., Shimono, Y., Funakoshi, Y., Chayahara, N., Toyoda, M., Kiyota, N., Takao, S., Kono, S., Nakatsura, T., & Minami, H. (2015). Comparison of 2D- and 3D-culture models as drug-testing platforms in breast cancer. *Oncology Reports, 33*(4), 1837-1843.

Imparato, G., Urciuolo, F., & Netti, P. A. *In Vitro* three-dimensional models in cancer research: a review. *International Materials Reviews, 60*(6), 297–311.

Januskeviciene, I., & Petrikaite, V. (2019). Heterogeneity of breast cancer: The importance of interaction between different tumor cell populations. *Life Sciences, 239*, 117009.

Jiang, Y., Zhang, H., Wang, J., Liu, Y., Luo, T., & Hua, H. (2022). Targeting extracellular matrix stiffness and mechanotransducers to improve cancer therapy. *Journal of Hematology & Oncology, 15*(34), 1-15.

Jing, X., Yang, F., Shao, C., Wei, K., Xie, M., Shen, H., & Shu, Y. (2019). Role of hypoxia in cancer therapy by regulating the tumor microenvironment. *Molecular Cancer, 18*(1), 157.

Junttila, M. R., & de Sauvage, F. J. (2013). Influence of tumour micro-environment heterogeneity on therapeutic response. *Nature, 501*(7467), 346-354.

Kapałczyńska, M., Kolenda, T., Przybyła, W., Zajączkowska, M., Teresiak, A., Filas, V., Ibbs, M., Bliźniak, R., Łuczewski, Ł., & Lamperska, K. (2018). 2D and 3D cell cultures - a comparison of different types of cancer cell cultures. *Archives of medical science: AMS*, *14*(4), 910–919.

Katira, P., Bonnecaze, R. T., & Zaman, M. H. (2013). Modeling the mechanics of cancer: effect of changes in cellular and extra-cellular mechanical properties. *Frontiers in Oncology, 3*, 145.

Koch, C. J. (2002). Measurement of absolute oxygen levels in cells and tissues using oxygen sensors and 2-nitroimidazole EF5. *Methods in Enzymology, 352*, 3-31.

Landon-Brace, N., Cadavid, J. L., Latour, S., Co, I. L., Rodenhizer, D., Li, N. T., Wu, N. C., Bugbee, E., Chebotarev, A., Zhang, J., Wouters, B. G., & McGuigan, A. P. (2021). An Engineered Patient-Derived Tumor Organoid Model That Can Be Disassembled to Study Cellular Responses in a Graded 3D Microenvironment. *Advanced Functional Materials, 31*(41), 2105349.

Larrañeta, E., Stewart, S., Ervine, M., Al-Kasasbeh, R., & Donnelly, R. F. (2018). Hydrogels for Hydrophobic Drug Delivery. Classification, Synthesis and Applications. *Journal of Functional Biomaterials, 9*(1), 13.

Lawson, D. A., Kessenbrock, K., Davis, R. T., Pervolarakis, N., & Werb, Z. (2018). Tumour heterogeneity and metastasis at single-cell resolution. *Nature Cell Biology, 20*(12), 1349-1360.

Madu, C. O., Wang, S., Madu, C. O., & Lu, Y. (2020). Angiogenesis in Breast Cancer Progression, Diagnosis, and Treatment. *Journal of Cancer, 11*(15), 4474-4494.

Martinez-Ordonez, A., Seoane, S., Avila, L., Eiro, N., Macia, M., Arias, E., Pereira, F., Garcia-Caballero, T., Gomez-Lado, N., Aguiar, P., Vizoso, F., & Perez-Fernandez, R. (2021). POU1F1 transcription factor induces metabolic reprogramming and breast cancer progression via LDHA regulation. *Oncogene, 40*, 2725-2740.

McCarthy, J. B., Skubitz, A. P., Qi, Z., Yi, X. Y., Mickelson, D. J., Klein, D. J., & Furcht, L. T. (1990). RGD-independent cell adhesion to the carboxy-terminal-heparin-binding fragment of fibronectin involves heparin-dependent and -independent activities. *The Journal of Cell Biology, 110*(3), 777-787.

Mohan, C. M., Lee, T. Y., Guiliano, A. E., & Cui, X. Current Status of Breast Organoid Models. *Frontiers in Bioengineering and Biotechnology, 9*, 745943.

Park, K. M., Lewis, D., & Gerecht, S. (2017). Bioinspired Hydrogels to Engineer Cancer Microenvironments. *Annual Review of Biomedical Engineering, 19*, 109-133.

Petroni, S., Caldarola, L., Scamarcio, R., Giotta, F., Latorre, A., Mangia, A., & Simone, G. (2016). FISH testing of HER2 immunohistochemistry 1+ invasive breast cancer with unfavorable characteristics. *Oncology Letters, 12*(5), 3115-3122.

Petrova, V., Annicchiarico-Petruzzelli, M., Melino, G., & Amelio, I. (2018). The hypoxic tumour microenvironment. *Oncogenesis, 7*(1), 10.

Qian, J., & Rankin, E. B. (2019). Hypoxia-Induced Phenotypes that Mediate Tumor Heterogeneity. *Advances in Experimental Medicine and Biology, 1136*, 43-55.

Qureshi-Baig, K., Ullman, P., Haan, S., & Letellier, E. (2017). Tumor-Initiating Cells: a critical review of isolation approaches and new challenges in targeting strategies. *Molecular Cancer, 16*(1), 40.

Reid, S. E., Kay, E. J., Neilson, L. J., Henze, A. T., Serneels, J., McGhee, E. J., Dhayade, S., Nixon, C., Mackey, J. B., Santi, A., et al. (2017). Tumor matrix stiffness promotes metastatic cancer cell interaction with the endothelium. *The EMBO Journal, 36*(15), 2373-2389.

Rodenhizer, D., Cojocari, D., Wouters, B. G., & McGuigan, A. P. (2016). Development of TRACER: tissue roll for analysis of cellular microenvironment and response. *Biofabrication, 8,* 045008.

Rodig, S. J. (2020). Growing Adherent Cells for Staining. *Cold Spring Harbor protocols, 2020*(8), 099614.

Ruoslahti, E. (1984). Fibronectin in cell adhesion and invasion. *Cancer Metastasis Reviews, 3*, 43-51.

Sahai, E., Astsaturov, I., Cukierman, E., DeNardo, D. G., Egeblad, M., Evans, R. M., Fearon, D., Greten, F. R., Hingorani, S. R., Hunter, T., et al. (2020). A framework for advancing our understanding of cancer-associated fibroblasts. *Nature Reviews Cancer, 20*, 174-186.

Salemme, V., Centonze, G., Cavallo, F., Defilippi, P., & Conti, L. (2021). The Crosstalk Between Tumor Cells and the Immune Microenvironment in Breast Cancer: Implications for Immunotherapy. *Frontiers in Oncology, 11*, 610303.

Semenza, G. L. (2012). Hypoxia-inducible factors in physiology and medicine. *Cell, 148*(3), 399-408.

Seoane, J., & De Mattos-Arruda, L. (2014). The challenge of intratumour heterogeneity in precision medicine. *Journal of Internal Medicine, 276*(1), 41-51.

Sflomos, G., Dormoy, V., Metsalu, T., Jeitziner, R., Battista, L., Scabia, V., Raffoul, W., Delaloye, J. F., Treboux, A., Fiche, M., et al. (2016). A Preclinical Model for ERa-Positive Breast Cancer Points to the Epithelial Microenvironment as Determinant of Luminal Phenotype and Hormone Response. *Cancer Cell, 29*(3), 407-422.

Shahali, A., Ghanadian, M., Jafari, S. M., & Aghaei, M. (2018). Mitochondrial and caspase pathways are involved in the induction of apoptosis by nardosinen in MCF-7 breast cancer cell line. *Research in pharmaceutical sciences, 13*(1), 12-21.

Shinoda, H., Shannon, M., & Nagai, T. (2018). Fluorescent Proteins for Investigating Biological Events in Acidic Environments. (2018). *International Journal of Molecular Science, 19*(6), 1548.

Siolas, D. & Hannon, G. J. (2013). Patient Derived Tumor Xenografts: transforming clinical samples into mouse models. *Cancer Research, 73*(17), 5315-5319.

Sledge, G. W. (2014). Past, Present, and Future Challenges in Breast Cancer Treatment. *Journal of Clinical Oncology, 32*(19), 1979-1986.

Toepke, M. W. & Beebe, D. J. (2006). PDMS absorption of small molecules and consequences in microfluidic applications. *Lab on a chip, 6*(12), 1484-1486.

Torre, L. A., Siegel, R. L., Ward, E. M., & Jemal, A. (2016). Global Cancer Incidence and Mortality Rates and Trends – An Update. *Cancer Epidemiology, Biomarkers, and Prevention, 25*(1), 16-27.

Trayes, K. P., & Cokenakes, S. E. H. (2021). Breast Cancer Treatment. *American Family Physician, 104*(2), 171-178.

Ullah, M. F. (2019). Breast Cancer: Current Perspectives on the Disease Status. *Advances in Experimental Medicine and Biology, 1152*, 51-64.

Van Loo, G., Saelens, X., van Gurp, M., MacFarlane, M., Martin, S. J., & Vandenabeele, P. (2002). The role of mitochondrial factors in apoptosis: a Russian roulette with more than one bullet. *Cell Death and Differentiation, 9*(10), 1031-1042.

van Meer, B. J., de Vries, H., Firth, K. S. A., van Weerd, J., Tertoolen, L. G. J., Karperien, H. B. J., Jonkheijm, P., Denning, C., IJzerman, A. P., & Mummery, C. L. (2017). Small molecule absorption by PDMS in the context of drug response bioassays. *Biochemical and biophysical research communications, 482*(2), 323-328.

Venkatesh, G. H., Bravo, P., Elsayed, W. S. M., Amirtharaj, F., Wojtas, B., Khouzam, R. A., Nawafleh, H. H., Mallya, S., Satymoorthy, K., Dessen, P., et al. (2020). Hypoxia increases mutational load of breast cancer cells through frameshift mutations. *Oncoimmunology, 9*(1), 1750750.

Vodermark, D., Shibata, T., & Brown, J. M. (2001). Green fluorescent protein is a suitable reporter of tumor hypoxia despite an oxygen requirement for chromophore formation. *Neoplasia, 3*(6), 527-534.

Wan, L., Neumann, C. A., & LeDuc, P. R. (2020). Tumor-on-a-chip for integrating a 3D tumor microenvironment: chemical and mechanical factors. *Lab on a chip, 20*(5), 873-888.

West, C. M. L. (2022). Hypoxia does not predict lack of benefit from adjuvant radiotherapy for patients with early stage breast cancer. *British Journal of Cancer, 126*(8), 1111-1112.

Wong, C. H., Siah, K. W., & Lo, A. W. (2019). Estimation of clinical trial success rates and related parameters. *Biostatistics, 20*(2), 273-286.

Woods, M. L., Koch, C. J., & Lord, E. M. (1996). Detection of individual hypoxic cells in multicellular spheroids by flow cytometry using the 2-nitroimidazole, EF5, and monoclonal antibodies. *International Journal of radiation oncology, biology, physics, 34*(1), 93-101.

Wu, T., & Dai, Y. (2017). Tumor microenvironment and therapeutic response. *Cancer Letters, 387*, 61-68.

Yan, M., Jene, N., Byrne, D., Millar, E. K. A., O-Toole, S. A., McNeil, C. M., Bates, G. J., Harris, A. L., Banham, A. H., Sutherland, R. L., & Fox, S. B. (2011). Recruitment of regulatory T cells is correlated with hypoxia-induced CXCR4 expression, and is associated with poor prognosis in basal-like breast cancers. *Breast Cancer Research, 13*(2), R47.

Ye, I. C., Fertig, E. J., DiGiacomo, J. W., Considine, M., Godet, I., & Gilkes, D. M. (2018) Molecular Portrait of Hypoxia in Breast Cancer: A Prognostic Signature and Novel HIF-Regulated Genes. *Molecular Cancer Research, 16*(12), 1889-1901.

Yeo, S. K., & Guan, J. L. (2018). Breast Cancer: Multiple Subtypes within a Tumor? *Trends in Cancer, 3*(11), 753-760.

Yuan, Y. (2016). Spatial Heterogeneity in the Tumor Microenvironment. *Cold Spring Harbor Perspectives in Medicine, 6*(8), a026583.

Zeng, W., Liu, P., Pan, W., Singh, S. R., & Wei, Y. (2015). Hypoxia and hypoxia inducible factors in tumor metabolism. *Cancer Letters, 356*(2 Pt A), 263-267.

Zhang, J. Y., Zhang, F., Hong, C. Q., Giuliano, A. E., Cui, X. J., Zhou, G. J., Zhang, G. J., & Cui Y. K. (2015). Critical protein GAPDH and its regulatory mechanisms in cancer cells. *Cancer biology & medicine, 12*(1), 10-22.

Zhang, M., Gao, C. E., Chen, W. L., Tang, Y. Y., Nie, J. Y., Shen, L. D., Ma, X., & Chen, D. D. (2018). Opposite response to hypoxia by breast cancer cells between cell proliferation and cell migration: A clue from microRNA expression profile. *Oncology Letters, 15*(3), 2771-2780.

Zhao, X., Liu, L., Li, R., Wei, X., Luan, W., Liu, P., & Zhao, J. (2018). Hypoxia-Inducible Factor 1-α (HIF-1α) Induces Apoptosis of Human Uterosacral Ligament Fibroblasts Through the Death Receptor and Mitochondrial Pathways. *Medical Science Monitor, 24*, 8722-8733.

Appendix A

Table A. Primer sequences and properties used in qRT-PCR.

Gene	Host species	F/R	Sequence (5' → 3')	Prod Length (bp)	Tm (ºC)
BACT	Human	F	GAGCACAGAGCCTCGCCTTT	166	62.79
		R	CCCACGATGGAGGGGAAGAC		61.97
VEGFA	Human	F	TCCTGGAGCGTGTACGTTGG	160	62.15
		R	CCTTGCAACGCGAGTCTGTG		62.16
BNIP3	Human	F	CTCAGCATGAGGAACACGAGC	146	61.33
		R	GTGGAGGTTGTCAGACGCCTT		62.58
P4HA1	Human	F	GGAGGATGAATGGGACAAGCC	144	60.75
		R	ACCGTCTCCAAGTCTCCTGTT		60.76
SLC2A1	Human	F	ACAGGCTTCGTGCCCATGTA	129	61.84
		R	GATGGAGTCCAGGCCGAACA		61.9
LDHA	Human	F	GATCTCATTGCCACGCGCC	161	62.17
		R	AGCACCAACCCCAACAACTG		61.04
PFKFB4	Human	F	GCTTGGGCAGGAACTTCAGC	131	61.87
		R	GCAGGCCCACCATGACAATG		61.95
DDIT4	Human	F	GAGTCCCTGGACAGCAGCAA	138	62.12
		R	CAGCAGCTGCATCAGGTTGG		61.93
FUT11	Human	F	CCAGCCCTCACACATGGACT	135	61.85
		R	TCCGAGTGGGGCCAAAGAAA		61.71
TCAF2	Human	F	AGCCTGTCCGTCAGTCCCTA	142	62.15
		R	GGAGTTCACTGGGGATGGGG		61.93
TGFB3	Human	F	CAACTGCTGACTTCGCGCTC	169	62.22
		R	CCTCGGCTTGTCTTCTGCCT		62.18
MGAT2	Human	F	CGCTCAGTTCTGGCCGTCTA	156	61.93
		R	GCTTCGTCTCCGTCCTCTCC		62.00
UGT1A1	Human	F	ACTGCCTTCACCAAAATCCACT	183	60.42
		R	TTCCAGTGTACCGCCACAGG		62.11
CLDN1	Human	F	GAGGGGCTGTGGATGTCCTG	118	62.26
		R	CAACCACCATCAAGGCACGG		61.87
S100A4	Human	F	GCTTCTGAGATGTGGGCTTGC	138	61.88
		R	TGTCACCCTCTTTGCCCGAG		62.11
TGFB1	Human	F	GAGTTGTGCGGCAGTGGTTG	122	62.39
		R	GCCGGTAGTGAACCCGTTGAT		62.70
FGF7	Human	F	GCTCAAGTTGCACCAGGCAG	97	62.14
		R	TTGCTGTGACGCTGTTTGCT		61.38
FGF2	Human	F	GGGAGAAGAGCGACCCTCAC	95	61.95
		R	AGCCAGGTAACGGTTAGCACA		61.72
PDGFA	Human	F	TACCTCGCCCATGTTCTGGC	120	62.25
		R	TCCGGAGTCTATCTCCAGGAGTC		62.08

PDGFB	Human	F	CGGAGTCGGCATGAATCGCT	98	62.96
		R	AAAGCTCCTCGGGAATGGGG		61.93
PLAU	Human	F	GCGACTCCAAACGAACTGTGA	177	61.13
		R	GTGCTGGCCTTTCCTCGGTA		62.18
IL-6	Human	F	GTGTTGCCTGCTGCCTTCC	200	61.92
		R	TCTGCCAGTGCCTCTTTGCT		62.06
IL-8	Human	F	CACACTGCGCCAACACAGAA	96	61.71
		R	TCTCCACAACCCTCTGCACC		61.77
MMP2	Human	F	TGGGCAGTTGCTAAGGGCTC	82	62.48
		R	AGGTTGCAGCTCTCCTTGGG		62.13
MMP9	Human	F	ACTGGCGATTCTCTGAGGGC	161	61.97
		R	GCCTGTGTACACCCACACCT		62.05
MMP11	Human	F	GCTACCCAGCATTGGCCTCT	140	62.28
		R	GCCCAGGACTGGCTTTTCAC		61.53
TIMP1	Human	F	CGGGGCTTCACCAAGACCTA	147	61.55
		R	ACGGGACTGGAAGCCCTTTT		61.72
HIF1A	Human	F	AGGGACGGAGATTTTCTTCAAGC	196	60.87
		R	TCTGGCTGCATCTCGAGACTTT		61.73
HIF3A	Human	F	GGCACCATGGACTGGCAAGA	116	62.77
		R	TGAGCCAGCTGGTACAGCAC		62.45
GAPDH	Human	F	AGGGCCGGACAACTCTTTT	122	59.16
		R	TTACTCCTTGGAGGCCATGT		58.33
YWHAZ	Human	F	ACTTTTGGTACATTGTGGCTTCAA	94	59.60
		R	CCGCCAGGACAAACCAGTAT		60.04

Appendix B

Table B. T-SLICE design criteria and steps taken to achieve them.

Design Criteria	Resolution
Imageable	• Culture cells between two parallel, closely spaced glass coverslips that are optically transparent • Use optically transparent polymer polydimethylsiloxane as the housing substrate to separate the glass coverslips
Tunable	• Create T-SLICE devices via PDMS soft lithography in 3D-printed molds that can be easily adjusted in size using CAD software
Cost-effective	• Use inexpensive materials to make it widely accessible to other life sciences laboratories • Total cost of materials to make one device: $1.60 • Devices can be UV sterilized and reused
User-friendly	• Incorporate commonly used laboratory techniques in T-SLICE culture design • 2D tissue culture, 3D spheroid culture
High content	• Optical transparency facilitates live-imaging • Pair live-imaging with –omic analyses
High throughput	• Low cell number requirement (~10,000 cancer cells per device) • Fits in a 6-well plate, enabling several T-SLICE devices to be set up in parallel